

Mathematical modeling for designing new treatment strategies with Granulocyte-Colony Stimulating Factor

Catherine Foley

Doctor of Philosophy



Department of Mathematics & Statistics
McGill University
Montreal, Canada

June 2008

A thesis submitted to McGill University in partial fulfilment of the requirements of the degree of Doctorate of Philosophy.

© 2008 Catherine Foley

Dedication

I dedicate this thesis to my son Olivier, who was born during the course of this thesis work and who brings a lot of happiness and inspiration into my life.

Acknowledgments

This work would not have been possible without the help and support of many people. I would like to express my deepest gratitude to my supervisor, Dr. Michael Mackey, whose expertise, understanding, and patience, contributed to make my graduate experience an enriching one. I greatly appreciated his guidance, his critical sense as well as his good advice in several situations.

I would also like to thank the McGill Applied Mathematics group as well as all the members of the Centre of Nonlinear Dynamics in Physiology and Medicine at McGill University for creating such a great environment for research. In particular, special thanks to Dr. Peter Swain, Dr. Caroline Colijn and Raluca Apostu for support and valuable discussions.

I gratefully acknowledge the financial support of the Natural Sciences and Engineering Research Council of Canada (NSERC), the Fonds Québécois de la Recherche sur la Nature et les Technologies (FQRNT) and the Institut des Sciences Mathématiques (ISM).

Un merci très spécial à ma famille, qui m'a toujours encouragée et supportée dans mes divers projets. Merci particulièrement à Véronique et à ma mère Esther pour toutes les scéances de gardiennage qui m'ont permis de mener à terme cette thèse. Merci également à mes amis ainsi qu'à tous ceux qui ont suivis mon parcours, pour leurs encouragements et intérêt.

Finalement, et non les moindres, merci à Frédéric pour sa patience et son soutien moral ainsi qu'à notre petit Olivier pour sa joie de vivre et tout le bonheur qu'il apporte dans nos vies.

Abstract

Mathematical modeling can help providing better understanding of the nature and characteristics of regulatory processes in hematology. We first review different mathematical approaches used for modeling so-called dynamical hematological diseases, which are characterized by oscillations in one or more blood cell lines. Then, we present two delay differential equation (DDE) models of the hematopoietic system designed for the study of the effects of Granulocyte-Colony Stimulating Factor (G-CSF) administration. G-CSF is used clinically for treating subjects presenting low numbers of white blood cells, a condition referred to as neutropenia that can result from different causes. However, even though G-CSF is widely used in clinical practice, it is not clear whether the standard G-CSF administration schedule is optimal. The aim of this work is to study alternative treatment regimens that would optimize the use of G-CSF using a mathematical modeling approach. The first model we propose is a comprehensive model that considers G-CSF administration for cyclical neutropenia, a dynamical disorder characterized by oscillations in the circulating neutrophil count. The second model focuses on the effects of two recombinant forms of G-CSF (filgrastim and pegfilgrastim) for the treatment of chemotherapy-induced neutropenia. For each model, we use a combination of mathematical analysis and numerical simulations to study alternative G-CSF treatment regimens that would be efficient while reducing the amount of drug. We found that the dynamical properties of the model could be exploited for designing better G-CSF treatment strategies.

Résumé

La modélisation mathématique est un outil qui permet d'obtenir une meilleure compréhension des différents processus de régulation en hématologie. Dans un premier temps, nous revisons différentes approches qui sont utilisées pour modéliser les maladies hématologiques dites dynamiques. Celles-ci sont caractérisées par la présence d'oscillations dans le niveau d'un ou de plusieurs types de cellules sanguines. Ensuite, nous présentons deux nouveaux modèles d'équations différentielles à délais (EED) du système hématopoïétique, qui sont dédiés à l'étude des effets de l'administration du *granulocyte-colony stimulating factor* (G-CSF). Le G-CSF est utilisé en pratique pour traiter les patients dont le niveau de globules blancs est faible, une condition appelée neutropénie, qui peut survenir dans plusieurs contextes. Cependant, même si le G-CSF est largement utilisé dans le milieu médical, il n'est pas clair que le protocole d'administration standard soit optimal. L'objectif de cette thèse est d'étudier des protocoles de traitement alternatifs qui optimiseraient l'utilisation du G-CSF en utilisant une approche de modélisation mathématique. Le premier modèle que nous proposons est un modèle qui inclut tous les types de cellules sanguines et qui considère l'administration du G-CSF dans le cas de la neutropénie cyclique, une maladie caractérisée par la présence d'oscillations dans le nombre de globules blancs, de plaquettes et de globules rouges. Dans le second modèle, nous nous intéressons aux effets de deux formes de G-CSF (filgrastim et pegfilgrastim) qui sont utilisés pour traiter la neutropénie qui survient fréquemment suite à la chimiothérapie. Pour chacun des modèles, nous utilisons une combinaison d'analyse mathématique et de simulations numériques pour étudier des traitements alternatifs de G-CSF qui seraient efficaces tout en réduisant la quantité de médicament utilisée. Nos résultats suggèrent que les propriétés dynamiques du système pourraient être exploitées afin d'élaborer de meilleures stratégies de traitement.

Contents

Dedication	i
Acknowledgments	ii
Abstract	iii
Résumé	iv
List of Figures	ix
List of Tables	x
1 Introduction	1
1.1 Presentation of the subject	1
1.2 Organization of the thesis	2
2 Dynamic Hematological Disease: A review	4
2.1 Introduction	4
2.2 Normo- and Pathophysiological Hematopoiesis	5
2.2.1 Normal hematopoiesis	5
2.2.2 Dynamical diseases in hematology	8
2.3 Mathematical Models of Hematopoiesis	12
2.3.1 DDE models	13
2.3.2 ODE models	15
2.3.3 Age-structured models	17
2.3.4 Other models	19
2.4 Modeling Periodic Hematological Diseases	20
2.4.1 Modeling periodic autoimmune hemolytic anemia	21
2.4.2 Modeling cyclical thrombocytopenia	25
2.4.3 Modeling cyclical neutropenia	28

2.4.4	Modeling periodic chronic myelogenous leukemia	35
2.5	Discussion	38
2.6	Appendix	40
2.6.1	Method for converting a PDE model into a DDE model	40
2.6.2	The Linear chain Trick	43
3	G-CSF treatment of canine cyclical neutropenia: A comprehensive mathematical model	45
3.1	Introduction	46
3.2	Data and Methods	48
3.2.1	Data	48
3.2.2	Model and Data Fitting	48
3.3	Results	49
3.4	Discussion	55
3.5	Appendix: The model	57
3.5.1	Model structure	57
3.5.2	Parameter estimation	61
3.5.3	Simulated-Annealing	64
4	Optimizing G-CSF treatment following chemotherapy	67
4.1	Introduction	68
4.2	Background	70
4.2.1	Granulopoiesis	70
4.2.2	Treating neutropenia using G-CSF treatment	71
4.3	Mathematical model	72
4.3.1	Description of the main part of the model	73
4.3.2	Description of the G-CSF model	77
4.4	Numerical simulations	80
4.4.1	Simulation without G-CSF treatment	81
4.4.2	Simulating G-CSF (filgrastim) treatment	82
4.4.3	Simulating Filgrastim effects following chemotherapy	83
4.4.4	Simulation of Pegfilgrastim responses following chemotherapy	92
4.5	Bifurcation and multistability	93

4.6	Discussion	96
4.7	Appendix	97
4.7.1	Derivation of the model	97
4.7.2	Derivation of the fraction of bound G-CSF receptors ($F(G)$)	100
4.7.3	Parameter estimation	101
4.7.4	Analytical derivation of steady state values	110
5	Conclusion	113
5.1	Discussion	113
5.2	Future work	116
	References	117

List of Figures

2.1	Schema of the hematopoietic system	7
2.2	Examples of experimental data for four hematological diseases	9
2.3	Schematic representation an age-structured model of erythropoiesis	22
2.4	Schematic representation of a DDE model for granulopoiesis	30
2.5	Schematic representation of a DDE model for the full hematopoietic system	33
2.6	Generic example of a curve that separates the $a - t$ plane (method of characteristics)	42
3.1	Serial neutrophil data and simulations for Dogs 100, 118 and 127	50
3.2	Serial neutrophil data and simulation results for Dogs 101, 113, 117 and 128	51
3.3	Effects of varying G-CSF treatment frequency	53
3.4	Effects of changing initiation time of G-CSF treatment	54
3.5	Schematic diagram of the model	58
3.6	Predicted serum G-CSF time series compared to digitized data from Stute et al. (1992)	62
4.1	Schema of the main part of the model	75
4.2	A two-compartment model for subcutaneous administration of G-CSF	78
4.3	Effects of varying G-CSF dose	82
4.4	Data from Morstyn et al. (1989) showing the effects of varying the time and duration of filgrastim administration	86
4.5	Simulation of 2 cycles of chemotherapy and daily filgrastim ($5\mu\text{g}/\text{kg}$)	87
4.6	Minimum and maximum neutrophil values during G-CSF treatment for both filgrastim ($5\mu\text{g}/\text{kg}/\text{day}$) and pegfilgrastim ($100\mu\text{g}/\text{kg}$) with respect to the starting day of G-CSF treatment following chemotherapy	88

4.7	Effects of varying the duration of filgrastim treatment	89
4.8	Effects of the duration of daily filgrastim ($5\mu\text{g}/\text{kg}$) over 2 cycles of chemotherapy	90
4.9	Simulation of filgrastim ($5\mu\text{g}/\text{kg}$) given only for one day the next day after chemotherapy	91
4.10	Effects of changing the starting day of pegfilgrastim treatment	92
4.11	Bistable behaviour in the model	95
4.12	Simulation of daily filgrastim ($5\mu\text{g}/\text{kg}$) and pegfilgrastim ($100\mu\text{g}/\text{kg}$) on cancer patients	107
4.13	Simulation of bolus subcutaneous injection using the G-CSF model	109

List of Tables

3.1	Normal steady state parameters appropriate for dogs.	63
3.2	Parameters used for computation for each dog	64
4.1	Parameters of the model (steady state values).	106

Contributions of Authors

This thesis is a collection of paper that have been published, accepted or submitted to peer-reviewed journals.

A version of Chapter 2 has been accepted in Journal of Mathematical Biology (C. Foley and M.C. Mackey. Dynamic Hematological Disease: A review, J. Math. Biol., 2008). The majority of this paper constitutes Chapter 2. However, the last paragraph of the section on Modeling cyclical neutropenia (Treatment of Cyclical Neutropenia with G-CSF) of the published paper has been removed from Chapter 2 because this material is actually covered in Chapter 3. CF and MCM both contributed to the manuscript, but CF wrote the majority of the manuscript.

Chapter 3 has been published in Journal of Experimental Hematology (C. Colijn, C. Foley, and M.C. Mackey. G-CSF treatment of canine cyclical neutropenia: A comprehensive mathematical model. Exp. Hematol., 35:898-907, 2007). This paper has been done in collaboration with Caroline Colijn and Michael C.Mackey, who contributed equally to this study. CC and CF participated in developing the mathematical model partially based on previous work of MCM, analyzing the data and performing the numerical simulations. All authors wrote the paper and checked the final version of the manuscript.

Chapter 4 has been submitted to Journal of Theoretical Biology (C. Foley and M.C. Mackey. Optimizing G-CSF treatment following chemotherapy, Journal of Theoretical Biology, 2008.) CF and MCM both participated in the development of the mathematical model and wrote the manuscript, but CF wrote the majority of the manuscript. CF also performed the parameter estimation and numerical simulations.

Chapter 1

Introduction

In this Chapter, we briefly present the characteristics of the regulation and production of blood cells. We also introduce the clinical features of the use of granulocyte-colony stimulating factor (G-CSF) for treating low levels of white blood cells. A comprehensive introduction to the subject is presented in Chapter 2.

1.1 Presentation of the subject

Red blood cells, white blood cells and platelets are all derived from the same source: the hematopoietic stem cells. Production of these different cell types (hematopoiesis) is very important and gives rise to an enormous number of cells. For example, adult humans produce the equivalent of their body weight in red cells, white cells and platelets every 7 years (Mackey (2001)). To better understand the mechanisms involved in the regulation of hematopoiesis, several mathematical models have been put forward over the past few decades. In particular, the existence of periodic hematological disorders, in which the levels of one or more cell types display oscillations, have been shown to be very useful. Indeed, with the use of dynamical systems theory, bifurcation theory and other mathematical tools, the modeling and analysis of their dynamical properties has revealed interesting insight into the underlying control mechanisms for this system. A comprehensive review of the different mathematical approaches used for modeling four periodic hematological diseases (periodic auto-immune hemolytic anemia, cyclical thrombocytopenia, cyclical neutropenia and periodic chronic myelogenous leukemia) is presented in Chapter 2.

The most studied periodic dynamical disorder is probably cyclical neutropenia (CN), a disease in which blood neutrophils counts oscillate between normal and barely detectable levels. Neutrophils act as the primary defense of the organism against infection. Thus, neutropenia, a condition in which the neutrophil levels are low, often leads to an increased risk of infections and can have serious consequences. The standard treatment for CN is daily doses of granulocyte-colony stimulating factor (G-CSF), which has the effect of stimulating neutrophil production. Although this treatment has been proven to be efficient, it is expensive and may have some undesirable side effects. In Chapter 3, we develop a delay differential equation (DDE) model of the hematopoietic system that we couple with an ordinary differential equation (ODE) pharmacokinetic model of G-CSF. Parameters of the model are based on experimental data from seven CN dogs. Using numerical simulations, we study alternative G-CSF treatment strategies for each of the seven dogs. We show that G-CSF administration may lead to different qualitative responses.

Neutropenia often occurs following chemotherapy and G-CSF is also used for treating chemotherapy-induced neutropenia. Two distinct forms of G-CSF are used clinically: filgrastim (daily doses) and pegfilgrastim (only one dose per chemotherapy cycle). In Chapter 4, we develop a DDE model for the production of neutrophils, coupled with an ODE model for G-CSF administration (parameters differ for filgrastim and pegfilgrastim). This model focuses on known effects of G-CSF following chemotherapy by using explicit functions for modeling amplification, aging velocity and death rates. The aim of this study is to optimize G-CSF treatment schedules by studying the effects of varying the starting day of G-CSF treatment as well as its duration. Numerical simulations and analysis of the dynamical properties of the model are performed and reveal the coexistence of two stable solutions.

1.2 Organization of the thesis

Chapter 2 provides a comprehensive review of dynamical hematological diseases and presents the different mathematical methods used for modeling hematopoiesis. It is based on a paper that has been accepted for publication (C. Foley and M.C. Mackey. Dynamical Hematological Disease: A review, *Journal of Mathematical Biology*, 2008). Chapter 3 studies alternative G-CSF treatment strategies for cyclical neutropenia using a

full model of the hematopoietic system. This work has been published (C. Colijn, C. Foley and M. C. Mackey. G-CSF treatment of canine cyclical neutropenia: A comprehensive mathematical model, *Experimental Hematology*, 35, 898-907, 2007). Chapter 4 proposes a new DDE model and uses it to study non-standard schedules for two forms of G-CSF following chemotherapy. A version of this chapter has been submitted for publication (C. Foley and M. C. Mackey. Optimizing G-CSF treatment following chemotherapy, *Journal of Theoretical Biology*, 2008). The thesis concludes with a discussion and possible future work in Chapter 5.

Chapter 2

Dynamic Hematological Disease: A review

Dynamic hematological diseases (also called periodic hematological diseases) are characterized by oscillatory behaviours in one or more cell lines. They have been intensively modeled due to their interesting dynamical nature. In this chapter, we review the basic characteristics of four periodic hematological disorders (periodic auto-immune hemolytic anemia, cyclical thrombocytopenia, cyclical neutropenia and periodic chronic myelogenous leukemia) and examine the role that mathematical modeling and numerical simulations have played in our understanding of the origin of these diseases and in the regulation of hematopoiesis.

A version of this chapter has been accepted for publication: C. Foley and M.C. Mackey, Dynamical Hematological Disease: A review, *Journal of Mathematical Biology*, 2008.

Although the majority of the above-cited paper is part of this chapter, some material has been altered to give coherence and continuity to the thesis.

2.1 Introduction

Based on the analysis of simple mathematical models for Cheyne-Stokes respiration and periodic hematological diseases, Mackey and Glass (1977) speculated that there were dynamical diseases “... characterized by the operation of a basically normal physiological control system in a region of physiological parameters that produces pathological behavior.” Their work suggested “... the following approaches: (i) demonstrate the onset

of abnormal dynamics in animal models by gradual tuning of control parameters;’ (ii) gather sufficiently detailed experimental and clinical data to determine whether sequences of bifurcations \dots actually occur in physiological systems; and (iii) attempt to devise novel therapies for disease by manipulating control parameters back into the normal range.” This programme has been especially successful within a hematological context over the past three decades.

Periodic hematological diseases are particularly interesting from a modeling point of view, due to their dynamical behaviors. Mathematical models (and their numerical simulations) of periodic hematological disorders have contributed substantially to the understanding of general regulatory principles of hematopoiesis and also provided insight into clinically relevant treatment strategies. In this paper, we review some of the mathematical models that have been developed over the years and recount how they have been of use. In Section 2.2, we first review the normal aspects of the regulation and production of blood cells as well as the basic characteristics of some periodic hematological disorders. Then, in Section 2.3, we present the different mathematical tools that are typically useful for modeling in hematology. Section 2.4 reviews the approaches used for modeling four periodic hematological diseases, namely periodic auto-immune hemolytic anemia (AIHA), cyclical thrombocytopenia (CT), cyclical neutropenia (CN) and periodic chronic myelogenous leukemia (PCML). For each of these diseases, we review the mathematical models as well as the knowledge of the disease gained from their mathematical analysis. The paper concludes with a discussion in Section 2.5.

2.2 Normo- and Pathophysiological Hematopoiesis

In this section, we briefly review normal hematopoiesis and provide a short description of some hematological diseases that have helped to elucidate the regulatory mechanisms of hematopoiesis.

2.2.1 Normal hematopoiesis

Hematopoiesis is the term used to describe the production of blood cells. This process is initiated in the bone marrow by the hematopoietic stem cells (HSCs). These cells are self replicating, and produce all types of blood cells. The HSC can produce partially differentiated progenitor cells (assayed by the colony-forming units (CFU-Mix)), which

can then differentiate into committed cells that give rise to one of the cell lineages: thrombocytes (platelets), erythrocytes (red blood cells (RBC)) or leucocytes (white blood cells (WBC)) (see Figure 2.1). Although all blood cells originate from this common source, the mechanisms that regulate their production are not completely clear.

Nevertheless, the production of erythrocytes (erythropoiesis) and platelets (thrombopoiesis) appears to be regulated by specific cytokines via a negative feedback mechanisms whereas granulopoiesis is perhaps more complicated and thus less clearly understood. We briefly present these processes below.

The growth factor (cytokine) mainly involved in the regulation of erythrocyte production is erythropoietin (EPO). EPO production adjusts to the demand for oxygen in the body such that if there is a decrease in the O_2 levels in tissues, there will be an increase in EPO levels. This, in turn, will trigger increased production of primitive erythrocytes precursors (colony-forming units-erythroid (CFU-E)) partially mediated by interfering with apoptosis in these cells (Hardee et al. (2006), Koury and Bondurant (1991)). These cells will mature and eventually (after a maturation delay) produce new erythrocytes. As a result, the erythrocyte population will be increased and so will the oxygen carrying capacity of the blood. Hence, EPO mediates a negative feedback such that a decrease (increase) in the number of erythrocytes leads to an increase (decrease) in erythrocyte production.

The regulation of platelet production (thrombopoiesis) involves similar feedback mechanisms mediated by the cytokine thrombopoietin. If the circulating platelets count is decreased, it triggers thrombopoietin production which then stimulates maturation of the platelet progenitor cells (colony-forming units-megakaryocyte (CFU-Meg)). This eventually leads to an increase in platelet production, again partially mediated by a decrease in megakaryocyte apoptosis (Ritchie et al. (1997)).

There are three types of leucocytes, namely the lymphocytes, the granulocytes and the monocytes. We will focus our attention on granulopoiesis (production of granulocytes) and more specifically on neutrophils, which constitute the most abundant type of granulocyte, since cyclical neutropenia is the periodic hematological disease on which the greatest amount of published clinical data exists. The mechanisms regulating granulopoiesis involve the cytokine granulocyte-colony stimulating factor (G-CSF), which is the main regulator of neutrophil production (Kaushansky et al. (1996)). It stimulates the formation of neutrophils from hematopoietic stem cells, accelerates the formation of neutrophils in the bone marrow and stimulates their release from the bone marrow into

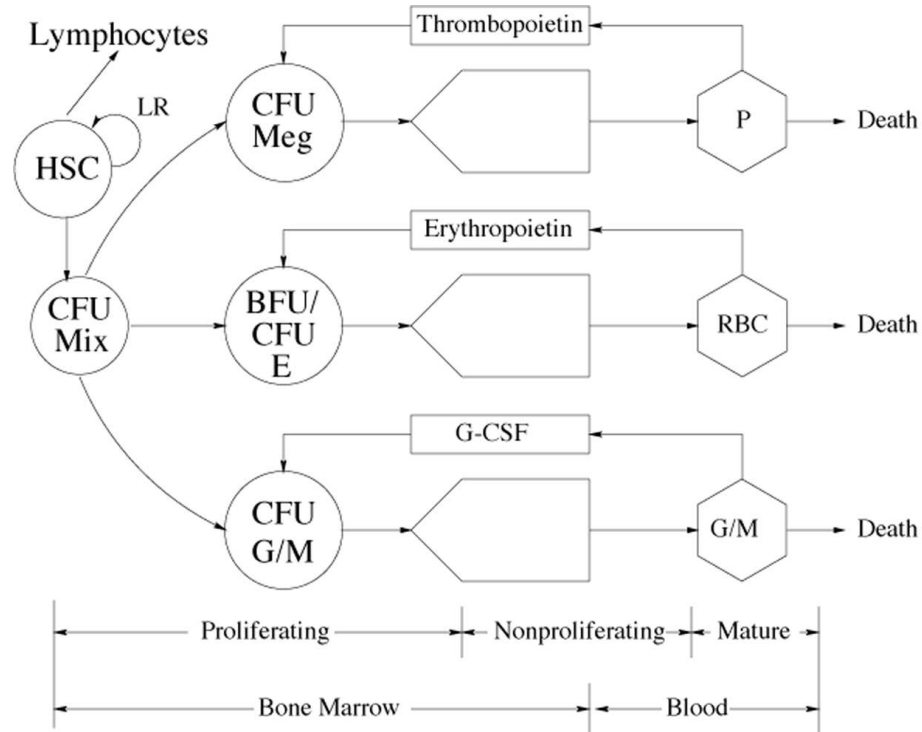


Fig. 2.1 Schema of the hematopoietic system, giving a schematic representation of the architecture and control of platelet (P), red blood cell (RBC), and monocyte (M) and granulocyte (G) (including neutrophil, basophil and eosinophil) production. Presumptive control loops mediated by thrombopoietin (TPO), erythropoietin (EPO), and the granulocyte colony stimulating factor (G-CSF) are indicated, as well as a local regulatory (LR) loop within the pluripotent hematopoietic stem cell (HSC) population. CFU (BFU) refers to the various colony (burst) forming units (Meg = megakaryocyte, Mix = mixed, E = erythroid, and G/M = granulocyte/monocyte) which are the *in vitro* analogs of the *in vivo* committed stem cells (CSC). Taken from Haurie et al. (1998) with permission.

the blood. Although the exact mechanisms by which G-CSF acts are still unclear, it has been shown to decrease the transit time through the neutrophil postmitotic pool and increase maturation rate (Lord et al. (1989), Price et al. (1996)) while interfering with apoptosis (Basu et al. (2002)). Several studies have shown an inverse relationship between the serum levels of G-CSF and the number of circulating neutrophils (Kearns et al. (1993b), Mempel et al. (1991), Takatani et al. (1996), Watari et al. (1989)).

2.2.2 Dynamical diseases in hematology

Periodic hematological disorders are classical examples of dynamical diseases (Glass and Mackey (1988); Mackey and Glass (1977)). Because of their dynamical properties, they offer an almost unique opportunity for understanding the nature of the regulatory processes involved in hematopoiesis. Periodic hematological disorders are characterized by oscillations in the number of one or more of the circulating blood cells with periods on the order of days to months (Haurie et al. (1998)). In this section, we briefly review the clinical aspects of four periodic hematological disorders (see Figure 2.2 for examples of experimental data for each disease). The first two, periodic auto-immune hemolytic anemia (AIHA) and cyclical thrombocytopenia (CT), involve oscillations in only one cell lineage. In the other two diseases, cyclical neutropenia (CN) and periodic chronic myelogenous leukemia (PCML), there is cycling in all of the major blood cell groups. This suggests that these disorders may involve a dynamic destabilization at the stem cell level, leading to oscillations in all cell lineages.

Periodic auto-immune hemolytic anemia

Auto-immune hemolytic anemia (AIHA) results from an abnormality of the immune system that produces autoantibodies, which attack red blood cells as if they were substances foreign to the body. It leads to an abnormally high destruction rate of the red blood cells. Periodic AIHA is a rare form of hemolytic anemia in humans (Ranlov and Videbaek (1963)) characterized by oscillatory erythrocyte numbers about a depressed level. The origin of the disease is unclear. Periodic AIHA, with a period of 16 to 17 days in hemoglobin and reticulocyte counts, has been induced in rabbits by using red blood cell auto-antibodies (Orr et al. (1968)).

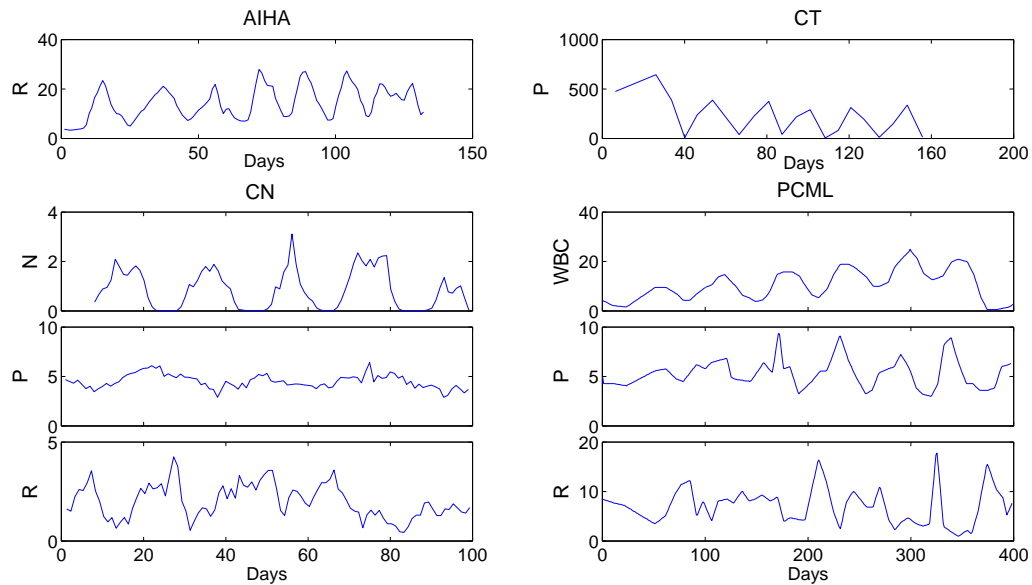


Fig. 2.2 Examples of experimental data for four hematological diseases. AIHA: Reticulocyte numbers ($\times 10^4$ cells/ μL) in an AIHA subject. Adapted from Orr et al. (1968) with permission. CT: Cyclical fluctuations in platelet counts ($\times 10^3$ cells/ μL). From Yanabu et al. (1993). CN: Circulating neutrophils ($\times 10^3$ cells/ μL), platelets ($\times 10^5$ cells/ μL) and reticulocytes ($\times 10^4$ cells/ μL) in a cyclical neutropenic patient. From Guerry et al. (1973) with permission. PCML: White blood cell (top) ($\times 10^4$ cells/ μL), platelet (middle) ($\times 10^5$ cells/ μL) and reticulocyte (bottom) ($\times 10^4$ cells/ μL) counts in a PCML patient. From Chikkappa et al. (1976) with permission.

Cyclical thrombocytopenia

Platelets are blood cells whose function is to take part in the clotting process, and thrombocytopenia denotes a reduced platelet (thrombocyte) count. In cyclical thrombocytopenia (CT), platelet counts oscillate generally from very low values (1×10^9 cells/L) to normal ($150 - 450 \times 10^9$ platelets/L) or above normal levels (2000×10^9 cells/L) (Swinburne and Mackey (2000)). These oscillations have been observed with periods varying between 20 and 40 days (Cohen and Cooney (1974)). In addition, patients may exhibit a variety of clinical symptoms indicative of impaired coagulation such as purpura, petechiae, epistaxis, gingival bleeding, menorrhagia, easy bruising, possibly premenstrually, and gastrointestinal bleeding (Swinburne and Mackey (2000)). There are two proposed origins of cyclical thrombocytopenia. One is of auto-immune origin and most prevalent in females. The other is of amegakaryocytic origin, more common in males.

Autoimmune cyclical thrombocytopenia is characterized by a shortened platelet lifespan at the time of decreasing platelet counts (Beutler et al. (1995)). This is consistent with normal to high levels of bone marrow megakaryocytes and with an increased destruction rate of circulating platelets (Swinburne and Mackey (2000)). Autoimmune CT has also been postulated to be a rare form of idiopathic (immune) thrombocytopenic purpura (ITP) (Beutler et al. (1995)).

The amegakaryocytic form of CT is characterized by oscillations in bone marrow megakaryocytes preceding the platelet oscillations (Balduini et al. (1993); Bernard and Caen (1962); Dan et al. (1991); Engstrom et al. (1966)). In this second type of CT, platelet oscillations are thought to be due to a cyclical failure in platelet production (Bernard and Caen (1962); Cohen and Cooney (1974); Dan et al. (1991); Engstrom et al. (1966); Hoffman et al. (1989); Lewis (1974)). The platelet lifespan is usually normal (Lewis (1974)) and antibodies against platelets are not detected (Hoffman et al. (1989)). Although it has been suggested that the failure of platelet production could arise at the stem cell level (Kimura et al. (1996)), it is generally thought that the cycling originates at the megakaryocyte level (Dan et al. (1991); Hoffman et al. (1989)). For a more detailed review of CT, see (Swinburne and Mackey (2000); Santillan et al. (2000)).

It has been hypothesized that autoimmune and amegakaryocytic cyclical thrombocytopenia have a different dynamic origin (Santillan et al. (2000)). This is

supported by Swinburne and Mackey (2000), who noted that the patients diagnosed as having the autoimmune CT generally have shorter periods (13-27 days) than those classified as amegakaryocytic (27-65). Moreover, they reported that autoimmune patients typically show platelet oscillations from low to normal levels, whereas amegakaryocytic subjects generally show oscillations from above normal to below normal levels of platelets.

Cyclical neutropenia

In a normal individual, the number of circulating neutrophils is relatively constant with an average of about 2.0×10^9 cells/L. Neutropenia is a term that designates a low number of neutrophils, thus indicating that the individual is less effective at fighting infections. Cyclical neutropenia is characterized by oscillations in the number of neutrophils from normal to very low levels (less than 0.5×10^9 cells/L). The period of these oscillations is usually around 3 weeks for humans, although periods up to 45 days have been observed (Haurie et al. (2000b)). The period in which the absolute neutrophil count (ANC) is very low (also called severe neutropenia) usually lasts for about a week in humans. This period is associated with symptoms such as mouth ulcers, periodic fever, pharyngitis, sinusitis, otitis and other infections, some of which can sometimes be life-threatening. Fortunately, CN is effectively treated with daily administration of the growth factor G-CSF, which has the effect of reducing the period of the oscillations and increasing both the oscillation amplitude and the value of the ANC nadir. This has the overall effect of decreasing the period of severe neutropenia. We will see in Section 2.4.3 how mathematical modeling has been used to design cheaper and more effective G-CSF treatment strategies.

Our understanding of CN has been greatly aided by the existence of a similar disease in grey collies (Haurie et al. (1999b)). The canine disorder shows the same characteristics as in humans, except that the period of the oscillations is usually between 11 and 15 days. The existence of this animal model has allowed the collection of a variety of data that would have been difficult, if not impossible, to obtain in humans.

A major characteristic of CN is that the oscillations are not only present in neutrophils, but also in platelets, monocytes and reticulocytes (Haurie et al. (1998)), which is the reason CN is sometimes referred to as periodic hematopoiesis (Palmer et al. (1996)). This observation suggests that the source of the oscillations may lie in the stem cell compartment. Although it is a rare disorder, cyclical neutropenia is probably the most

extensively studied periodic hematological disorder. The availability of an animal model and its dynamical properties makes it suitable for mathematical modeling and several modeling studies have indeed aided our understanding of the basic mechanisms of this disease, as we review in Section 2.4.3.

Periodic chronic myelogenous leukemia

Leukemia is a cancer of the blood or bone marrow characterized by an abnormal proliferation of blood cells, usually leucocytes. Chronic myelogenous leukemia (CML) is distinguished from other leukemias by the presence of a genetic abnormality in blood cells, called the Philadelphia chromosome, which is a translocation between chromosomes 9 and 22 that leads to the formation of the BcrAbl fusion protein (O'Dwyer et al. (2000)). This protein is thought to be responsible for the dysfunctional regulation of myelocyte growth and other features of CML (Melo (1996)). (For more details about CML, see Grignani (1985)).

A dynamical disease of particular interest is periodic chronic myelogenous leukemia (PCML), characterized by oscillations in circulating cell numbers that occur primarily in leucocytes, but may also occur in the platelets and reticulocytes (Fortin and Mackey (1999)). The leucocyte count varies periodically, typically between values of 30 and 200×10^9 cells/L, with a periods ranging from 40 to 80 days. In addition, oscillation of platelets and reticulocytes may occur with the same period as the leucocytes, around normal or elevated numbers (Fortin and Mackey (1999); Henderson et al. (1996)). As in cyclical neutropenia, the hypothesis that the disease originates from the stem cell compartment is supported by the presence of oscillations in more than one cell lineage.

2.3 Mathematical Models of Hematopoiesis

Mathematical models have been used for modeling biological processes for decades. With the advances in technology and the increasing amount of available data, mathematical models and simulation techniques provide ways of better understanding the underlying mechanisms of biological processes. In hematological modeling, several mathematical tools and computational methods are used: differential equations (partial, ordinary or delay), stochastic processes, Boolean networks, Bayesian theory, multivariate statistics, decision trees, etc. For a review, see Roeder (2006) and Viswanathan and Zandstra

(2003). The choice of the mathematical tools often depends on the desired level of description of the model. For instance, one could model processes at small scale (e.g. at the molecular or the cellular levels), or on a larger scale (model the whole system). Mathematical models of in vivo hematopoietic regulatory systems using a stochastic formulation have not been extensively developed, primarily because of the lack of corresponding data for stem cells and their progeny. Since they are widely used, we focus in this chapter on models that use differential equations: ordinary differential equations (ODE), partial differential equations (PDE), or delay differential equations (DDE). In this section, we first discuss the different types of delay differential equations and show how some DDE systems could be reduced to an ODE system using the linear chain trick. Second, we present a typical setting for a model, based on biological aspects of hematopoiesis and show that this could be modeled by an age-structured model (PDE). We then show that this PDE model can be reduced to a DDE model. Finally, we briefly comment other types of models in Section 2.3.4.

2.3.1 DDE models

Delay-differential equations (DDEs) are a large and important class of dynamical systems. They often arise in biological systems where time lags naturally occur (MacDonald (1978b)). In particular, in hematology several processes are controlled through feedback loops and these feedbacks are generally operative only after a certain time, thus introducing a delay in the system feedback. The general form of a DDE for $x(t) \in R^n$ is

$$\frac{dx}{dt} = f(t, x(t), x_\tau), \quad (2.1)$$

where x_τ is the delayed variable ($x(t - \tau)$) and f is a functional operator in $R \times R^n \times C^1$. There are different kinds of delay-differential equations: with discrete fixed delays, with distributed delays and with state-dependent delays. In this section, we briefly discuss these different types of DDEs and give some examples of how they have arisen in modeling hematological problems.

DDE with constant delays

Delay differential equations with constant delays take the form

$$\frac{dx}{dt} = f(x(t), x(t - \tau_1), x(t - \tau_2), \dots, x(t - \tau_n)), \quad (2.2)$$

where the quantities $\tau_i, i = 1, 2, \dots, n$ are positive constants. For simplicity, consider the DDE with a single constant delay:

$$\frac{dx}{dt} = f(x(t), x(t - \tau)). \quad (2.3)$$

To obtain a solution of Equation (2.3) for $t > 0$, one needs to specify a history function on $[-\tau, 0]$. Indeed, recall that for an ordinary differential equation (ODE) system with n variables, one would only need to specify the initial values $x(0)$ for each of the n state variables. In order to solve a DDE, one needs to specify not only the value at $t = 0$, but also all the past values of $x(t)$ over the interval $[-\tau, 0]$. Since one needs to specify an “infinite” number of values, DDEs are often viewed as infinite-dimensional systems.

Constant delay differential equations are often used in modeling in hematology (Bernard et al. (2003); Beuter et al. (2003); Haurie et al. (1998); Mackey (1979a)). For example, let $X(t)$ represent the circulating cell population of a certain type of blood cell, assume that γ is the random rate of loss of cells in the circulation and F is the flux of cells from the previous compartment. Then, the dynamics of the number of circulating cells will have the generic form

$$\frac{dX}{dt} = -\gamma X + F(X(t - \tau)), \quad (2.4)$$

where τ is the average length of time required to go through the compartment (time delay). Typically, F is taken to be a monotone decreasing function of X to mimic the negative feedback loops of the system.

DDE with distributed delays

Delays arise in biological systems because of properties inherent to the different processes (time lag due to maturation, transmission of an impulse, etc.). Although constant delays may be an excellent approximation of the time lag involved, one might want to account for the distribution of time delay. Indeed, in a real system, it is much more likely that

events related to the delay (maturation time for example) are distributed with a density that is not a delta function. A distribution of delays is then be more appropriate and the DDE becomes an integro-differential equation of the form

$$\frac{dx}{dt} = f \left(x(t), \int_{-\infty}^t x(\tau)G(t - \tau) d\tau \right). \quad (2.5)$$

The density $G(u)$ of the distribution function is referred to as the memory function or the kernel and is normalized, i.e.

$$\int_0^{\infty} G(u) du = 1.$$

This type of model can also be interpreted as allowing for a stochastic element in the duration of the delay (MacDonald (1978b)). Examples of such models in hematology are found in Blythe et al. (1984), Haurie et al. (2000b) and Hearn et al. (1998). Also, we will see in Section 2.3.2 that for some densities $G(u)$, Equation (2.5) can be equivalently viewed as a system of ordinary differential equations.

DDE with state-dependent delays

Another type of delay differential equation occurs when the delay depends on a state variable. For example, one could imagine that the maturation time for a blood cell depends on the amount of growth factor in the circulation as, for example, is the case with the maturation time of neutrophil precursors in humans (Price et al. (1996)). An example of a model with a state-dependent delay can be found in Mahaffy et al. (1998a), but it is fair to say that models of hematopoietic regulation with state dependent delays have not appeared because of the paucity of data for the analytic variation of delays with respect to state variables.

2.3.2 ODE models

Delay differential equations naturally arise in modeling biological systems. However, since DDEs are infinite-dimensional systems, they are difficult to analyze and handle numerically. For some forms of delays, the so-called linear chain trick (MacDonald (1978b)) enables the model to be written as an equivalent finite-dimensional system of ordinary differential equations. Next, we present a simple example of this method which

is a specific example of the more general considerations of Fargue (1973, 1974). Consider the following DDE system with a distributed delay:

$$\frac{dx_1}{dt} = f \left(x_1(t), \int_{-\infty}^t x_1(\tau) G(t - \tau) d\tau \right), \quad (2.6)$$

with the special choice of the density of the gamma distribution for the memory function

$$G(u) = G_a^p(u) = \frac{a^{p+1} u^p}{p!} e^{-au}, \quad (2.7)$$

where a is a positive number and p is a positive integer or zero. Note that the function $G(u)$ has a maximum at $u = p/a$ and that, as a and p increase, keeping p/a fixed, the kernel approaches a delta function and the distributed delay approaches the discrete time delay with $\tau = p/a$. Moreover, it is clear that the following three properties are satisfied:

$$\begin{aligned} \lim_{u \rightarrow \infty} G_a^p(u) &= 0, \\ G_a^p(0) &= 0 \text{ for } p \neq 0, \\ G_a^0(0) &= a. \end{aligned} \quad (2.8)$$

The central idea of the method is to replace the distributed delay by an extension of the set of variables. Define $p + 1$ new variables as

$$x_{j+1} = \int_{-\infty}^t x_1(\tau) G_a^{j-1}(t - \tau) d\tau \quad j = 1, 2, \dots, p + 1, \quad (2.9)$$

and set

$$x_{p+2} := \int_{-\infty}^t x_1(\tau) G(t - \tau) d\tau. \quad (2.10)$$

Then, using the properties of G one can show that these new variables satisfy a sequence of linear ODEs (see the Appendix for a detailed derivation). Solving the following system is thus equivalent to solving the DDE problem (2.6), given that the new variables are

given appropriate initial values:

$$\begin{aligned}\frac{dx_1}{dt} &= f(x_1, x_{p+2}) \\ \frac{dx_{j+1}}{dt} &= a(x_j - x_{j+1}) \quad j = 1, 2, \dots, p+1, \\ \frac{dx_{p+2}}{dt} &= a(x_{p+1} - x_{p+2}).\end{aligned}\tag{2.11}$$

The linear chain trick could be useful for numerical computations since it reduces the problem to an ODE system, for which several numerical methods are available. However, this method cannot be used for all sorts of delays (for more details about the method and some examples, see MacDonald (1978b)). Within a hematological context, Hearn et al. (1998) were unable to use this technique in their model of neutrophil production because the estimated value of p in the experimentally determined distribution of delays was not an integer. Other models (Loeffler and Pantel (1990); Loeffler et al. (1989); Schmitz et al. (1993, 1994, 1995, 1990)) have used constructs somewhat analogous to the system (2.11). Introducing a delay in a system could be thought of as a way of including age-structure in the model. For instance, one could think of setting up a detailed model in which the population dynamics is described by several maturation stages. If enough detail is known about the time spent in each stage, one could then associate a differential equation (ordinary or delayed) with each stage. However, detailed data such as these are often (usually) not available. Alternatively, one could lump together all the stages and reduce the model to only one DDE where the delay is the total maturation time. Another option would be to use partial differential equations, as we will discuss in the next section.

2.3.3 Age-structured models

We now present a typical PDE model used in several applications. Based on Figure 2.1, one can see that the production of any of the cell types takes many steps. Indeed, a cell starts from the hematopoietic stem cell and then its progeny go through a number of stages before being released into the circulation. One could model this process by associating a partial differential equation for the cell density function with each stage, which describes the population in the compartment as a function of the variables age a and time t (Rubinow and Lebowitz (1975)). The model also contains feedback control

elements (rate of apoptosis, rate of production, etc.) that regulate the release of cells from one compartment to the other. The number of compartments depends on the data available which determines the maximum level of detail appropriate for the model. For instance, a model of erythropoiesis could have one compartment for each recognizable stage of erythrocytes precursors, or alternatively merge some of the compartments together and thus reduce the model dimensions. In the following, we will present some results using only a generic compartment. The treatment for a larger model is the same. We then show that by partial integration we can express this problem as a delay differential equation model. Age-structured models provide a means of understanding the regulation of hematopoiesis. Examples in the literature can be found in Adimy and Crauste (2003), Adimy and Pujon-Menjouet (2001, 2003), Bélair et al. (1995), Dyson et al. (1998), Mackey and Rudnicki (1994), Mahaffy et al. (1998a), Ostby et al. (2003, 2004), Rubinow and Lebowitz (1975) and Santillan et al. (2000).

Let $x(t, a)$ be the cell density at time t and age a in a generic compartment. We assume that cells disappear (die) at a rate $\gamma(t)$. We also assume that the cells in the compartment age with a velocity $V(t)$ and that a cell enters a compartment at age $a = 0$ and exits this compartment at age $a = \tau$. Therefore, the equation satisfied by $x(t, a)$ is an time-age equation (advection, or reaction-convection, equation):

$$\frac{\partial x}{\partial t} + V(t) \frac{\partial x}{\partial a} = -\gamma(t)x \quad t > 0, a \in [0, \tau], \quad (2.12)$$

The right hand side in this equation represents the rate at which cells in the age interval a to $a + \delta a$ disappear at time t . To represent the manner in which new cells enter the compartment, we define the boundary condition (B.C.) $x(t, 0) = H(t)$. Finally, to fully represent the problem, we specify the initial condition (I.C.) $x(0, a) = \phi(a)$. In the Appendix, we show that by partial integration of equation (2.12), we can reformulate this problem as a delay differential equation. Using the method of characteristics (Webb (1985)), we obtain the following delay differential equation:

$$\frac{dX}{dt} = V(t) \left[H(t) - H(t - T_\tau) \exp \left(- \int_0^{T_\tau} \gamma(w) dw \right) \right] - \gamma(t)X(t), \quad (2.13)$$

where $X(t)$ is the total number of cells ($X(t) = \int_0^\tau x(t, a) da$) and T_τ satisfies

$\tau = \int_{t-T_\tau}^t V(w) dw$. Note that if γ is a constant, Equation (2.13) reduces to

$$\frac{dX}{dt} = V(t) [H(t) - H(t - T_\tau)e^{-\gamma T_\tau}] - \gamma X(t). \quad (2.14)$$

In addition, if the aging velocity is constant ($V(t) = V$), we have that T_τ satisfies

$$\tau = \int_{t-T_\tau}^t V dw = VT_\tau,$$

which implies that $T_\tau = \tau/V$. Hence, if γ and V are constant, we obtain a delay differential equation with constant delay:

$$\frac{dX}{dt} = V(t) [H(t) - H(t - \tau/V)e^{-\gamma\tau/V}] - \gamma X(t). \quad (2.15)$$

2.3.4 Other models

In this section, we briefly discuss some other types of mathematical models. As mentioned above, several approaches have been used for modeling hematopoiesis (for example DDE, ODE or PDE models). However, it is sometimes appropriate to combine these approaches in one model as in Vainstein et al. (2005). In this work, the authors used a PDE model which includes a distributed delay for the compartment transition time and a constant delay for the cell cycle duration. Others have included probabilistic aspects in the model, as in Lasota and Mackey (1984) where the authors used a probabilistic approach to model to cellular maturation of proliferative cells.

Besides the PDE models presented in Section 2.3.3, other types of partial differential equations have been used. For instance, a reaction-diffusion model for leukemia is proposed in Bessonov et al. (2005). This type of model accounts for spatial variables, which are not considered ODEs, DDEs and in the previously discussed PDE models. In Ducrot and Volpert (2008), they proposed a reaction-diffusion system of equations in a porous medium to describe the evolution of leukemia in the bone marrow. They showed the existence of two stationary solutions, one of them corresponds to the normal case and another one to the pathological case.

Finally, a different technique has recently been used in Bessonov et al. (2006). In this work, the authors used a multi agent approach and created software to study

hematopoiesis at the cell population level with the individually based approach. This computational model is aimed at studying different features of hematopoiesis and may be useful as an interface between theoretical work on population dynamics and experimental observations.

2.4 Modeling Periodic Hematological Diseases

Based on the dynamical properties of the periodic hematological diseases, a number of mathematical models have been put forward to better understand the mechanisms responsible for the onset of the observed oscillations in blood cell counts. This mathematical modeling of periodic hematological diseases has helped our understanding of the mechanisms of hematopoiesis.

These models fall into two major categories and reference to Figure 2.1 will help place these in perspective. The first broad group identifies the origin of the oscillations as a destabilization of the peripheral control loops. In this case, the cell production is adjusted relative to the number of mature cells in the blood and mediated by one of the three cytokines (EPO, TBO and G-CSF). The second group of models focuses on the existence of oscillations in many of the peripheral cell lineages (neutrophils, platelets and erythroid precursors, see Figure 2.1). It assumes that oscillations arise in the common stem cell populations through a loss of stability in the stem cell population that is hypothesized to be independent of feedback from peripheral circulating cell types. Thus, this would represent a relatively autonomous oscillation driving the three major lines of differentiated hematopoietic cells (Colijn et al. (2006a)).

In this section, we review a number of mathematical models of the hematopoietic system and show how dynamical disorders have helped understanding the mechanisms involved. First, we review modeling of erythropoiesis guided by the dynamics of periodic auto-immune hemolytic anemia, and then turn to a consideration of thrombopoiesis drawing on the features of cyclical thrombocytopenia. Recall that each of these two disorders only involve oscillations in one cell line. Then, we turn to a review of large scale models drawing inspiration from the data and characteristics of cyclical neutropenia and periodic chronic myelogenous leukemia.

2.4.1 Modeling periodic autoimmune hemolytic anemia

In an early model of erythropoiesis, Mackey (1979a) examined the role of peripheral erythrocyte destruction rate on the onset of AIHA using a simple constant delay differential equation model for the regulation of erythrocyte production. The model defines the rate of change of the circulating density of erythrocytes (E (cells/kg)) by

$$\frac{dE}{dt} = -\gamma E + \beta(E_\tau), \quad (2.16)$$

where $E_\tau = E(t - \tau)$, β is the cellular production rate in the early erythroid series cells and γ (day^{-1}) is the peripheral erythrocyte destruction rate. The delay τ represents the total average number of days between the entrance of a cell into the erythroid series and the release of a mature erythrocyte into the blood. As mentioned in Section 2.2, erythropoiesis is regulated by a negative feedback mediated by the cytokine erythropoietin (EPO). This is modeled by using a monotone decreasing Hill function for the production rate β :

$$\beta(E) = \beta_0 \frac{\theta^n}{\theta^n + E^n}, \quad (2.17)$$

where β_0 (cells/kg/day) (the maximum production rate), θ (cells/kg), and n are parameters. (Hill functions are often used for regulatory feedback expressions since they frequently can be fit to existing clinical or laboratory data, and offer a form that is easy to deal with analytically.) Mackey (1979a) performed a linear stability analysis of this model and showed that a supercritical Hopf bifurcation occurs when the death rate of circulating erythrocytes is increased above a certain critical value. This transition from damped to stable oscillations would characterize the onset of periodic AIHA and account for the experimentally observed characteristics of AIHA.

In their study, Bélair et al. (1995) developed an age-structured model that incorporates the fact that the population of precursor cell matures at differing rates depending on the EPO concentration, which itself varies according to the amount of oxygen carried in blood. They developed a PDE model similar to the one presented in Section 2.3.

Assuming constant maturing velocity, the authors were then able to reduce their model to a threshold-type DDE with two constant delays, using the method we presented in Section 2.3.

Even though the bifurcation analysis performed on this model agreed surprisingly well

with experimental observations in an induced autoimmune hemolytic anemia, this model was less than satisfactory in predicting the response of a normal patient to a blood loss as in a blood donation. In their paper, Mahaffy et al. (1998a) expanded the previous model of Bélair et al. (1995) to account for the active degradation of older cells and to include the possibility of significant apoptosis. Next, we present the equations of this extended age-structured model for hematopoiesis that includes apoptosis and active degradation of the oldest mature cells.

The precursor cells begin from a pool that have differentiated into a self-sustaining population which eventually leads to the production of mature erythrocytes. The model considers two populations of cells: the precursor cells, denoted by $p(t, \mu)$ (see below), and the mature non-proliferative cells, denoted by $m(t, \nu)$. Figure 2.3 shows a cartoon representation of the model.

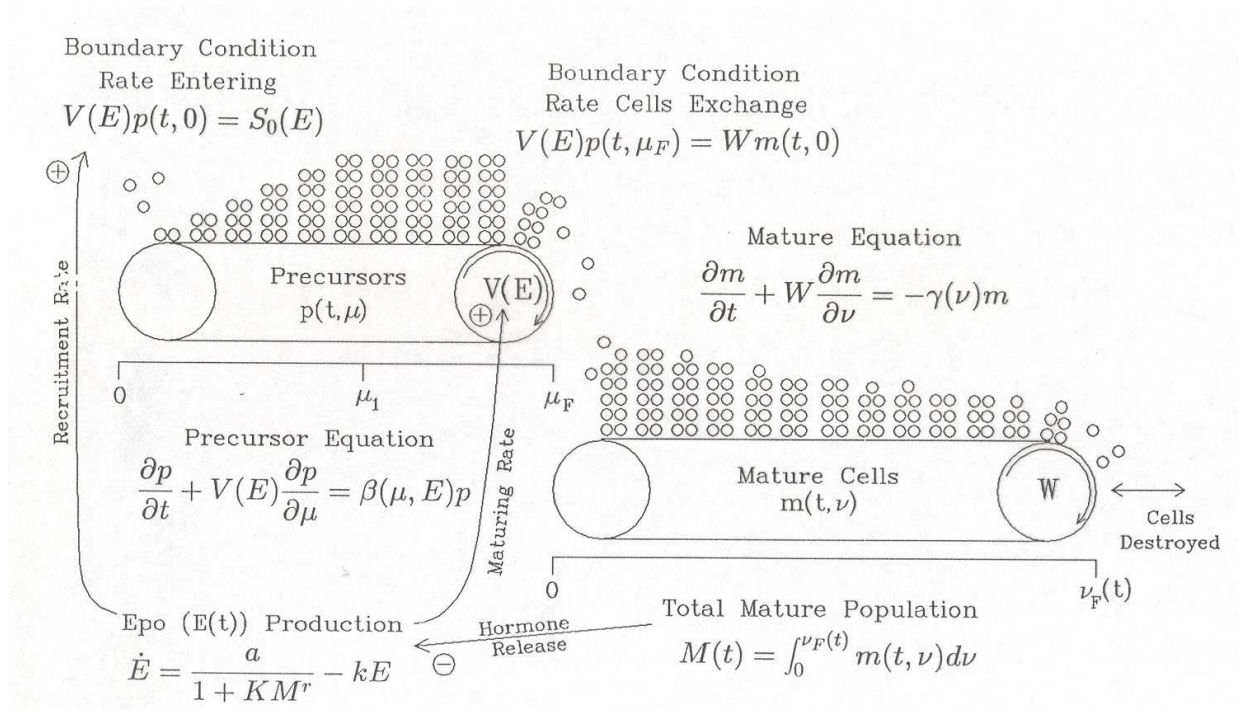


Fig. 2.3 Schematic representation of the age-structured model of erythropoiesis, taken from Mahaffy et al. (1998a) with permission.

Let $p(t, \mu)$ denote the population of precursor cells at time t and age μ , and let $V(E)$ be the velocity of maturation, which may depend on the hormone (EPO) concentration, E . If $S_0(E)$ is the number of cells recruited into the proliferating precursor population, then

the entry of new precursor cells into the age-structured model will satisfy the boundary condition

$$V(E)p(t, 0) = S_0(E). \quad (2.18)$$

Let the birth rate for proliferating precursor cells be $\beta(\mu, E)$ and $\alpha(\mu, E)$ represent the death rate through apoptosis. Let $h(\mu - \bar{\mu})$ be the density of the distribution of maturity levels of the cells when released into the circulating blood, where $\bar{\mu}$ represents the mean age of mature precursor cells and

$$\int_0^{\mu_F} h(\mu - \bar{\mu})d\mu = 1.$$

The disappearance rate function is given by:

$$H(\mu) = \frac{h(\mu - \bar{\mu})}{\int_{\mu}^{\mu_F} h(s - \bar{\mu})ds}.$$

With these conditions the age-structured model for the population of precursor cells with $t > 0$ and $0 < \mu < \mu_F$ satisfies:

$$\frac{\partial p}{\partial t} + V(E)\frac{\partial p}{\partial \mu} = V(E)[\beta(\mu, E)p - \alpha(\mu, E)p - H(\mu)p]. \quad (2.19)$$

Now, let $m(t, \nu)$ be the population of mature non-proliferating cells at time t and age ν . Assume that the mature cells age at a rate W , which is considered to be a constant for erythropoiesis since the aging process appears to depend only on the number of times that an erythrocyte passes through the capillaries. From the disappearance rate function, the boundary condition for cells entering the mature population is given by

$$Wm(t, 0) = V(E) \int_0^{\mu_F} h(\mu - \bar{\mu})p(t, \mu)d\mu, \quad (2.20)$$

where the maturity level μ_F represents the maximum age for a cell reaching maturity. The authors assumed that destruction of erythrocytes occurs by active removal of the oldest cells. The immune system recognizes erythrocytes that are no longer efficient and tags them with special markers, which then signals macrophages (white blood cells) to degrade them. For erythrocytes, if one assumes either a finite source of markers or a fixed

number of macrophages, then there is a constant flux of the oldest erythrocytes that are dying. From a modeling point of view, this results in a moving boundary condition with the age of the oldest erythrocyte, $\nu_F(t)$, varying in t . The boundary condition is then given by

$$(W - \dot{\nu}_F(t))m(t, \nu_F(t)) = Q, \quad (2.21)$$

where Q is the fixed erythrocyte removal rate (for a full derivation, see Mahaffy et al. (1998a)). If $\gamma(\nu)$ is the death rate of mature cells (depending only on age), then the partial differential equation describing $m(t, \nu)$ is given by:

$$\frac{\partial m}{\partial t} + W \frac{\partial m}{\partial \nu} = -W\gamma(\nu)m, \quad t > 0, \quad 0 < \nu < \nu_F(t), \quad (2.22)$$

where the maximum age, $\nu_F(t)$, is determined by (2.21).

As in the simple DDE model of Mackey (1979a), the EPO level E is governed by a differential equation with a negative feedback, depending on the total population of mature cells, $M(t)$, defined by

$$M(t) = \int_0^{\nu_F(t)} m(t, \nu) d\nu. \quad (2.23)$$

The differential equation for E is thus:

$$\frac{dE}{dt} = \frac{a}{1 + KM^r} - kE, \quad (2.24)$$

where k is the decay constant for the hormone and the rate of EPO production is given by a monotone decreasing Hill function.

The partial differential equations and their boundary conditions given by Eqns. (2.18)-(2.22) describe the age-structured model for erythropoiesis. The hormone EPO exerts control in the model through the boundary conditions, the birth and death of precursor cells, and the velocity of aging. Using the method of characteristics and the techniques presented in Section 2.3, one can reduce this system of equations to a system of threshold delay equations. Moreover, if one makes some simplifying assumptions (see Mahaffy et al. (1998a) for the details), it further reduces this system to a system of delay differential equations with a fixed delay and one state dependent delay and it transform

the constant flux boundary condition (2.21) to

$$Q = (1 - \dot{\nu}_F(t))e^{\beta\mu_1}e^{-\gamma\nu_F(t)}S_0(E(t - T - \nu_F(t))). \quad (2.25)$$

The following system of delay differential equations with a fixed delay T and a state dependent delay occurring in the equation governing the age at which mature cells die is obtained:

$$\begin{aligned} \frac{dM(t)}{dt} &= e^{\beta\mu_1}S_0(E(t - T)) - \gamma M(t) - Q, \\ \frac{dE(t)}{dt} &= f(M(t)) - kE(t), \\ \frac{d\nu_F(t)}{dt} &= 1 - \frac{Qe^{-\beta\mu_1}e^{\gamma\nu_F(t)}}{S_0(E(t - T - \nu_F(t)))}. \end{aligned} \quad (2.26)$$

Analysis of the characteristic equation for the linearized model demonstrated the existence of a Hopf bifurcation when the destruction rate of erythrocytes is increased, as in the previous models by Bélair et al. (1995) and Mackey (1979a). Parameters of the model have been estimated from experimental data. Numerical simulations were performed for both periodic auto immune hemolytic anemia in rabbits and blood donation in humans and compared with experimental data. Even though the extension of the model presented in Mahaffy et al. (1998a) leads to the same conclusion about the origin of periodic AIHA, the moving boundary condition has the advantage of better capturing the physiological reality of apoptosis in circulating cells. Moreover, the model is sufficiently general to characterize other hematopoietic lines. In particular, a similar age-structured model has been used for modeling cyclical thrombocytopenia, as we will see in the next section.

2.4.2 Modeling cyclical thrombocytopenia

A number of studies have presented models for the regulation of thrombopoiesis. Some considered only a simple thrombopoiesis feedback (Bélair and Mackey (1987); Gray and Kirk (1971); von Schulthess and Gessner (1986)) whereas other models are more physiologically detailed (Apostu and Mackey (2008); Eller et al. (1987); Györi and Eller (1987); Wichmann et al. (1979)). Nevertheless, they all assume that the production of platelets is regulated by a negative feedback loop mediated by thrombopoietin (TPO). In their study, von Schulthess and Gessner (1986) suggested that the normal platelet control

system was biased close to a stability boundary and that this was the origin of the oscillatory platelets counts observed in some normal individuals (Morley (1969)). Bélair and Mackey (1987) specifically considered the case of cyclical thrombocytopenia. Based on the analysis of their model, they hypothesized that an increased destruction rate of circulating platelets could give rise to the characteristic oscillations in the circulating platelet counts seen in CT, an hypothesis that has recently been modified in Apostu and Mackey (2008) using a more comprehensive model. Santillan et al. (2000) developed an age-structured model for the regulation of platelet production that we briefly present below.

The development of the mathematical model for thrombopoiesis in Santillan et al. (2000) follows earlier age-structured mathematical models for erythropoiesis (Bélair et al. (1995)), bearing in mind that the primary difference between the processes of erythropoiesis and thrombopoiesis is in the development of the precursor cells. In erythropoiesis, the stem cells undergo rapid proliferation and differentiation until they reach the stage of reticulocytes, where the cells simply mature to become circulating erythrocytes. In thrombopoiesis, the stem cells proliferate, then become megakaryocytes that no longer proliferate, but undergo nuclear endoreduplication. These megakaryocytes have different ploidy values at maturation and release differing numbers of platelets. In order to simplify calculations and based on the relative frequencies of megakaryocytes in various ploidy classes, the authors chose to divide the megakaryocyte populations into three classes, denoted by $m_i(t, \mu)$, $i = 0, 1, 2$. As before, t represents time and μ represents the age of the megakaryocyte.

The partial differential equations describing the development of the megakaryocytes are given by:

$$\frac{\partial m_0}{\partial t} + \frac{\partial m_0}{\partial \mu} = -k_0(T)m_0, \quad (2.27)$$

$$\frac{\partial m_1}{\partial t} + \frac{\partial m_1}{\partial \mu} = k_0(T)m_0 - k_1(T)m_1, \quad (2.28)$$

$$\frac{\partial m_2}{\partial t} + \frac{\partial m_2}{\partial \mu} = k_1(T)m_1, \quad (2.29)$$

where $k_i(T)$ is the transfer rate from ploidy class i to ploidy class $i + 1$. The domain for these partial differential equations is $t > 0$ and $0 < \mu < \mu_F$.

Relevant boundary conditions for each population were included. The remaining equations for the circulating platelets $p(t, \mu)$ and its boundary condition are similar to the ones presented in Section 2.4.1 for erythrocytes and will not be presented here. They used a constant flux boundary condition as derived in Mahaffy et al. (1998a) and a negative feedback ODE for regulation of thrombopoietin.

Despite some difficulties in estimating parameters of this age-structured model, the model numerically reproduced the normal human response to a bolus injection of TPO. The dynamic characteristics of the autoimmune version of cyclical thrombocytopenia were reproduced if the rate of platelet destruction in the circulation is elevated to more than twice the normal value. The authors hypothesized that the amegakaryocytic version of cyclical thrombocytopenia, with its longer periods and different dynamic clinical presentation could potentially find an explanation in considerations of the dynamics of the hematopoietic stem cell.

Recently, a more comprehensive mathematical model was used to understand the clinical data of patients with cyclical thrombocytopenia (Apostu and Mackey (2008)). This model is based on the work of Colijn and Mackey (2005a) (presented in Section 2.4.3 and Figure 2.5) and accounts for all cell lineages (erythrocytes, leucocytes and platelets). The authors found that it was not possible to induce oscillations in the platelet compartment without destabilizing the neutrophil compartment using the model of Colijn and Mackey (2005a). They found that using a constant platelet differentiation rate (instead of a rate depending on the circulating platelet levels), the hematopoietic model was then able to generate oscillations in platelets while maintaining the other cells lines at their steady state values. Their model successfully duplicates the platelet counts in CT patients and agrees qualitatively with clinical data. However, it supports only partially the conclusions drawn from the previous modeling study of Santillan et al. (2000), where CT was hypothesized to be due to an increased platelet destruction rate. Indeed, their numerical experiments showed that more than one parameter had to be modified to reproduce clinical data. Using a simulated-annealing method (see Section 3.5.3, they concluded that a variation in the megakaryocyte maturity, a slower relative growth rate of megakaryocytes, as well as an increased random destruction of platelets are the critical elements generating the platelet oscillations in CT. Moreover, the authors believe that both types of CT are due to a Hopf bifurcation in the platelet dynamics, but that the parameter change inducing the bifurcation might depend on the type of cyclical thrombocytopenia. Their model

raises a number of clinical issues that will have to be resolved in the future.

2.4.3 Modeling cyclical neutropenia

Due to its interesting dynamics and its clinical and laboratory manifestations, cyclical neutropenia is probably the most studied periodic hematological disease. A number of mathematical models have been put forward to attempt to model this disorder, and they fall into two major categories (see Figure 2.1 to place them in perspective). For other reviews, see Colijn et al. (2006a); Dunn (1983); Fisher (1993); Haurie et al. (1998). The first group of models identifies the origin of CN with a loss of stability in the peripheral negative feedback control loop. Typical examples of models of this type which have specifically considered CN are Kazarinoff and van den Driessche (1979), King-Smith and Morley (1970), MacDonald (1978a), Morley (1979), Morley et al. (1969), Morley and Stohlman (1970), Reeve (1973), Schmitz (1988), Schmitz et al. (1993), Schmitz et al. (1994), Schmitz et al. (1995), Schmitz et al. (1990), Shvitra et al. (1983), von Schulthess and Mazer (1982), and Wichmann et al. (1988).

The second group of models builds upon the existence of oscillations in many of the peripheral cellular elements (neutrophils, platelets, and erythroid precursors, see Figure 2.1) and postulates that the origin of CN is in the common hematopoietic stem cell (HSC) population. A loss of stability in the stem cell population is hypothesized to be independent of feedback from peripheral circulating cell types and would thus represent a relatively autonomous oscillation driving the three major lines of differentiated hematopoietic cells. In their study, Hearn et al. (1998) concluded that there is no consistent way in which a destabilization of the peripheral loop alone can give rise to the characteristics of CN. It seemed more likely that the oscillations of CN originate from the hematopoietic stem cell population as was originally proposed in earlier work by Mackey (1978a, 1979b). Some mathematical models coupled a stem cell compartment with the peripheral loop for granulocytes (Bernard et al. (2003); Haurie et al. (2000b); Hearn et al. (1998)) whereas others present a more complex model showing the stem cells coupled to all major cell lines (Colijn and Mackey (2005a)). For a complete review, see Colijn et al. (2006a).

We present two of these models that have given significant insight into the origin of cyclical neutropenia. Then, we show how these models have been used to improve

existing treatment for CN.

Origin of Cyclical Neutropenia

Bernard et al. (2003) presented a two variable delay differential equation (DDE) system that has negative feedback loops in both the peripheral loop and the stem cell loop. Figure 2.4 illustrates the two compartments of the model: the hematopoietic stem cell (HSC) compartment (denoted S) and the neutrophil compartment (denoted N). The HSCs are assumed to be self-renewing, and thus cells in the resting (G_0) phase can either enter the proliferative phase at rate $K(S)$ or differentiate into neutrophils (N) at rate $F(N)$. As the neutrophil precursors differentiate, their numbers are amplified by a factor A , which accounts for both successive divisions and cell loss due to apoptosis. It is also assumed that apoptosis occurs during the proliferative phase at rate γ_s and that mature neutrophils die at rate α . As can be seen in Figure 2.4, the system is controlled by two negative feedback loops. The first one regulates the rate $K(S)$ of reentry of HSCs to the proliferative cycle, and it operates with a delay τ_s (the cell cycle time) that accounts for the time required to produce two daughter cells from one mother cell. The second loop regulates the rate $F(N)$ of HSC differentiation into mature neutrophils. It operates with a delay τ_N that accounts for the transit time through the neutrophil precursor compartment.

Mathematically, this model translates into the following two variable delay differential equation (DDEs) form. The equations for the two variables N and S can be derived from a time-age-maturation formulation, or written directly from consulting Figure 2.4. For the compartment N , the loss is the efflux to death αN and the production of mature neutrophils is equal to the influx $F(N)S$ from the HSC compartment times the amplification A . Since one needs to take into account the transit time τ_N , the total production of mature neutrophils is $AF(N(t - \tau_N))S(t - \tau_N)$, or equivalently $AF(N_{\tau_N})S_{\tau_N}$ (recall that $N_{\tau_N} = N(t - \tau_N)$). This leads to the total rate of change of N given by

$$\frac{dN}{dt} = -\alpha N + AF(N_{\tau_N})S_{\tau_N}. \quad (2.30)$$

For the second variable, the loss from the compartment S is the flux reentering the proliferative phase, $K(S)S$, plus the efflux going into differentiation, $F(N)S$. The production of S is equal to the flux of cells reentering and surviving the proliferative

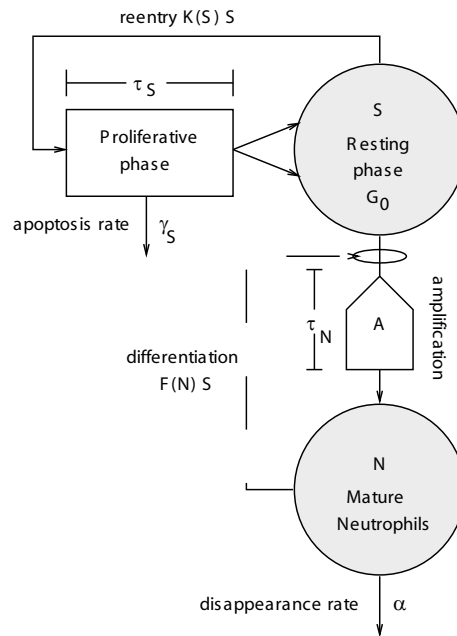


Fig. 2.4 Schematic representation of the mathematical model of Bernard et al. (2003). Two feedback loops control the entire process through the proliferation rate $K(S)$ and the differentiation rate $F(N)$. Taken from Bernard et al. (2003) with permission.

phase, given by $K(S_{\tau_S})S_{\tau_S}e^{-\gamma S_{\tau_S}}$, times the cell division factor 2. The dynamics of S is then described by

$$\frac{dS}{dt} = -F(N)S - K(S)S + 2K(S_{\tau_S})S_{\tau_S}e^{-\gamma S_{\tau_S}}. \quad (2.31)$$

The feedback functions $F(N)$ and $K(S)$ are monotone decreasing Hill functions, similar to the one used in Mackey (1979a):

$$F(N) = f_0 \frac{\theta_1^n}{\theta_1^n + N^n}, \quad (2.32)$$

and

$$K(S) = k_0 \frac{\theta_2^s}{\theta_2^s + S^s}. \quad (2.33)$$

$F(N)$ controls the number of neutrophils (N) while $K(S)$ regulates the level of HSCs (S). This model was sufficiently simple that it was possible to perform a complete bifurcation analysis that highlighted the dynamical features of CN (Bernard et al. (2003)). Using a combination of mathematical analysis and computational tools, Bernard et al. (2003) showed that the origin of cyclic neutropenia is probably due to an increased apoptosis rate in the recognizable and committed neutrophil precursors, leading to a destabilization of the hematopoietic stem cell compartment through a supercritical Hopf bifurcation. This has the effect of generating oscillations in the HSC population. This result was in accordance with previous modeling studies (Haurie et al. (2000b)) and agrees with experimental data on grey collies. This model could also be used to study the effects of G-CSF treatment on CN, as we will see in the next section. First we present a more sophisticated model of the hematopoietic system that has also been used to study cyclical neutropenia.

As mentioned, CN is characterized by oscillations in all major cell lines (neutrophils, reticulocytes and platelets). This motivated the development of a comprehensive mathematical model that includes not only the neutrophils and HSC, but also the platelets and red blood cells. This allowed a more realistic approach since one could then study the response of the hematopoietic system when considering all cell lines. In addition, the model simulations could thus be compared with data for platelets and erythrocytes. Colijn and Mackey (2005b) developed a comprehensive model that contains

four compartments: the HSC (Q), the neutrophils (N), the erythrocytes (R) and the platelets (P). This model combines a number of compartmental models we have reviewed in previous sections: the stem cell and neutrophil dynamics are based on the model in Bernard et al. (2003), and the erythrocyte and platelet compartment are simplified models based on Mahaffy et al. (1998a) and Santillan et al. (2000) respectively. The circulating cells are coupled to each other via their common origin in stem cell compartment. Regulatory negative feedback loops determine how much differentiation from the stem cells each cell line will undergo. Since it takes several days to produce a mature cell from a newly differentiated cell, time delays appear in the equations. The model consists of a set of four coupled delay differential equations. Their derivation is similar to Equations (2.30) and (2.31) from Bernard et al. (2003)'s model and is based on Figure 2.5:

$$\begin{aligned}
\frac{dQ}{dt} &= -\beta(Q)Q - (\kappa_N + \kappa_R + \kappa_P)Q + 2e^{-\gamma_S\tau_S}\beta(Q_{\tau_S})Q_{\tau_S}, \\
\frac{dN}{dt} &= -\gamma_N N + A_N \kappa_N(N_{\tau_N})Q_{\tau_N}, \\
\frac{dR}{dt} &= -\gamma_R R + A_R \left\{ \kappa_R(R_{\tau_{RM}})Q_{\tau_{RM}} - e^{-\gamma_R\tau_{RS}} \kappa_R(R_{\tau_{RM}+\tau_{RS}})Q_{\tau_{RM}+\tau_{RS}} \right\}, \\
\frac{dP}{dt} &= -\gamma_P P + A_P \left\{ \kappa_P(P_{\tau_{PM}})Q_{\tau_{PM}} - e^{-\gamma_P\tau_{PS}} \kappa_P(P_{\tau_{PM}+\tau_{PS}})Q_{\tau_{PM}+\tau_{PS}} \right\}.
\end{aligned} \tag{2.34}$$

Analogous to Eq. (2.32) and (2.33) we have

$$\begin{aligned}
\beta(Q) &= k_0 \frac{\theta_2^s}{\theta_2^s + Q^s}, & \kappa_N(N) &= f_0 \frac{\theta_1^n}{\theta_1^n + N^n}, \\
\kappa_P(P) &= \frac{\bar{\kappa}_p}{1 + K_p P^r}, & \kappa_R(R) &= \frac{\bar{\kappa}_r}{1 + K_r R^{m_e}},
\end{aligned} \tag{2.35}$$

where the first two functions are the same as in Bernard et al. (2003). For a complete derivation, see Colijn and Mackey (2005b). This model was applied to both PCML (Section 2.4.4) and CN.

The authors used a simulated annealing approach (see Section 3.5.3) and clinical data from dogs and humans to estimate the model parameters. The model supported the hypothesis on the origin of CN put forward in Bernard et al. (2003) and showed that realistic CN oscillations in neutrophils and platelets can result from an increased apoptosis rate in the neutrophil precursors. Interestingly, in order to mimic clinical data,

it was also necessary to decrease the rate of differentiation into the neutrophil line and the maximal rate of re-entry of the stem cells into the proliferative phase.

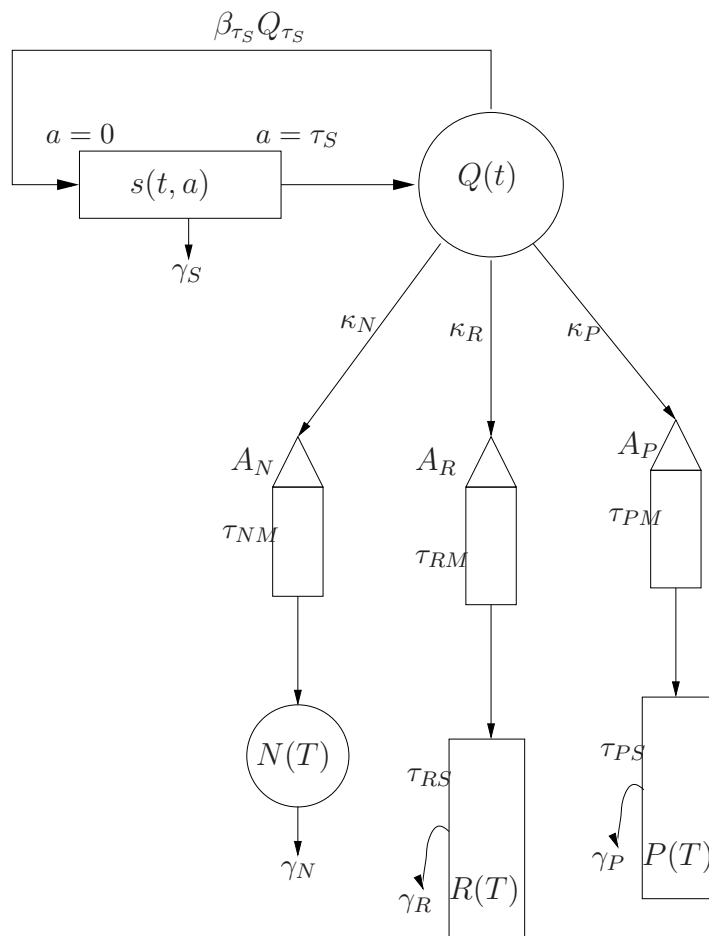


Fig. 2.5 Schematic representation of the comprehensive mathematical model of Colijn and Mackey (2005a) including the HSC and the three differentiated cell lines. Each cell lineage is controlled by a negative feedback loop. Taken from Colijn and Mackey (2005a) with permission.

A bifurcation analysis was performed on the model. This analysis predicted that changes in the platelet compartment can have long-term effects on the nature of the oscillations. Simulations show that temporarily increasing the platelet amplification factor A_P will often induce the simulations to jump from an oscillating solution to the coexisting stable solution. Oscillations were thereby abolished. While there are limitations to the clinical applicability of these results because of the difficulties in administering a drug such as

thrombopoietin, the ability of the platelet dynamics to affect the long-term behavior of the whole hematopoietic system is theoretically intriguing.

In the next section, we show how the model of Bernard et al. (2003) could be used to explore different G-CSF treatment strategies for CN. In Chapter 3, we will adapt Colijn and Mackey (2005b)'s model for studying alternative G-CSF therapy regimens.

Treatment of Cyclical Neutropenia with G-CSF

Treatment for cyclical neutropenia typically involves daily G-CSF administration. This is an effective treatment since it has the overall effect of decreasing the period of severe neutropenia by increasing the nadir and the amplitude of the oscillations as well as decreasing their period (Haurie et al. (1998)). However, G-CSF is expensive (about \$45 000 per year for a 70 kg adult treated daily) and may cause undesirable side effects. In this section, we show how mathematical modeling can illuminate the effects of different G-CSF treatment schemes.

Foley et al. (2006), using the model of Bernard et al. (2003) presented earlier, analyzed alternate G-CSF treatment schemes. Even though the effects of G-CSF have been included implicitly in the model through the feedback function $F(N)$, it can be shown that by using physiologically relevant parameter values, this model can replicate the characteristics of CN and the effects of G-CSF administration. Mimicking CN can be achieved by increasing the rate of apoptosis for the neutrophil precursors, i.e. decreasing the amplification parameter A (which accounts for cell death). To simulate the effects of G-CSF in CN the authors modified five of the eleven parameters of the model: decrease apoptosis in both the HSC (decrease γ_s) and in the neutrophil precursors compartment (increase A), decrease the duration of both the proliferative and differentiating phases (τ_n and τ_s) as well as increasing the parameter θ_1 in the feedback function. This yields two sets of parameters of interest (for untreated CN and CN under G-CSF treatment).

Assuming that the five parameters vary linearly between the untreated CN state and the G-CSF treated values, the authors expressed the five relevant parameters as a function of a new parameter T , in such a way that $T = 0$ corresponds to untreated CN and $T = 1$ corresponds to the treated state. Increasing T was therefore associated with increasing G-CSF concentration. A complete bifurcation analysis was then performed using this G-CSF parameter (T).

Interesting dynamical features of the model were found. The bifurcation analysis agreed with the clinical aspects of G-CSF administration (increased amplitude and decreased period of the oscillations Haurie et al. (1999a,b)), as expected. However, some cases have been reported in the literature in which G-CSF treatment abolished significant oscillations (Hammond et al. (1989); Haurie et al. (1998, 1999a)). Interestingly, the model also accounts for this effect of G-CSF administration. Indeed, for $T = 1$ (G-CSF treatment), a stable steady state (corresponding to annihilation of oscillations) coexists with a stable large amplitude oscillation. This bistability in the system is interesting since it suggests that by properly designing the treatment administration scheme, one might stabilize the neutrophil count to a desirable level and could potentially reduce the amount of G-CSF required in treatment. In Foley et al. (2006), the authors exploited this bi-stability and showed that, depending on the starting time of the G-CSF treatment, the neutrophil count could either be stabilized or show large amplitude oscillations. Using computer simulations, they also showed that other G-CSF treatment schemes (such as administering G-CSF every other day) could be effective while using less G-CSF, hence reducing the cost of treatment and side effects for patients.

The model of Bernard et al. (2003) grasped the essential features of the system while being simple enough to carry out the detailed analysis and simulations presented in Foley et al. (2006). It gave insight into the dynamics of the system but it had two major shortcomings. First, the model included neither erythrocyte nor platelet dynamics even though clinical data indicates oscillations in those cell lines in CN patients. Thus it is not known if the results would be consistent with observed platelet and reticulocyte data. Second, G-CSF kinetics are implicitly included in the model and are based on a pseudo-equilibrium assumption on the kinetics of G-CSF clearance, which is a simplification. Therefore, the simulations did not take into account the pharmacokinetics of G-CSF. In Chapter 3, we study different G-CSF treatment strategies using Colijn and Mackey (2005b)'s model to which we add a two-compartment pharmacokinetic model for G-CSF administration.

2.4.4 Modeling periodic chronic myelogenous leukemia

As for cyclical neutropenia, periodic chronic myelogenous leukemia (PCML) is an interesting dynamical disease of the hematopoietic system in which oscillating levels of

circulating leukocytes, platelets and/or reticulocytes are observed. Typically all of these three differentiated cell types have the same oscillation period, but the relation of the oscillation mean and amplitude to the normal levels is variable. The hypothesis that oscillations originate in the stem cells is related to the fact that oscillations of the same period occur in different cell lines. However, in several mathematical models, only one cell line, or one line coupled to the stem cells, is represented. In particular, Pujo-Menjouet et al. (2005) explored how long-period oscillations (as seen in PCML) could arise within the context of a G_0 stem cell model. They used a two-dimensional DDE model and they performed a careful mathematical analysis. They studied when stability was lost and oscillations occur, and how various parameters modify the period of these oscillations. They also considered a limiting case of the original model in order to compute an explicit solution and give an exact form of the period and the amplitude of oscillations. They showed that the main parameters controlling the period are the cellular loss (the differentiation rate δ and the apoptosis rate γ), while the cell regulation parameters (proliferation rate β and cell cycle duration τ) mainly influenced the amplitude. In Pujo-Menjouet and Mackey (2004), the authors used the same model and determined the local stability conditions and showed under what conditions a Hopf bifurcation may occur. They interpreted the role of each parameter in the loss of stability, and then examined a simpler model to try to deduce possible changes at the stem-cell level that might be responsible for the characteristics of PCML.

In these papers, the models assumed a constant cell cycle duration, leading to a system of nonlinear differential equations with discrete delays. In Adimy et al. (2005a, 2006), the authors assumed that all cells do not divide at the same age, introducing a distributed delay in the two-dimensional nonlinear differential equation system. The dynamics and stability of this model were analyzed in Adimy et al. (2005a,b, 2006). In particular, the authors showed the existence of a Hopf bifurcation and applied their results to periodic chronic myelogenous leukemia. They showed that their model can display long periods of peripheral cell oscillations (as seen in PCML) for relatively short cell cycle duration. Adimy et al. (2006) studied the action of growth factors on the hematopoietic system using a DDE model. They assumed growth factors act on the rate of introduction in the proliferative phase and applied their model to PCML. Then, in Adimy and Crauste (2007) they considered the action of growth factors on apoptosis using a three-dimensional DDE system with distributed delay, concluding that the action of growth factors can lead to

the existence of oscillating solutions in the stem cell population.

All these models only consider one cell line coupled with the stem cells and do not include platelet and erythrocyte regulation. Thus, it is not clear whether their hypothesis would be consistent with observed platelet and erythrocyte data in PCML. For this reason, the comprehensive model for the regulation of the hematopoietic system (Colijn and Mackey (2005b)) presented in Section 2.4.3 was used to examine the possible origins of PCML. Based on estimates of parameters for a typical normal human, the authors systematically explored the changes in some of these parameters necessary to account for the quantitative data on leukocyte, platelet and reticulocyte cycling in 11 patients with PCML, using two different fitting procedures (the Marquardt Levenberg procedure as well as simulated annealing). Both methods gave qualitative and quantitative agreement with the published data on PCML in reproducing the period, amplitudes and mean values of the oscillating cell types as well as the relative phase differences between them. This indicates that the model is capable of duplicating the overall features of the coupled oscillations of the different cell lines.

Based on their analysis and numerical simulations, the oscillatory nature of PCML could be generated through a bifurcation in the dynamics of the coupled HSC compartment and the regulation of differentiated leukocytes. The critical model parameter changes required to simulate the periodic chronic myelogenous leukemia patient data were the amplification in the leukocyte line (A_N), the differentiation rate from the stem cell compartment into the leukocyte line (f_0), and the rate of apoptosis in the stem cell compartment (γ_S). In particular, their model system was very sensitive to changes in γ_S , suggesting that changes in the numbers of proliferating stem cells might be important in generating PCML. Note also that a high-frequency oscillation on top of the typical long time periods oscillations was often seen in their numerical simulations. Colijn et al. (2006b) analyzed a two-compartment DDE model for stem cell and neutrophil populations and showed how such oscillations can be understood in the context of slow periodic stem cell oscillations. They suggested that these observed intermittent high frequency oscillations are likely to be partially due to the system dynamics, and not simply result from noise and fluctuations in the biological parameters.

2.5 Discussion

Due to their interesting dynamical characteristics, hematological periodic diseases are good candidates for using mathematical modeling and bifurcation theory to better understand the underlying mechanisms of hematopoiesis and even to potentially understand how clinical treatment affects dynamics.

We have reviewed four dynamical diseases and presented different mathematical models that have aided our understanding of the origin and features of these diseases. Several types of mathematical models have been used and the choice typically depends on the availability of data and the overall objective of the study. Due to advances in measurement technology, an increasing amount of cellular and molecular data is being generated. Their analysis and the complexity of the underlying mechanisms require the contribution of mathematical models and computational methods. Indeed, mathematical modeling and simulation techniques contribute to the discovery of regulatory principles and may also provide clinical predictions. In particular, we illustrated how one could use mathematical models to optimize standard G-CSF treatment for cyclical neutropenia. The same ideas may be used for other diseases if enough clinical data are made available for appropriate parameter estimations. Indeed, despite major advancement in new technologies, some quantities are still difficult to measure or estimate, making the parameter estimation a limitation for mathematical modeling.

In conclusion, we also mention three other recent studies that have used computational methods for specific clinical applications. First, Engel et al. (2004) used an ODE model for studying the effects of 10 different multi-cycle poly-chemotherapies on leucocytes in lymphoma patients. Their model provides quantitative predictions for different G-CSF chemotherapy schedules (Engel et al. (2004); Scholz et al. (2005)). Second, the PDE model in (Ostby et al. (2003, 2004)) was successfully applied to clinical results for granulocyte reconstitution after high-dose chemotherapy with stem cell and G-CSF support in breast cancer patients. Finally, we mention the work of Skomorovski and Agur (2001) and Skomorovski et al. (2003), who developed a computer tool that simulates thrombopoietin (TPO) administration schedules on the platelets number and on the cell counts of different bone marrow compartments. This tool is aimed at suggesting improved drug protocols for patients suffering from low blood platelet levels. In our opinion, these are other examples which show that clinical biology and dynamical modeling should not

be regarded as independent fields, but rather as complementary parts of biology. We hope that readers will appreciate that mathematical modeling is a process that constantly evolves as the predictions of the models are iterated against data and clinical findings, and the results of the past three decades in modeling the of dynamical hematological diseases is an example of this. For example, the original model for PCML in Mackey and Glass (1977) bears little resemblance to the more recent model of Colijn and Mackey (2005b) and indeed the original model of Mackey and Glass (1977) is inconsistent with the currently available clinical data. Likewise, the earlier model of Mackey (1978a) identified apoptosis within the stem cell compartment as the likely culprit in the generation of the oscillations of CN. This led, in turn, to laboratory and clinical investigations that did, indeed, identify significantly higher than normal levels of apoptotic cells in the bone marrow *but the apoptosis was occurring in the committed neutrophil precursors!* This model has been revisited a number of times Bélair and Mackey (1987); Bernard et al. (2003); Colijn and Mackey (2005b,a); Mackey and Rudnicki (1994); Mahaffy et al. (1998b); Pujo-Menjouet et al. (2005); Pujo-Menjouet and Mackey (2004); Santillan et al. (2000) as knowledge has improved, and conclusions drawn from subsequent models has led to an evolution of our understanding of this disease as well as the treatment of it using G-CSF.

The reader will, no doubt, also realize that each model has its positive and negative aspects. The level of detail of the model depends on the availability and quality of the data and also on the questions we want to address. The more detail, the more complicated the model will be. A mathematical analysis might then be hard to undertake and the conclusions may only be based on numerical experiments which many, including us, find less than satisfactory. On the other hand, a simple model may be easier to analyze and mathematical analysis can give more insights into the dynamical properties or the underlying system, but it may oversimplify and fail to capture some important features of the reality.

The issue of model complexity is intimately tied to the issue of the dimensionality of the parameter space, and this is tied directly to one of the quandaries that faces every modeler. The more complex the model, the more parameters that must be estimated. It is a virtual truism in mathematical biology that one is almost never able to obtain all of the parameters in a model from the same laboratory or clinical setting using the same procedures and techniques and subjects. So, as mathematical model construction is

something of an art in itself the same can be said for parameter estimation. Experience suggests that the hardest part of the modeling exercise is in obtaining decent parameter estimations.

2.6 Appendix

2.6.1 Method for converting a PDE model into a DDE model

As presented in Section 2.3.3, we consider the cell density $x(t, a)$ at time t and age a in a generic compartment. We assume that $x(t, a)$ satisfies the following time-age equation (advection, or reaction-convection, equation):

$$\frac{\partial x}{\partial t} + V(t) \frac{\partial x}{\partial a} = -\gamma(t)x \quad t > 0, a \in [0, \tau], \quad (2.A.1)$$

with boundary condition (B.C.):

$$x(t, 0) = H(t) \quad (2.A.2)$$

and initial condition (I.C.)

$$x(0, a) = \phi(a). \quad (2.A.3)$$

Next, we show that by partial integration of equation (2.A.1), we can reformulate this problem as a delay differential equation.

Integrating with respect to the age variable a , we obtain

$$\begin{aligned} & \int_0^\tau \frac{\partial x(t, a)}{\partial t} da + \int_0^\tau V(t) \frac{\partial x(t, a)}{\partial a} da = - \int_0^\tau \gamma(t)x(t, a) da \\ \implies & \frac{dX}{dt} + V(t) [x(t, \tau) - x(t, 0)] = -\gamma(t)X(t), \end{aligned}$$

where $X(t)$ is the total number of cells:

$$X(t) = \int_0^\tau x(t, a) da.$$

We can then substitute the boundary condition $x(t, 0) = H(t)$ to give

$$\frac{dX}{dt} = V(t)[H(t) - x(t, \tau)] - \gamma(t)X(t). \quad (2.A.4)$$

We next need to find an expression for $x(t, \tau)$. This can be done by directly solving Equation (2.A.1) using the method of characteristics. We define a new (dummy) independent variable s and let $x(s) = x(t(s), a(s))$. Thus, we obtain

$$\frac{dx}{ds} = \frac{\partial x}{\partial t} \frac{dt}{ds} + \frac{\partial x}{\partial a} \frac{da}{ds} = -\gamma(t)x.$$

This defines a set of three ODEs for $t > 0$ and $a \in [0, \tau]$ as follows:

$$\frac{dt}{ds} = 1 \quad \Longrightarrow \quad t(s) = t(0) + s \quad (2.A.5)$$

$$\frac{da}{ds} = V(t) \quad \Longrightarrow \quad a(s) = a(0) + \int_0^s V(w) dw \quad (2.A.6)$$

$$\frac{dx}{ds} = -\gamma(t)x \quad \Longrightarrow \quad x(s) = x(0) \exp\left(-\int_0^s \gamma(t(w), a(w)) dw\right). \quad (2.A.7)$$

Denote by \mathcal{C} the curve emanating from the point $(t, a) = (0, 0)$, and separating the (t, a) plane into two distinct regions \mathcal{R}_1 and \mathcal{R}_2 (cf. Figure 2.6). The curve \mathcal{C} is defined by

$$\mathcal{C} = \left\{ (t, a) \mid t(s) = s \text{ and } a(s) = \int_0^s V(w) dw \text{ for } s \in [0, s_T] \right\}, \quad (2.A.8)$$

where the value of s_T corresponds to the value of s required to reach age $a = \tau$. Thus, s_T must satisfy

$$\tau = \int_0^{s_T} V(w) dw. \quad (2.A.9)$$

The solution $x(t, a)$ takes a different form depending on whether it lies in region \mathcal{R}_1 or region \mathcal{R}_2 . Recall that the general solution is given by Equation (2.A.7)

$$x(s) = x(0) \exp\left(-\int_0^s \gamma(t(w), a(w)) dw\right).$$

Therefore, we need to find an expression for $x(0)$ and s as a function of a and t in order to obtain the expression for $x(t, a) := x(t(s), a(s))$. Recall also that we are interested in the value $x(t, \tau)$.

1. **If $(t(0), a(0)) \in \mathcal{R}_1$:** Then, it can be seen from Figure 2.6 that $t(0) = 0$. Hence, we have $t(s) = s$ and $a(s) = a(0) + \int_0^s V(w) dw$ with $0 < a(0) < \tau$. Using the initial

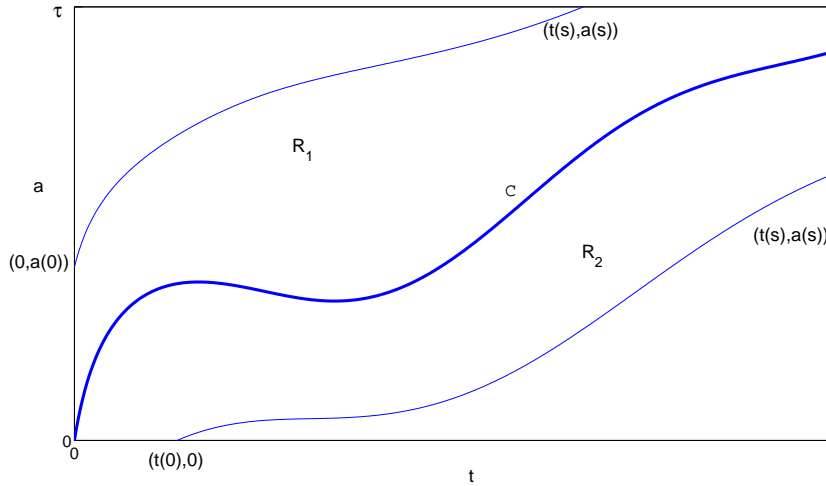


Fig. 2.6 Generic example of the curve \mathcal{C} that separates the $a - t$ plane into regions \mathcal{R}_1 and \mathcal{R}_2 .

condition (2.A.3), this implies that $x(0) = \phi \left(a - \int_0^t V(w) dw \right)$ and therefore, we obtain

$$x(t, \tau) = \phi \left(\tau - \int_0^t V(w) dw \right) \exp \left(- \int_0^t \gamma(w) dw \right).$$

2. **If $(t(0), a(0)) \in \mathcal{R}_2$:** Then, from Figure 2.6, one can see that $a(0) = 0$ and thus $a(s) = \int_0^s V(w) dw$ and $t(s) = t(0) + s$. Hence, using the boundary condition (2.A.2), we have $x(0) = H(t - s)$. Now, we need to find an expression for s . This is defined implicitly using the expression for $a(s)$. Indeed, we have that s represents the time required for age a to increase from 0 to $a(s)$. Moreover,

$$a(s) = \int_0^s V(t(w)) dw = \int_0^s V(t(0) + w) dw = \int_{t(0)}^{t(0)+s} V(\sigma) d\sigma.$$

Recall also that we are interested in $x(t, \tau)$. Thus, let us define by T_τ the time needed for the age variable to go from 0 to τ , i.e.:

$$\tau = \int_0^{T_\tau} V(w) dw. = \int_{t-T_\tau}^t V(w) dw. \quad (2.A.10)$$

Therefore, the expression for $x(t, \tau)$ reads as follows:

$$x(t, \tau) = H(t - T_\tau) \exp\left(-\int_0^{T_\tau} \gamma(w) dw\right),$$

where T_τ satisfies equation (2.A.10).

Therefore, from the method of characteristics the solution $x(t, \tau)$ is

$$x(t, \tau) = \begin{cases} \phi\left(\tau - \int_0^t V(w) dw\right) \exp\left(-\int_0^t \gamma(w) dw\right) & \text{if } (t, a) \in \mathcal{R}_1 \\ H(t - T_\tau) \exp\left(-\int_0^{T_\tau} \gamma(w) dw\right) & \text{if } (t, a) \in \mathcal{R}_2, \end{cases}$$

with T_τ satisfying $\tau = \int_{t-T_\tau}^t V(w) dw$. Since we are interested in long term behaviour, we consider only the case where $(t, a) \in \mathcal{R}_2$ (from Figure 2.6, one can see that region \mathcal{R}_2 includes the t -axis whereas \mathcal{R}_1 is bounded by $a = \tau$.) We obtain

$$x(t, \tau) = H(t - T_\tau) \exp\left(-\int_0^{T_\tau} \gamma(w) dw\right).$$

Substituting in equation (2.A.4), this yields the general solution for $X(t)$

$$\frac{dX}{dt} = V(t) \left[H(t) - H(t - T_\tau) \exp\left(-\int_0^{T_\tau} \gamma(w) dw\right) \right] - \gamma(t)X(t). \quad (2.A.11)$$

2.6.2 The Linear chain Trick

In this section, we present the derivation of the ODE system obtained using the linear chain trick (see MacDonald (1978b) for more details and examples). Consider the following DDE system with a distributed delay:

$$\frac{dx_1}{dt} = f\left(x_1(t), \int_{-\infty}^t x_1(\tau)G(t-\tau) d\tau\right), \quad (2.A.12)$$

with the special choice of the density of gamma distribution (2.7) for the memory function. Note that this trick works only for some particular memory functions. Using definitions (2.9) and (2.10) and properties (2.8), we show that we can express the DDE problem (2.A.12) as the $(p+2)$ -dimensional ODE system (2.11). First, substituting the

definition of x_{p+2} into Equation (2.A.12) directly leads to the first differential equation

$$\frac{dx_1}{dt} = f(x_1, x_{p+2}).$$

Next, we derive the expression for $\frac{dx_{j+1}}{dt}$, $j = 1, \dots, p+1$. From the Leibniz integral rule, we have that

$$\begin{aligned} \frac{dx_{j+1}}{dt} &= \frac{d}{dt} \left(\int_{-\infty}^t x_1(\tau) G_a^{j-1}(t-\tau) d\tau \right) \\ &= x_1(t) G_a^{j-1}(0) + \lim_{u \rightarrow \infty} G_a^{j-1}(u) + \int_{-\infty}^t x_1(\tau) \frac{d}{dt} G_a^{j-1}(t-\tau) d\tau. \end{aligned} \quad (2.A.13)$$

From the three properties of $G_a^{j-1}(u)$ presented above, the first and second terms on the right hand side vanish, except for the case $j = 1$ where the first term is equal to ax_1 .

Also, one can easily show that the derivatives of $G_a^{j-1}(t-\tau)$ are given by

$$\begin{aligned} \frac{d}{dt} G_a^0(t-\tau) &= -a G_a^0(t-\tau), \\ \frac{d}{dt} G_a^{j-1}(t-\tau) &= a [G_a^{j-2}(t-\tau) - G_a^{j-1}(t-\tau)] \quad (j = 2, 3, \dots, p+2). \end{aligned}$$

Hence, substituting in Equations (2.A.13) and using definition (2.9), we obtain the required set of differential equations for x_j ($j = 2, 3, \dots, p+2$):

$$\frac{dx_2}{dt} = ax_1 - a \int_{-\infty}^0 x_1(\tau) G_a^0(t-\tau) d\tau = ax_1 - ax_2, \quad (2.A.14)$$

$$\frac{dx_{j+1}}{dt} = a \left[\int_{-\infty}^t x_1(\tau) (G_a^{j-2}(t-\tau) - G_a^{j-1}(t-\tau)) d\tau \right] = ax_j - ax_{j+1}. \quad (2.A.15)$$

Chapter 3

G-CSF treatment of canine cyclical neutropenia: A comprehensive mathematical model

In the last chapter, we reviewed different modeling approaches in hematology, mainly based on the study of periodic hematological disorders. In particular, modeling of cyclical neutropenia (CN) and analysis of its dynamical properties has provided insights on the origin of the disease and potentially helped in the design of new G-CSF treatment regimens. Indeed, Foley et al. (2006) proposed alternative G-CSF treatment strategies for cyclical neutropenia using a combination of analytical and numerical tools. However, their model did not account for the pharmacokinetics of G-CSF and did not consider the platelets and erythrocytes, in which oscillations are also observed in CN. In this chapter, we resolve these issues by proposing a comprehensive mathematical model of the mammalian hematopoietic system that couples the pharmacokinetics of G-CSF to the hematopoietic stem cell, neutrophil, platelet, and erythrocyte dynamics. We then study the effects of varying the treatment initiation time, and whether injections are given daily, every other day, or every three days.

A version of this chapter has been published: C. Colijn, C. Foley and M. C. Mackey. G-CSF treatment of canine cyclical neutropenia: A comprehensive mathematical model, *Experimental Hematology*, 35, 898-907, 2007.

3.1 Introduction

All blood cells are derived from the hematopoietic stem cells (HSC), which are undifferentiated cells having a high proliferative potential. These multipotent stem cells can proliferate and mature to form all types of blood cells (platelets, leucocytes and erythrocytes). Production in these cell lines is regulated by a variety of cytokines, including erythropoietin (EPO), which mediates the regulation of erythrocyte production, thrombopoietin (TPO), which regulates production of platelets (but may also affect other cell lines), as well as granulocyte colony-stimulating factor (G-CSF), which regulates leukocyte numbers.

In Colijn and Mackey (2005a,b) a comprehensive mathematical model for the regulation of hematopoiesis was presented. This work was motivated by the existence of several hematological diseases that display a highly dynamic nature characterized by oscillations in one or more of the circulating cell lines (Haurie et al. (1998)). Examples of these are cyclical neutropenia, periodic chronic myelogenous leukemia, cyclical thrombocytopenia and periodic hemolytic anemia.

In this chapter, we concentrate on cyclical neutropenia, a rare hematological disorder characterized by oscillations in the circulating neutrophil count. These levels fall from normal to barely detectable levels with a typical period of 19 to 21 days in humans (Haurie et al. (1998); Guerry et al. (1973); Dale and Hammond (1988)), even though periods up to 40 days have been observed (Haurie et al. (1998)). These oscillations in the neutrophil count are generally accompanied by oscillations with similar period in the platelets, lymphocytes and reticulocytes (Haurie et al. (1998, 2000a)). Cyclical neutropenia also occurs in grey collies with periods on the order of 11 to 16 days (Haurie et al. (1998, 1999b, 2000a)). This animal model has provided extensive experimental data that has enriched our understanding of cyclical neutropenia.

Though the gene modified responsible for canine cyclical neutropenia has been identified (Horwitz et al. (2004)), the dynamic origin of the cycling is only partially understood. Because of its interesting dynamical nature, many mathematical models have been formulated to attempt to answer this question. While many have modeled cyclical neutropenia as arising only from destabilization of neutrophil dynamics (King-Smith and Morley (1970); Morley et al. (1969)), the work of Bernard et al. (2003) and Colijn and Mackey (2005a) suggest that the origin of cyclical neutropenia lies in a destabilization of

the combined HSC and neutrophil control system. The hypothesis that oscillations originate in the stem cells is supported by the observation that in cyclical neutropenia oscillations are also present in platelets and reticulocytes.

Cyclical neutropenia in humans is often treated using granulocyte colony stimulating factor (G-CSF) (Hammond et al. (1989)), which is known to interfere with apoptosis (Koury (1992); Park (1996); Migliaccio et al. (1990); Williams and Smith (1993)).

Treatment protocols typically call for daily subcutaneous injection of G-CSF at 3 to 5 μg per kg of body weight (Ozer et al. (1997); Dale et al. (2003)). This represents a current cost of over US\$45,000 per year for a 70 kg adult. Clearly it would be of enormous economic benefit if the same clinical effects could be achieved with less G-CSF. A few alternative treatment strategies in humans have been reported in which various administration schemes have been used (Jayabose and Sandoval (1994); Dicato et al. (1992); Danielson and Harmenberg (1992); Dale et al. (2003)).

In Bernard et al. (2003), a two-compartment model accounting for a destabilization of the HSC compartment was used to mimic the dynamical behavior of the hematopoietic system under G-CSF treatment. In Foley et al. (2006) the authors showed that, depending on the starting date of the G-CSF treatment, the neutrophil count could either be stabilized or show large amplitude oscillations (both behaviors have been observed experimentally (Hammond et al. (1989))). Their model suggested that other G-CSF treatment schemes (such as administering G-CSF every other day) could be effective while using less G-CSF. However, this model included neither erythrocyte nor platelet dynamics even though clinical data indicates oscillations in those cell lines in cyclical neutropenia patients. Thus it is not known if the results would be consistent with observed platelet and reticulocyte data. Second, the simulations did not take into account the pharmacokinetics of G-CSF.

In this chapter, we present a new model for assessing the effects of G-CSF treatment in cyclical neutropenia. To do this, we augment the comprehensive model of the hematopoietic system from Colijn and Mackey (2005a) by coupling it with a two-compartment pharmacokinetic model that accounts for G-CSF kinetics. The details of the mathematical model are presented in the Appendix.

3.2 Data and Methods

3.2.1 Data

We used data on seven grey collies generously supplied by Dr. David C. Dale (University of Washington School of Medicine, Seattle) and previously analyzed in Haurie et al. (1999b). All of these dogs showed statistically significant cycling in neutrophils and/or platelets, according to the Lomb periodogram analysis carried out in Haurie et al. (1999b). The Lomb periodogram is equivalent to power spectrum analysis but is tailored for unevenly sampled data sets. It is used to detect periodicity in the blood counts before and during treatment with G-CSF. Data for neutrophils, erythrocytes and platelets were available both for untreated dogs as well as dogs receiving daily G-CSF.

3.2.2 Model and Data Fitting

We have developed a mathematical model that couples the pharmacokinetics of G-CSF to the hematopoietic stem cell, neutrophil, platelet and erythrocyte dynamics. The model is based on the work of Colijn and Mackey (2005a) and is described in the Appendix. Briefly, it consists of 4 delay differential equations each describing the time evolution of one of the cell types, coupled to two equations representing the changing levels of G-CSF in the subcutaneous tissue and in the circulation. The G-CSF compartment adds 10 parameters, which are estimated from the literature (see Table 3.1 in the Appendix). In Colijn and Mackey (2005a), the hematological portion of the present model was fitted to observed data for cyclical neutropenic dogs and human patients, both untreated and receiving G-CSF treatment. To do this, a simulated annealing optimization method was used to minimize the least squares difference between the simulation and the data (see Section 3.5.3 for more details on simulated annealing). Both the platelet and neutrophil counts were matched for dogs with untreated cyclical neutropenia, and (separately) for dogs undergoing daily treatment with G-CSF injections.

The results were that three of the model's parameters were identified as the most crucial in simulating the effects of cyclical neutropenia and its treatment with G-CSF: the amplification in the proliferating neutrophil precursors, the rate of apoptosis in the proliferating HSC's, and the maximal rate of differentiation from the HSC's into the neutrophil line. Interestingly, it was consistently necessary to change all of these to

account for the features of the data.

Here, we used the fits for 7 dogs *without* G-CSF treatment from Colijn and Mackey (2005a). For three of these, we then used the simulated annealing procedure to minimize the least squares difference between the simulation and the treated data, changing *only* the three most critical parameters. We then estimated, without fitting, the treated parameters for the remaining 4 dogs. At this point, the parameter sets successfully match the model simulations to data, without the new G-CSF compartment (i.e. the model is that of Colijn and Mackey (2005a)).

We now add the pharmacokinetic G-CSF compartment, to obtain our full model. The quality of the fits is preserved; in other words, the least squares difference between the model and simulations is as good, or better, with the G-CSF compartment than without, though the parameters were estimated for the model without it. (See Figures 3.1 and 3.2 and the discussion below).

At this point, having determined both the untreated and treated parameter values we are in a position to use simulation to explore the effects of different treatment strategies. We experiment with simulating treatment every day, every second day, and every three days, for each of the dogs. We also examine the effect of changing the time in the cycle when treatment is first initiated.

3.3 Results

The parameter sets for the first three dogs are given in the first three columns of Table 3.2 in the Appendix. In each case, we found that the neutrophil amplification increases substantially under G-CSF treatment, as does the rate of stem cell apoptosis, and the differentiation into the neutrophil line. We therefore predict similar changes for the remaining dogs (see the four last columns in Table 3.2 of the Appendix). There is some redundancy in the model, in that increasing the neutrophil amplification and the differentiation into the neutrophil line from the stem cells have similar effects. This is not unexpected, since the primary effect of both changes is to raise neutrophil levels.

Figure 3.1 shows the fit of the untreated and treated data for Dogs 100, 118 and 127 (for which we used the simulated annealing method for fitting the treated values of the parameters). Note that the simulations match the data reasonably well for the neutrophils as well as for the erythrocytes and platelets (not shown). This confirms that

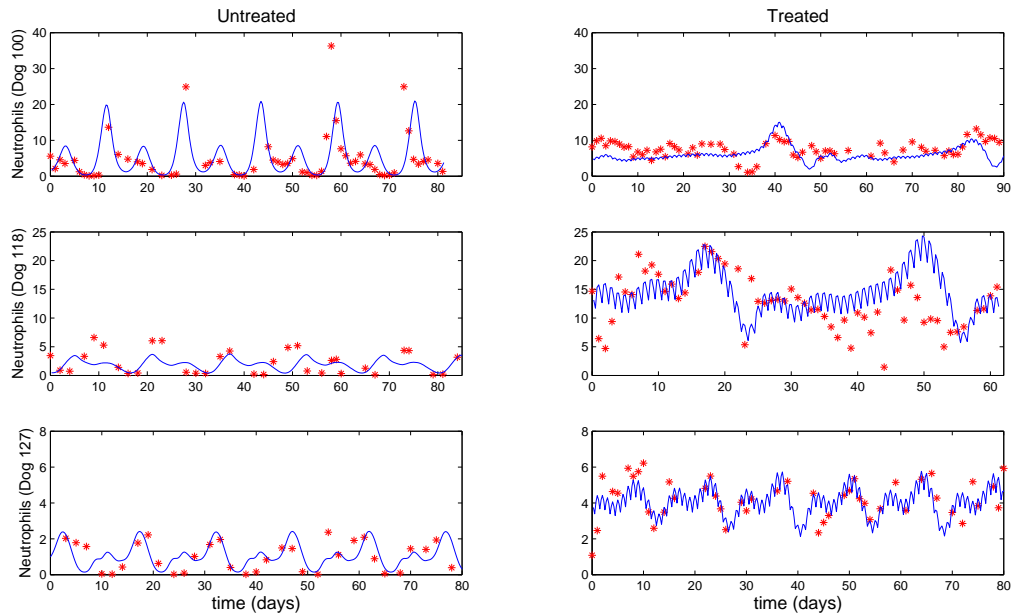


Fig. 3.1 Serial neutrophil data and simulations for Dogs 100, 118 and 127. (Data and simulations for platelets and erythrocytes are not shown). The left panel shows untreated data (points) and simulations (solid line). The right panel shows data and simulations for dogs under daily G-CSF treatment. Note that the model accounts for the different scalings in neutrophil counts. The simulations were obtained using parameters resulting from the simulated annealing method. Neutrophil units are 10^8 cells-kg $^{-1}$.

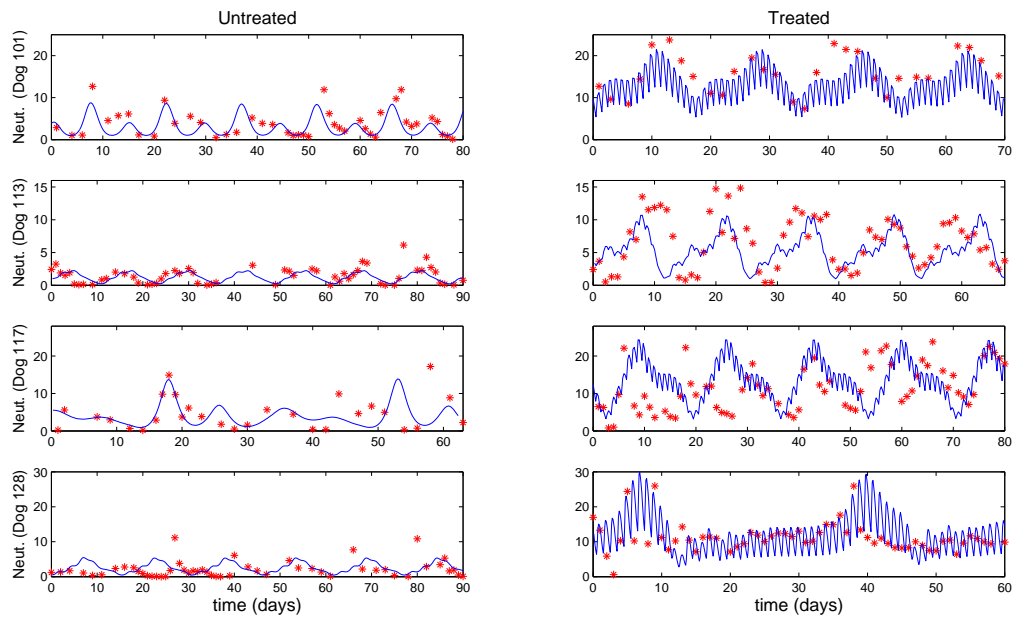


Fig. 3.2 Serial neutrophil data and simulation results for Dogs 101, 113, 117 and 128. The left panel shows data from untreated dogs (points) and simulations (solid line). The right panel shows data and simulations for dogs given daily G-CSF treatment. Note that the model accounts for the different scalings in neutrophil counts. The simulations were carried out using parameters estimated from the data from Dogs 100, 118 and 127. Neutrophil units are 10^8 cells- kg^{-1} .

the new model, with the G-CSF coupled to the cell population dynamics, is capable of reproducing the data. The least squares differences between the simulations and the data were not significantly less than the values reported in Colijn and Mackey (2005a). These simulations and data are for daily treatment.

Figure 3.2 shows the data and simulations for the other four dogs (Dogs 101, 113, 117 and 128), again with daily treatment. Recall that these were the estimated, not fitted, values for the treated parameters and note the quality of the fits. Thus, we are able to match observed data without automated parameter fitting based simply on an examination of the treated data and the parameter changes for Dogs 100, 118 and 127.

For each dog, we performed simulations comparing daily treatment, treatment every other day, and every three days. We find that particularly for Dogs 100, 101, 118 and 127, changing the period of the treatment can significantly affect the nature of the oscillations. Figure 3.3 shows the results of treating Dog 118 every other day, rather than every day. We have also explored the effects of changing the time at which the treatment is initiated. In most cases, this did not significantly change the long-term behavior. However, for Dog 127 the amplitude of the oscillations was significantly reduced when the treatment was initiated in the latter half of the cycle. More specifically, measured from day 1 (defined here to be the day when the neutrophil level reaches its minimum), we find that smaller oscillations occur if treatment is initiated on day 8 or afterwards, or on days 2 or 5 (see Figure 3.4). When treatment was initiated on other days, larger oscillations in the model resulted. We were aware from our previous study (Foley et al. (2006)) of similar models that there is the possibility that two or more qualitatively different states can be locally stable, and we have also found evidence for this in the present model. Namely, changing the treatment onset time from day 1 to day 8 for Dog 127 caused the simulation to stabilize to two very different types of behavior.

It should also be noted that increasing the G-CSF dosage in the model sometimes helped to stabilize oscillations (Dog 127), but in several cases (Dogs 100, 128 and 101) a dosage increase from 5 $\mu\text{g}/\text{kg}$ to a dosage in the range 15-25 $\mu\text{g}/\text{kg}$ caused some simulations to fail. In those simulations, the differentiation rate out of the stem cells was so high, and the apoptosis rate in the stem cells was so high, that the stem cell population was no longer able to maintain itself. For the other dogs, there was always a dosage that was sufficiently high to terminate the simulation, but it was sometimes a factor of 10 higher than the actual dosage given.

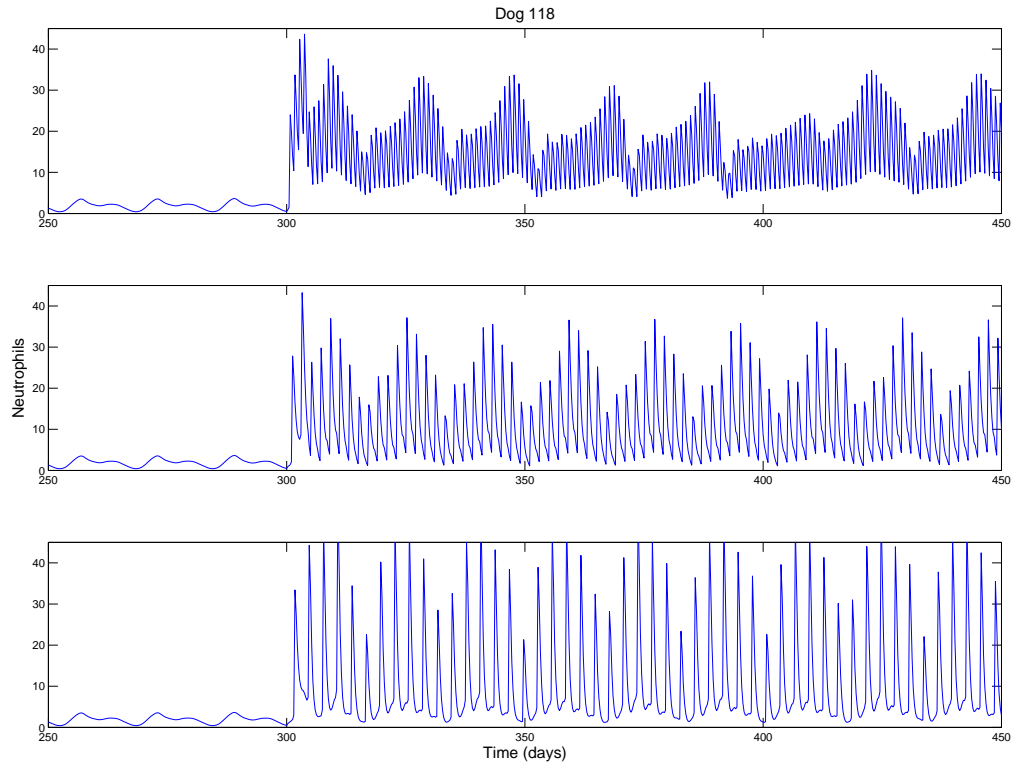


Fig. 3.3 Effects of varying G-CSF treatment frequency. Simulations for Dog 118 when we administer G-CSF daily (top panel), every other day (middle panel) and every third day (bottom panel). Treatment always starts on day 300. Notice the change in the amplitude of the oscillations depending on the treatment regime. Neutrophil units are in 10^8 cells-kg $^{-1}$.

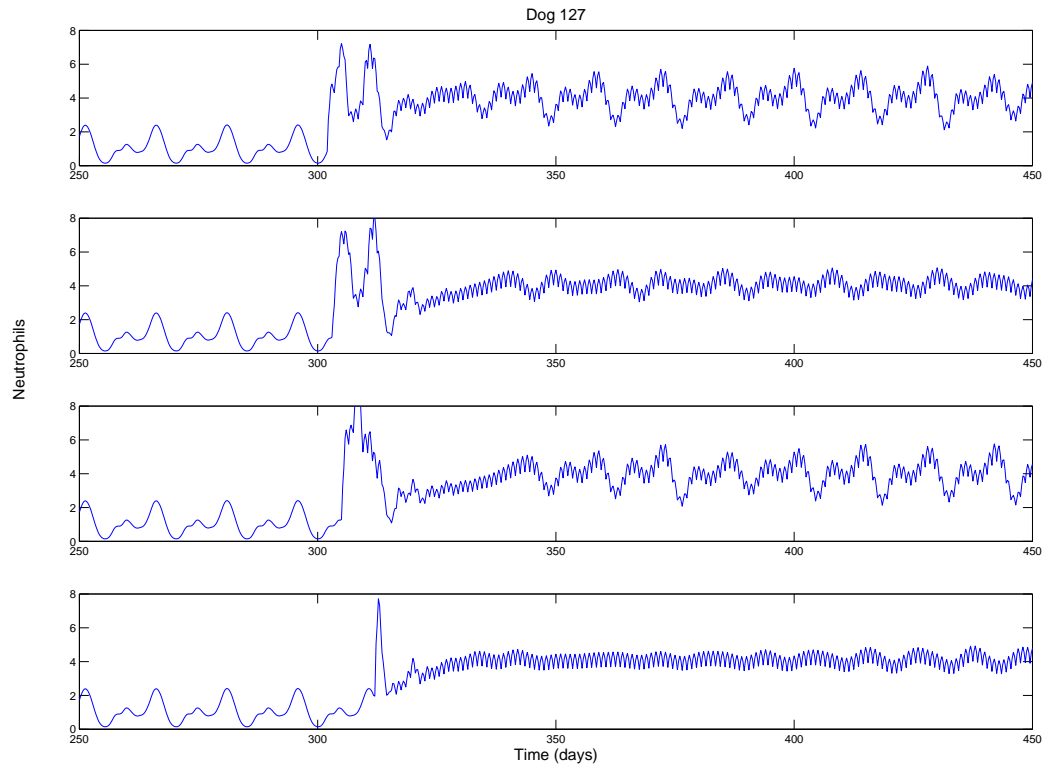


Fig. 3.4 Effects of changing initiation time of G-CSF treatment. Simulations for Dog 127 when we change the time at which daily G-CSF treatment is initiated. If day 1 represents the day at which the nadir occurs, we see starting treatment day (STD) is 1 (top), STD = 2 (second panel), STD = 4 (third panel) and STD = 9 (bottom). We can either have large amplitude oscillations (panels 1 and 3) or small oscillations (panels 2 and 4). Neutrophils are in units of $10^8 \text{cells}\cdot\text{kg}^{-1}$.

3.4 Discussion

We have developed a model of the hematopoietic system (including the bone marrow stem cells, circulating neutrophils, platelets and erythrocytes) that includes a pharmacokinetic model of G-CSF dynamics in tissue and in circulation. The model is able to account for the features of untreated, and G-CSF-treated, data for dogs with cyclical neutropenia. This is accomplished, starting with parameter fitting done in Colijn and Mackey (2005a), by fitting parameters for 3 dogs and thereby estimating, not fitting, parameters for 4 other dogs.

One of the most intriguing observations resulting from the parameter fitting in this study, as in Colijn and Mackey (2005a), is that to fit observed data for cyclical neutropenic dogs and human patients during G-CSF treatment it was necessary to assume that there was an increase in the rate of apoptosis in the stem cell compartment during G-CSF treatment, at the same time as the more expected increase in neutrophil amplification (consistent with an inhibition of apoptosis in the proliferating neutrophil precursors). The study we report here about treatment schedules indicates that changing the period of the treatment from daily to every other day, and then to every third day, almost always significantly alters the nature of the oscillations. Since G-CSF is costly and may have undesirable side effects, it may be worth exploring this option further in humans. Furthermore, we found in one case (Dog 127) that changing the time of onset of treatment to the latter half of the cycle (as measured by setting day 1 to be the day when the neutrophil level is minimal) results in much smaller amplitude oscillations in the treated simulation.

In the model, both of these interventions (changing the treatment period, and changing the onset time) had more significant effects on the oscillations than did changing the G-CSF dosage. Indeed, increasing the dosage was not seen to be a viable option in our simulations, as it frequently led to the termination of the simulation rather than to the stabilization of oscillations.

The observed data are highly variable from one dog to another, but the simulations can be individualized to account for this. This presents the possibility of using “real time” data for a given dog to individualize model simulations and make predictions about the effects of different treatment schedules.

Earlier modeling work also suggested that significantly different behavior would result

from different G-CSF treatment schedules. Our model substantiates this, and quantifies the effects using realistic G-CSF dynamics and yielding simulations that are directly comparable to observed data. Our central result is that in the model, changing the time of treatment initiation and/or the period of treatment may result in equally good, or better, long-term outcomes and may require less G-CSF. These changes would be practical to implement and, if less G-CSF were required, would reduce the risk of side effects as well as the cost of treatment.

3.5 Appendix: The model

3.5.1 Model structure

The model we have developed includes the hematopoietic stem cells, the neutrophils, platelets and erythrocytes, as well as tissue G-CSF levels and circulating G-CSF in the blood. The model has four distinct cellular compartments and two compartments representing G-CSF (c.f. Figure 3.5).

The stem cells are pluripotential and self-renewing, and can differentiate into the leukocyte, erythrocyte or platelet lines. Alternatively, the stem cells may re-enter the proliferative phase of the stem cell compartment, during which they undergo a random loss via apoptosis at rate γ_S . The stem cell compartment model is based on the original work of Mackey (1978b). The neutrophil, erythrocyte and platelet compartments are modeled after earlier efforts (Bernard et al. (2003); Santillan et al. (2000); Bélair et al. (1995); Mahaffy et al. (1998a)). G-CSF, meanwhile, is injected into the tissue compartment and enters the circulation from there. It is cleared from the circulation by two processes: a random loss, and a linear neutrophil-mediated clearance representing the fact that neutrophils take up circulating G-CSF (Stute et al. (1992); Takatani et al. (1996)); at very high G-CSF levels the neutrophil-mediated clearance is saturable, but at the concentrations relevant here, a linear approximation is accurate.

Our notation is as follows. The hematopoietic stem cells (HSC's) are denoted by Q (in units of 10^6 cells/kg, see Figure 3.5). The circulating neutrophils, erythrocytes and platelets are denoted N (units 10^8 cells/kg), R (units 10^{11} cells/kg) and P (units 10^{10} cells/kg), respectively. Each of the differentiation rates from the stem cell compartment into the cell lines depend on the number of circulating cells of the relevant type, so there is a feedback between the circulating cell numbers and the rates of differentiation. These are negative feedback functions, so when the number of circulating mature cells of a given line decreases, the corresponding differentiation rate κ increases to compensate. The rates of differentiation (units of days^{-1}) from the HSC's into the three circulating cell lines are denoted by $\kappa_N(N)$, $\kappa_R(R)$ and $\kappa_P(P)$, respectively. Tissue levels of G-CSF are denoted X (units $\mu\text{g}/\text{kg}$), and circulating G-CSF concentration is G (units $\mu\text{g}/\text{mL}$).

The effects of G-CSF on the system (injected with a temporal schedule $I(t)$) are ultimately represented by changes in the parameters A_N (the effective amplification in the neutrophil line between the HSC's and the circulating neutrophils), γ_S , (the rate of

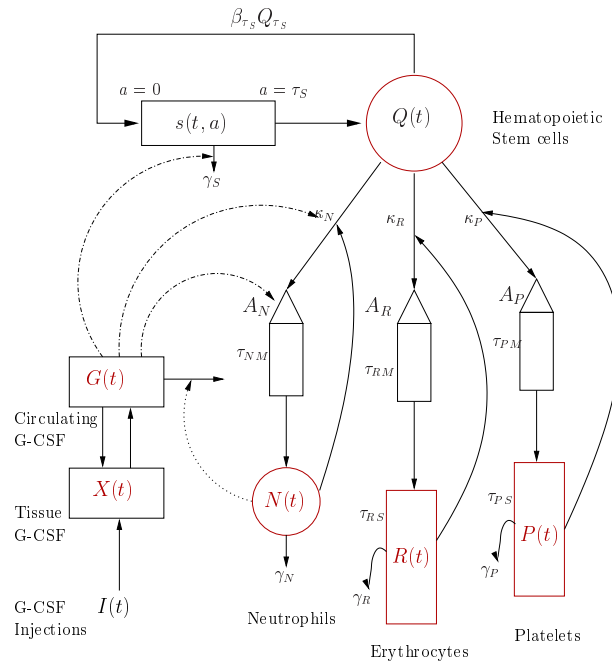


Fig. 3.5 Schematic diagram of the model. Solid lines reflect either the movement of cells or the influence of a cell population on a process, while dashed lines represent the coupling between the G-CSF dynamics and the hematological model. The notation $Q_{\tau_S} \equiv Q(t - \tau_S)$ indicates that there is a delay involved.

apoptosis in the HSC compartment), and θ_1 (through which G-CSF increases the level of differentiation from the stem cells into the neutrophil line). Only the circulating, and not the tissue, G-CSF has these effects. These particular effects are isolated because in Colijn and Mackey (2005a), these were the primary parameter changes that were found necessary for model simulations to match the observed laboratory and clinical data for dogs and humans with cyclical neutropenia undergoing G-CSF treatment. With this notation, and the convention that $X_\tau \equiv X(t - \tau)$, the model equations are

given by

$$\begin{aligned}
 \frac{dQ}{dt} &= -\beta(Q)Q - (\kappa_N + \kappa_R + \kappa_P)Q + 2e^{-\gamma_S\tau_S}\beta(Q_{\tau_S})Q_{\tau_S} \\
 \frac{dN}{dt} &= -\gamma_N N + A_N \kappa_N(N_{\tau_N})Q_{\tau_N} \\
 \frac{dR}{dt} &= -\gamma_R R + A_R \{ \kappa_R(R_{\tau_{RM}})Q_{\tau_{RM}} - e^{-\gamma_R\tau_{RS}} \kappa_R(R_{\tau_{RM}+\tau_{RS}})Q_{\tau_{RM}+\tau_{RS}} \} \\
 \frac{dP}{dt} &= -\gamma_P P + A_P \{ \kappa_P(P_{\tau_{PM}})Q_{\tau_{PM}} - e^{-\gamma_P\tau_{PS}} \kappa_P(P_{\tau_{PM}+\tau_{PS}})Q_{\tau_{PM}+\tau_{PS}} \} \\
 \frac{dX}{dt} &= I(t) + k_T V_B G - k_B X \\
 \frac{dG}{dt} &= \frac{k_B}{V_B} X - k_T G - (\alpha N + \gamma_G)G.
 \end{aligned} \tag{3.A.1}$$

The (negative) feedback functions are:

$$\begin{aligned}
 \beta(Q) &= k_0 \frac{\theta_2^s}{\theta_2^s + Q^s} \\
 \kappa_N(N) &= f_0 \frac{\theta_1^n}{\theta_1^n + N^n} \\
 \kappa_P(P) &= \frac{\bar{\kappa}_p}{1 + K_p P^r} \\
 \kappa_R(R) &= \frac{\bar{\kappa}_r}{1 + K_r R^{m_e}}.
 \end{aligned} \tag{3.A.2}$$

We must also specify an input function $I(t)$ that represents the subcutaneous G-CSF injections. We assume that this input is brief in duration, and that the total amount of G-CSF added corresponds to the desired dosage, namely

$$\int_{\text{before}}^{\text{after}} I(t) dt = \text{dosage}. \tag{3.A.3}$$

Note that if σ is small, a Gaussian-like input approximates a Dirac δ -function, and we can write

$$\int_{\text{before}}^{\text{after}} a e^{-t^2/\sigma^2} dt \approx \int_{-\infty}^{\infty} a e^{-t^2/\sigma^2} dt = a\sigma\pi.$$

Therefore to simulate periodic injections, we let

$$I(t) = H(t - d)ae^{-((t \bmod T) - T/2)^2/\sigma^2}, \quad (3.A.4)$$

where $H(t)$ denotes the Heaviside step function

$$H(t) = \begin{cases} 0 & t \leq 0 \\ 1 & t > 0. \end{cases}$$

The day on which treatment is initiated is denoted by d , and the Heaviside function simply turns the injections on. The term “ $t \bmod T$ ” ensures periodicity, and we require that $T \gg \sigma$ so that the approximation to the integral remains valid. Finally, we ensure that (3.A.3) holds by choosing the parameter a such that $a\sigma\pi = \text{dosage}$.

It remains only to describe how the G-CSF acts on the hematological portion of the model. As mentioned above, previous work Colijn and Mackey (2005a) indicated that G-CSF will raise A_N , γ_S and θ_1 . Thus, given that we begin with values for these parameters that we know match the treated data in the model without G-CSF kinetics, we want to have G-CSF injections cause fluctuations in those three parameters about their treated values.

We therefore write those parameters as functions of the circulating G-CSF (where in Colijn and Mackey (2005a,b) they were constant):

$$\begin{aligned} A_N &= A_N^{\text{untr}}(1 - H(t - d)) + H(t - d)(m_A(G - \bar{G}) + A_N^{\text{tr}}) \\ \gamma_S &= \gamma_S^{\text{untr}}(1 - H(t - d)) + H(t - d)(m_g(G - \bar{G}) + \gamma_S^{\text{tr}}) \\ \theta_1 &= \theta_1^{\text{untr}}(1 - H(t - d)) + H(t - d)(m_t(G - \bar{G}) + \theta_1^{\text{tr}}) \end{aligned} \quad (3.A.5)$$

The superscripts “tr” and “untr” respectively indicate values corresponding to treated and untreated data. The parameters m_A , m_g and m_t are slopes that specify how much A_N , γ_S and θ_1 change in response to a given change in G-CSF concentration, G . \bar{G} is the average G-CSF concentration for each data set. These were computed using the G-CSF model alone (without the cell types coupled to it), and using the average neutrophil levels in each data set.

The slopes were computed as follows:

$$\begin{aligned} m_A &= m(A_N^{\text{tr}} - A_N^{\text{untr}})/\bar{G} \\ m_g &= m(\gamma_S^{\text{tr}} - \gamma_S^{\text{untr}})/\bar{G} \\ m_t &= m(\theta_1^{\text{tr}} - \theta_1^{\text{untr}})/\bar{G}. \end{aligned} \tag{3.A.6}$$

In (3.A.5), m_A , m_g and m_t set the amount of fluctuation in A_N , γ_S and θ_1 . When the parameter m in (3.A.6) is 1, then when G falls to zero, A_N , γ_S and θ_1 drop all the way down to their average untreated levels. If $m < 1$, then they do not fall all the way to their untreated average levels when $G = 0$ but rather fluctuate about their treated levels with a lower amplitude.¹

3.5.2 Parameter estimation

There are a number of parameters to be estimated, and many of these have been considered in previous modeling studies (Colijn and Mackey (2005a,b); Bernard et al. (2003)). Our baseline parameters for the HSC compartment, and the neutrophil, platelet and erythrocyte compartments are the same as in Colijn and Mackey (2005a). Colijn and Mackey (2005a,b) can be consulted for an extensive discussion of how these parameters were determined.

Some of the pharmacokinetic parameters for the G-CSF portion of the model can be taken from published data on G-CSF kinetics. We require estimates of the transfer rates k_T and k_B , the volume V_B , and the parameters α and γ_G which give the clearance rate of G-CSF from the bloodstream.

Hayashi et al. (2001) and Kuwabara et al. (1994) determined $k_T = 0.06 \text{ hr}^{-1}$ and $V_B = 76 \text{ mL/kg}$, while Vainstein et al. (2005) give $\gamma = 0.06 \text{ hr}^{-1}$. We use $k_B = 0.25 \text{ hr}^{-1}$, which is larger than the value 0.1 given in Hayashi et al. (2001) but which we needed to reach the observed levels of G-CSF using the approximate $I(t)$ function input. It only remains to estimate α , which relates the number of circulating neutrophils to the clearance of G-CSF. Given a known value for N on the day of treatment, and the G-CSF concentration as a function of time, the half-life can be related to the clearance rate by $t_{1/2} = \ln 2/(\alpha N + \gamma)$. With the half-lives and circulating neutrophil counts in Stute et al.

¹This can be seen by re-arranging (3.A.5) and (3.A.6), setting $t > d$ to get $A_N - A_N^{\text{tr}} = m \frac{A_N^{\text{tr}} - A_N^{\text{untr}}}{\bar{G}} (G - \bar{G})$.

(1992) and Kearns et al. (1993a), this gives a range of $\alpha = 0.015 - 0.03$ kg/hr. To check the validity of this determination, and to ensure that the model is giving a reasonable description of G-CSF dynamics, we digitized a time series of G-CSF concentration from Stute et al. (1992) and fit the model simulations to these data. The fit is shown in Figure 3.6. The value of α from the fit is 0.03, consistent with the above estimate.

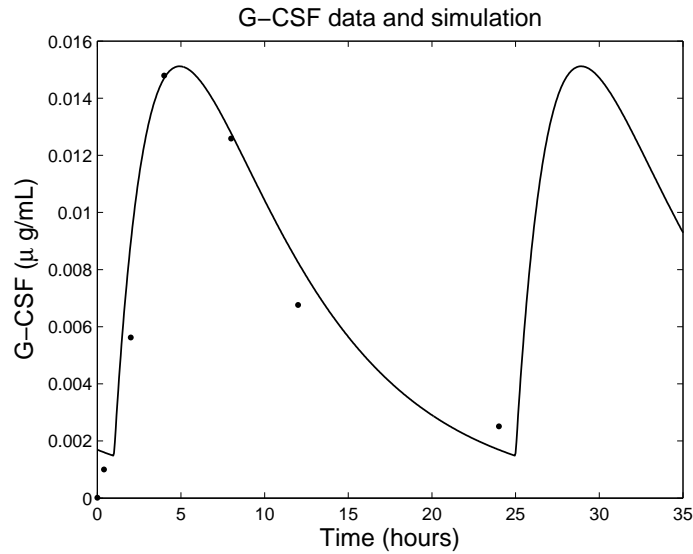


Fig. 3.6 Predicted serum G-CSF time series compared to digitized data from Stute et al. (1992).

Parameter Name	Value Used	Unit	Sources
Stem Cell Compartment			
Q_*	1.1	$\times 10^6$ cells/kg	Bernard et al. (2003)
γ_S	0.07	days ⁻¹	Bernard et al. (2003)
τ_S	2.8	days	Bernard et al. (2003); Abkowitz et al. (1988)
k_0	8.0	days ⁻¹	Bernard et al. (2003)
θ_2	0.5	$\times 10^6$	Bernard et al. (2003)
s	4	(none)	Bernard et al. (2003)
Neutrophil Compartment			
N_*	6.9	$\times 10^9$ cells/kg	Abkowitz et al. (1988); Beutler et al. (1995)
γ_N	2.4	days ⁻¹	Bernard et al. (2003); Deubelbeiss et al. (1975); Haurie et al. (2000b)
τ_{MN}	3.5	days	Bernard et al. (2003)
A_N	752	100's	Colijn and Mackey (2005a)
f_0	0.40	days ⁻¹	(calculated)
θ_1	0.36	$\times 10^8$ cells/kg	Bernard et al. (2003)
n	1	(none)	Bernard et al. (2003)
Erythrocyte Compartment			
R_*	3.5	$\times 10^{11}$ cells/kg	Mahaffy et al. (1998b)
γ_R	0.001	days ⁻¹	Mahaffy et al. (1998b)
τ_{RM}	6	days	Mahaffy et al. (1998b)
τ_{sum}	120	days	Mahaffy et al. (1998b)
τ_{ret}	2.8	days	Beutler et al. (1995)
A_R	5.63	10,000's	Beutler et al. (1995); Novak and Necas (1994)
$\bar{\kappa}_r$	0.5	days ⁻¹	(calculated)
K_r	0.0382	$(\times 10^{11} \text{ cells/kg})^{-1}$	Mahaffy et al. (1998b)
m_e	6.96	(none)	Mahaffy et al. (1998b)
Platelet Compartment			
P_*	2.14	$\times 10^{10}$ cells/kg	Santillan et al. (2000)
γ_P	0.15	days ⁻¹	Santillan et al. (2000)
τ_{PM}	7	days	Santillan et al. (2000)
τ_{PS}	9.5	days	Santillan et al. (2000)
A_P	28.2	1000's	Beutler et al. (1995)
$\bar{\kappa}_p$	1.17	days ⁻¹	(calculated)
K_p	11.66	$(\times 10^{10} \text{ cells/kg})^{-1}$	Santillan et al. (2000)
r	1.29	(none)	Santillan et al. (2000)
G-CSF compartment			
X_*	0.1	$\mu\text{g}/\text{kg}$	(calculated)
G_*	0	$\mu\text{g}/\text{ml}$	(calculated)
k_T	0.07	hours ⁻¹	Hayashi et al. (2001)
k_B	0.25	hours ⁻¹	fit
V_B	76	mL/kg	Hayashi et al. (2001)
α	0.03	kg/hr	Stute et al. (1992); Kearns et al. (1993a), fit
γ	0.07	hours ⁻¹	Vainstein et al. (2005), fit
a	2.2	$\mu\text{g} * \text{hours}/\text{kg}$	(calculated)
σ^2	0.001	hours ²	(calculated)
T	24	hours	(calculated)
\bar{G}	0.01	$\mu\text{g}/\text{ml}$	(calculated)
m	1	(none)	(calculated)

Table 3.1 Normal steady state parameters appropriate for dogs.

Parameter Name	Dog 100	Dog 118	Dog 127	Dog 101	Dog 113	Dog 117	Dog 128
A_N^{untr}	488	73.4	18.8	135.8	51	659	100
A_N^{tr}	912.4	866.4	68.3	900	200	2000	800
θ_1^{untr}	0.36	0.36	0.36	0.36	0.36	0.36	0.8
θ_1^{tr}	2.0	4.1	2.1	4	4	4	5
γ_s^{untr}	0.03	0.03	0.005	0.05	0.01	0.05	0.08
γ_s^{tr}	0.17	0.15	0.05	0.18	0.055	0.1	0.18
τ_S	2.80	2.80	2.80	2.52	2.45	2.52	2.52
k_0	1.45	1.21	1.34	1.03	1.5	1.59	1.90
f_0	0.30	0.69	1.44	0.81	0.48	0.17	0.5
A_R	5.63	5.63	5.63	5.80	5.63	5.80	5.63
τ_{PM}	7	7	7	6.9	5.27	6.9	7
A_P	21.63	49.38	30.88	91.74	6.15	14.0	21.0
κ_P	1.38	1.16	0.26	0.32	3.48	0.69	0.90
K_P	3.41	10.82	2.46	8.01	11.66	3.79	4.0
\bar{G}	0.008	0.0038	0.0083	0.008	0.01	0.008	0.005

Table 3.2 Parameters used for computation for each dog. The other parameters are the same as in Table 3.1.

3.5.3 Simulated-Annealing

Simulated annealing is an optimization approach derived from the physical cooling of metals. The algorithm explores the parameter space looking for a minimum of an energy function, which was given by the sum of square (3.A.7) in our case. At each step, the algorithm generates a random neighbor solution by perturbing the parameters. We used the Metropolis acceptance rule (Metropolis et al. (1953)) to determine whether we would move to the proposed perturbation of the parameters. If the energy of this new state was lower, the move was accepted. However, unlike other optimization procedures, in simulated annealing the current parameter set could also be altered to one which gives a higher energy. Such uphill moves were accepted with probability $P = e^{-\Delta ET}$ where T is the temperature. Thus, as T decreased, the probability that an uphill move was accepted decreased. The fact that uphill moves can be accepted allows for the system to be perturbed out of a local minima. Simulated annealing is know to be advantageous for optimization of energy functions containing several local minima.

To set up the algorithm, we needed to define an energy function and determine how the cooling, or annealing, would be done (i.e. define a cooling schedule). We used the same energy function and cooling schedule as in Colijn and Mackey (2005b). Briefly, since we aimed at fitting the model to data, the energy function was given by the following sum of squares:

$$\begin{aligned}
 E = & \sqrt{\sum_{i=1}^M \left(\frac{(N_i^s - L_i)^2}{\bar{N}^2} + \frac{(P_i^s - P_i)^2}{\bar{P}^2} \right) + \frac{(R_i^s - R_i)^2}{\bar{R}^2}} \\
 & + \delta \left[\frac{(\bar{N}^s - \bar{N})^2}{\bar{N}^2} + \frac{(\bar{P}^s - \bar{P})^2}{\bar{P}^2} + \frac{(\bar{R}^s - \bar{R})^2}{\bar{R}^2} \right] \\
 & + \delta \left[\frac{(\text{var}(N^s) - \text{var}(N))^2}{\text{var}(N)^2} + \frac{(\text{var}(P^s) - \text{var}(P))^2}{\text{var}(P)^2} + \frac{(\text{var}(R^s) - \text{var}(R))^2}{\text{var}(R)^2} \right],
 \end{aligned} \tag{3.A.7}$$

where N , P and R refer to neutrophils, platelets and red blood cells respectively. The superscript s indicates simulation whereas the lack of a superscript indicates observed data. The bars indicate that the mean has been taken, 'var' refers to the variance and the sum is taken over a total of M points. Although the energy function looks complicated, it is in fact simpler than it may appear. The first and dominant term (first line) is the square root of the usual sum of square, normalized by their means. The remaining terms (second and third lines), scaled by a small parameter δ , involve means and variances of the three blood cell types. These terms were added to force the solution to be oscillatory in order to account for the oscillations observed in platelets, neutrophils and reticulocytes. Without these terms, a steady state solution would frequently be obtained since a constant solution can have a lower sum of squares than an oscillatory solution than would be out of phase or having a different period. For more details, see Colijn and Mackey (2005b). We used the following geometric cooling schedule to determine how and when the temperature T will be decreased:

$$T_n = T_0 \alpha^n, \tag{3.A.8}$$

where $\alpha \in (0.995, 0.999)$. The initial temperature T_0 was chosen such that about half of attempted uphill moves were accepted initially. The temperature is decreased following (3.A.8) after the system has undergone a random walk of length n in the parameter

space. For more details about simulated annealing, see Salamon et al. (2002).

Chapter 4

Optimizing G-CSF treatment following chemotherapy

Granulocyte-colony stimulating factor (G-CSF) stimulates neutrophils production and is used clinically for treating neutropenia (low neutrophil levels). In chapter 3, we used a mathematical modeling approach and experimental data to study alternative G-CSF treatment regimens for cyclical neutropenia. We found that G-CSF can either increase or decrease the amplitude of the oscillations. These results suggest that administration of G-CSF can affect the dynamical behaviour of the granulopoiesis system. In this chapter, we are also interested in studying the effects of G-CSF administration, but for chemotherapy-induced neutropenia. Indeed, G-CSF is widely used in oncological practice for treating neutropenia and preventing infections that often follow chemotherapy treatment. To better study this situation, we develop a delay differential equation model for the regulation of neutrophil production. We use explicit functions for modeling the effects of G-CSF on the amplification factor, the postmitotic transit time and the apoptosis rates. Using a combination of analysis and numerical simulations, we use this model to study the effects of delaying G-CSF treatment following chemotherapy for two recombinant forms of G-CSF (filgrastim and pegfilgrastim). We also examine the consequences of varying the duration of filgrastim treatment and study some dynamical properties of the system.

A version of this chapter has been submitted for publication: C. Foley and M. C. Mackey. Optimizing G-CSF treatment following chemotherapy, *Journal of Theoretical Biology*,

2008.

The reference Foley and Mackey (2008) and the reference Colijn et al. (2007) are respectively presented in chapter 2 and in chapter 3.

4.1 Introduction

Hematopoiesis is the term that refers to the production of blood cells. This process is initiated in the bone marrow by the stem cells, which are self-renewing and which can differentiate and mature to produce all types of blood cells: the leucocytes (white blood cells or WBCs), the erythrocytes (also known as red blood cells (RBCs)) and platelets. Production of blood cells is regulated by cytokines (growth factors) via negative feedback mechanisms. Erythropoietin (EPO) regulates the production of red blood cells, thrombopoietin mediates platelets production whereas Granulocyte-Colony Stimulating Factor (G-CSF) regulates granulopoiesis (production of white blood cells).

Neutropenia refers to a condition in which the number of neutrophils is low. Neutrophils usually make up 50-70% of circulating white blood cells and serve as the primary defence against infections by destroying bacteria in the blood. Hence, having a reduced number of neutrophils makes the body less able to fight infection and this condition can sometimes become life-threatening. Neutropenia is said to be severe if the Absolute Neutrophil Count (ANC) is less than 500 cells per microlitre of blood (or equivalently, 0.38×10^8 cells/kg). Severe chronic neutropenia may be present at birth (congenital neutropenia) or may occur at any stage in life (acquired neutropenia). In particular, chemotherapy often causes neutropenia since it typically attacks cells indiscriminately regardless of whether malignant or normal. In fact, neutropenia is one the most frequent side-effects of chemotherapy (Rahman et al. (1997), Vainstein et al. (2005)). Administration of recombinant forms of the growth factor G-CSF has been shown to stimulate neutrophil production and is now the standard treatment for neutropenia. However, the clinical administration schedule of G-CSF is typically determined by trial and error and it is not clear if there is an optimal way of giving G-CSF after chemotherapy (Clark et al. (2005), Bennett et al. (1999)).

Some clinical studies have tried to optimize G-CSF timing following chemotherapy (Morstyn et al. (1989), Meisenberg et al. (1992), Butler et al. (1992), Fukuda et al. (1993), Koumakis et al. (1999)), but the conclusions vary between studies. The goal of

this chapter is to study G-CSF treatment strategies following chemotherapy using a mathematical modeling approach and supplemented by numerical simulations.

Over the past decades, mathematical modeling has provided insight into different aspects of biological system function. Several mathematical models have been used as tools for better understanding the nature of hematopoiesis and hematopoietic diseases (see Roeder (2006) and Foley and Mackey (2008) for reviews). Some of these models are very detailed and aimed at obtaining insight into biological mechanisms (Rubinow and Lebowitz (1975), Shochat et al. (2002), Vainstein et al. (2005)). They have several compartments and hence are often high dimensional and contain a large number of parameters. Other models focus on specific aspects of neutrophil production. These models can take various forms and present different levels of details. For instance, they could be formulated as partial differential equations (PDE) (Ostby et al. (2003)), delay differential equations (DDE) (Bernard et al. (2003), Foley et al. (2006)) or ordinary differential equations (ODE) (Panetta et al. (2003), Scholz et al. (2005), Shochat et al. (2007)).

Analysis and numerical simulations of such mathematical models can also provide a way of studying G-CSF treatment strategies in various contexts. For example, Ostby et al. (2003) proposed a reaction-diffusion partial differential equation (PDE) model for the hematopoietic reconstitution after high-dose chemotherapy and G-CSF treatment. They investigated the physiological effects of G-CSF on proliferation rate, maturation rate, mobilization and cell death relative to engraftment. Scholz et al. (2005) used an ODE model for computing the time dependent behaviour of cell numbers in each compartment under the influence of poly-chemotherapy and G-CSF administration. Their model includes self-regulating mechanisms that describe the effects of G-CSF administration and chemotherapy treatment. Shochat et al. (2007) developed a simple two-dimensional ODE system for the G-CSF-neutrophil dynamics using an axiomatic approach. They performed a detailed mathematical analysis to deduce interesting dynamical properties of the system. Finally, Foley et al. (2006) and Colijn et al. (2007) used DDE models to propose alternative G-CSF treatment schedules for cyclical neutropenia. However, in these models, G-CSF effects were implicitly included through negative feedback functions. The model we develop in here is a four-variable delay differential equation model coupled with a two-compartment ODE model that accounts for G-CSF subcutaneous administration. It is distinguished from previous DDE models by an explicit modeling of the effects of G-CSF administration on amplification, maturation and apoptosis rates.

Moreover, the model can reproduce currently available clinical data for two forms of recombinant G-CSF used in clinical practice (filgrastim and pegfilgrastim). We use it to study alternative time schedules for G-CSF following chemotherapy as well as dynamical aspects of the system.

This chapter is organized as follows. First, we review some aspects of granulopoiesis and present the standard clinical G-CSF treatment procedures following chemotherapy in Section 4.2. Then, in Section 4.3, we develop a new mathematical model for neutrophil production that accounts explicitly for G-CSF effects. This model is then used in Section 4.4 to numerically study alternative G-CSF schedules for two forms of G-CSF (filgrastim and pegfilgrastim). In Section 4.5, we study some dynamical properties of the model and conclude with a discussion in Section 4.6.

4.2 Background

In this section, we review the basic aspects of granulopoiesis and discuss how G-CSF is used for treating chemotherapy-induced neutropenia.

4.2.1 Granulopoiesis

Granulopoiesis is the term for the production of granulocytes. Neutrophils are the most abundant type of granulocytes. Neutrophil precursors in the bone marrow can be divided into two pools: the mitotic and the post-mitotic pools. Cells in the mitotic pool are proliferative and they consist of the progenitor cells, myeloblasts, promyelocytes and myelocytes. Cells in the post-mitotic pool are non-proliferative and they act as a reserve pool (or storage compartment) before entering the blood. They consist of metamyelocytes and the banded and segmented neutrophils. Under normal physiological conditions, the transit time through the mitotic pool is approximately 6 days (Israels and Israels (2002)). Then, cells are held in the bone marrow in the post-mitotic pool for about another 6 days (Price et al. (1996)) before being released into the circulation. When G-CSF levels are increased (either in response to an inflammatory process or by exogenous administration), the transit times through the mitotic and post-mitotic pools are reduced (Lord et al. (1989)). G-CSF acts on both precursor and mature cells by stimulating the effective proliferation of committed granulocytes progenitors (myeloblasts, promyelocytes and myelocytes), apparently by decreasing apoptosis. Administration of exogenous G-CSF is

known to increase the number of circulating neutrophils by increasing the number of mitotic cells, reducing the maturation time and releasing the bone marrow storage pool (Israels and Israels (2002), Lord et al. (1989), Price et al. (1996)).

4.2.2 Treating neutropenia using G-CSF treatment

G-CSF (granulocyte-colony stimulating factor) is a hematopoietic growth factor that stimulates the bone marrow to increase the production of neutrophils. Thus, this is the treatment of choice for neutropenia. It is produced naturally in the body, but recombinant forms of G-CSF (filgrastim (Neupogen), lenograstim (Granocyte) and pegfilgrastim (Neulasta)) are used as drugs to accelerate recovery from neutropenia. In this study, we will only consider filgrastim and pegfilgrastim. They are both G-CSF analogs produced by recombinant DNA technology. The gene for human granulocyte colony-stimulating factor is inserted into the genetic material of *Escherichia coli*. Recombinant G-CSF produced by *E. coli* is only slightly different from G-CSF naturally made in humans. Filgrastim is a small molecule which is rapidly filtered by the kidney and cleared from the blood, necessitating daily administrations. The pegylated filgrastim (pegfilgrastim) is the same molecule as filgrastim but to which a 20 kDa polyethylene glycol moiety has been added. This addition changes its pharmacokinetic properties and virtually eliminates renal clearance. Hence, whereas filgrastim is rapidly cleared after a subcutaneous dose, pegfilgrastim, a bigger molecule, has a much longer half life. Therefore, only a single administration after each cycle of chemotherapy is necessary for pegfilgrastim instead of a number of daily injections for filgrastim, thereby reducing cost and inconvenience to the patient.

Other than a difference in their clearance rate, both molecules have the same effects: they boost the number of neutrophils by decreasing the apoptosis rates in neutrophil precursors (Hannun (1997)) and thus increasing the effective amplification factor, and accelerating the transit time through the postmitotic pool (Lord et al. (1989), Price et al. (1996)).

Side effects

Even though G-CSF is a natural substance, a too high concentration may cause side effects such as bone pain, red and itchy skin, fever, chills and fluid retention, nausea, vomiting and diarrhea.

Clinical uses

G-CSF is used clinically to treat neutropenia in several situations. In particular, since a common side effect of many chemotherapeutic drugs is a reduction in the number of white blood cells, G-CSF is often given after chemotherapy to elevate the white blood cell production. It is usually given subcutaneously (injection under the skin) because the increase in neutrophil count is higher and the stimulated duration is longer than with an intravenous administration of the same dose (Hayashi et al. (2001)). In this study, we only consider the use of G-CSF following myelosuppressive chemotherapy on patients suffering from nonmyeloid types of cancer, e.g. we are assuming that a model of regulation of neutrophil production can be taken to represent a hematologically normal individual. Filgrastim (Neupogen)'s clinical guidance (www.neupogen.com) for cancer patients receiving myelosuppressive chemotherapy recommends a starting dose of $5 \mu\text{g}/\text{kg}/\text{day}$, subcutaneously. Doses may be increased in increments of $5 \mu\text{g}/\text{kg}$ for each chemotherapy cycle, according to the duration and severity of the ANC nadir. Neupogen should be administered no earlier than 24 hours after the administration of cytotoxic chemotherapy and it should be administered daily for up to 2 weeks, until the ANC has reached normal levels following the expected chemotherapy-induced neutrophil nadir.

The recommended dosage of Neulasta (pegfilgrastim) is a single subcutaneous injection of 6 mg administered once per chemotherapy cycle (clinical guidances www.neulesta.com). Neulasta should not be administered in the period between 14 days before and 24 hours after administration of cytotoxic chemotherapy.

4.3 Mathematical model

In this section, we describe a mathematical model for neutrophil regulation and production. This model is divided into two parts: the main compartment, which models the white blood cell production system, and the G-CSF compartment, which models G-CSF subcutaneous injections. The effects of G-CSF are included in the main compartment through different functions. This model will be used in section 4.4 to study the effects of different schedules of G-CSF following chemotherapy.

4.3.1 Description of the main part of the model

We consider a model with 5 compartments. Let $m(t, a)$, $s(t, a)$, $p(t, a)$, $n(t, a)$ and $w(t, a)$ be the population densities at time t and age a of proliferative stem cells, resting (G_0) stem cells, proliferative precursors cells, non-proliferative precursors and circulating white blood cells respectively (see Fig. 4.1). We make the following assumptions:

1. **Apoptosis:** We assume that in each of these compartments (except for the G_0 stem cell compartment), there is a random loss of cells due to apoptosis, at a rate denoted by $\gamma_s, \gamma_p, \gamma_n$ and γ_w for the proliferative stem cells, proliferative precursors, non-proliferative precursors and circulating neutrophils respectively. We assume that all of the apoptosis rates except γ_w depend on the G-CSF concentration $G(t)$.
2. **Ageing velocity:** We assume that the cells in each compartment age with a certain velocity $V_i(G), i = m, s, p, n, w$. In particular, we take V_m (proliferative stem cells), V_s (stem cells in G_0 phase), V_p (proliferative precursors) and V_w (white blood cells) to be equal to 1. On the other hand, we consider that the velocity for the non-proliferative precursors compartment ($V_n(G)$) depends explicitly on G-CSF because G-CSF is known to modify the maturation time of this population (Lord et al. (1989)). We assume that a cell enters the non-proliferative compartment at age $a = 0$ and exits this compartment at age $a = \tau_n$. Hence, if we increase $V_n(G)$, the transit time through that phase will decrease since it will take less time to go through the compartment.
3. **Differentiation rate:** We assume that the differentiation rate $\delta(W)$ from the resting G_0 stem cell compartment to the proliferative phase depends on the number of circulating neutrophils $W(t)$.
4. **Re-entry of G_0 phase stem cells into proliferation:** Cells in the resting G_0 phase (represented by $s(t, a)$) can either differentiate at a rate $\delta(W)$ or reenter proliferation at a rate $\beta(S)$ (we will assume β does not depend on $G(t)$). The function $\beta(S)$ is a decreasing Hill function and hence, as the number of cells in the G_0 phase decreases, the proliferation rate is increased. Cells enter the proliferative phase of the stem cells at age $a = 0$ and leave at age $a = \tau_s$. We assume that before entering the G_0 compartment, the cells divide into two daughter cells and hence we consider an amplification factor of 2.

5. **Amplification factor $A(G)$:** Cells exiting the proliferative phase are amplified by a factor $A(G)$. This accounts for the number of divisions occurring in the proliferative phase and it depends on the G-CSF concentration explicitly.

From Fig. 4.1, we can write down a partial differential equation satisfied by the cell density function for each compartment. We let a represents age and t time. The age-structured model for the cell populations can be written as:

$$\frac{\partial m}{\partial t} + \frac{\partial m}{\partial a} = -\gamma_s(G)m \quad t > 0, a \in [0, \tau_s] \quad (4.1)$$

$$\frac{\partial s}{\partial t} + \frac{\partial s}{\partial a} = -\delta(W)s - \beta(S)s \quad t > 0, a > 0 \quad (4.2)$$

$$\frac{\partial p}{\partial t} + \frac{\partial p}{\partial a} = -\gamma_p(G)p \quad t > 0, a \in [0, \tau_p] \quad (4.3)$$

$$\frac{\partial n}{\partial t} + V_n(G)\frac{\partial n}{\partial a} = -\gamma_n(G)n \quad t > 0, a \in [0, \tau_n] \quad (4.4)$$

$$\frac{\partial w}{\partial t} + \frac{\partial w}{\partial a} = -\gamma_w w \quad t > 0, a > 0. \quad (4.5)$$

Note that age a characterizes each compartment separately but time t is the same in all compartments. For instance, cells entering a given compartment are always characterized by $a = 0$. The right hand sides of these equations account for the cell loss. To completely determine the system, we also need to provide initial conditions and boundary conditions. We consider the following boundary conditions:

$$\begin{aligned} m(t, 0) &= \beta(S(t))S(t), & s(t, 0) &= 2m(t, \tau_s), \\ p(t, 0) &= \delta(W(t))S(t), & n(t, 0) &= A(G(t))p(t, \tau_p), \\ w(t, 0) &= n(t, \tau_n), \end{aligned}$$

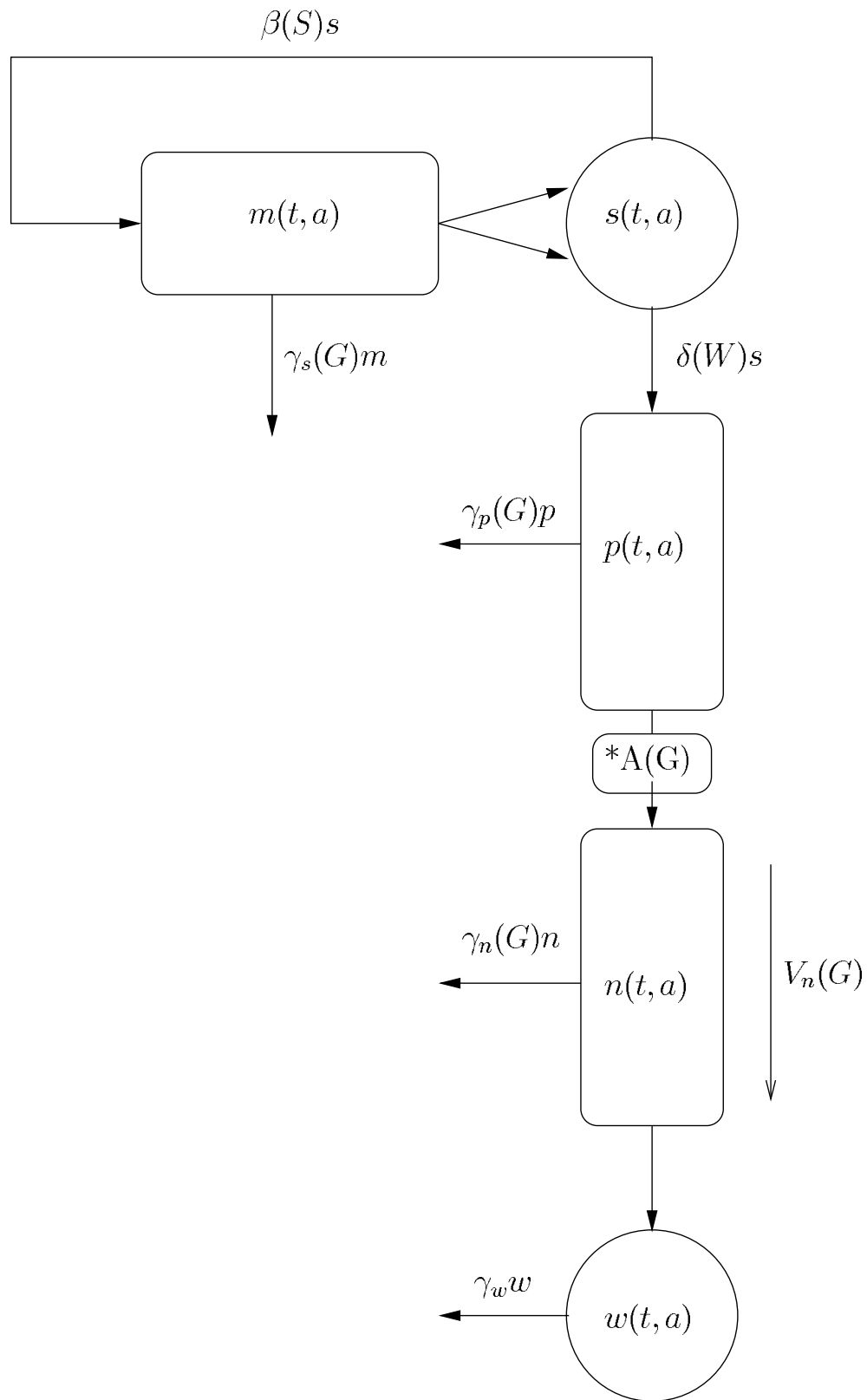


Fig. 4.1 Schema of the main part of the model. See the text for full details as well as the notation.

where $A(G)$ is the amplification factor from proliferative to non-proliferative neutrophil precursors and the total population of each type is defined as:

$$\begin{aligned} M(t) &= \int_0^{\tau_s} m(t, a) da, & S(t) &= \int_0^{\infty} s(t, a) da, \\ P(t) &= \int_0^{\tau_p} p(t, a) da, & N(t) &= \int_0^{\tau_n} n(t, a) da, \\ W(t) &= \int_0^{\infty} w(t, a) da. \end{aligned}$$

Also, we use initial conditions of the form

$$\begin{aligned} m(0, a) &= \phi_m(a) & a &\in [0, \tau_s] \\ s(0, a) &= \phi_s(a) & a &> 0 \\ p(0, a) &= \phi_p(a) & a &\in [0, \tau_p] \\ n(0, a) &= \phi_n(a) & a &\in [0, \tau_n] \\ w(0, a) &= \phi_w(a) & a &> 0. \end{aligned}$$

We assume that the re-entry into stem cell proliferation and differentiation in the neutrophil line are modeled by the same monotone decreasing Hill functions as in Colijn and Mackey (2005a). Therefore, when the stem cells level S decreases, $\beta(S)$ increases and stem cell production is increased. Similarly, when the neutrophil count is low, it increases the differentiation rate $\delta(W)$. The functions $\beta(S)$ and $\delta(W)$ are given by

$$\beta(S) = k_0 \frac{\theta_2^2}{\theta_2^2 + S^2} \quad (4.6)$$

$$\delta(W) = f_0 \frac{\theta_1}{\theta_1 + W}. \quad (4.7)$$

The aging velocity is related to the transit time through a given stage. Since we do not have any a priori information on how G-CSF decreases the time spent in the non-proliferative precursor phase, we postulate a simple bounded relationship:

$$V_n(G) = (V_{max} - 1) \frac{G}{G + b_v} + 1. \quad (4.8)$$

Note that this function is increasing so that the time spent in the phase is decreased as G increases. Recall that the amplification factor $A(G)$ also varies as a function of G-CSF. Again, as we have no a priori information on its shape, we assume a bounded relationship:

$$A(G) = (A_{max} - A_{min}) \frac{G}{G + b_A} + A_{min}. \quad (4.9)$$

Using the method presented in Section 2.6.1, we can integrate each equation and express the model as delay differential equations (DDE) for the total cell population numbers $S(t)$, $P(t)$, $N(t)$ and $W(t)$. The complete derivation of the DDE model is presented in the Appendix and yields the following equations:

$$\frac{dS}{dt} = 2\beta(S_{\tau_s})S_{\tau_s} \exp\left(\int_0^{\tau_s} -\gamma_s(G(t)) dt\right) - [\beta(S) + \delta(W)]S, \quad (4.10)$$

$$\frac{dP}{dt} = -\gamma_p(G)P + \delta(W)S - \delta(W_{\tau_p})S_{\tau_p} \exp\left(-\int_0^{\tau_p} \gamma_p(G(t)) dt\right), \quad (4.11)$$

$$\begin{aligned} \frac{dN}{dt} = & -\gamma_n(G)N + V_n(G)\delta(W_{\tau_p})S_{\tau_p} \exp\left(-\int_0^{\tau_p} \gamma_p(G(t)) dt\right) * \\ & * \left[A(G) - A(G_{\tau_n}) * \exp\left(-\int_0^{\tau_n} \gamma_n(G(t)) dt\right) \right], \end{aligned} \quad (4.12)$$

$$\frac{dW}{dt} = -\gamma_w W + A(G_{\tau_n})\delta(W_{\tau_p})S_{\tau_p} \exp\left(-\int_0^{\tau_p} \gamma_p(G(t)) dt - \int_0^{\tau_n} \gamma_n(G(t)) dt\right) \quad (4.13)$$

A subscript on a variable denotes a temporal delay in that variable ($x_\tau := x(t - \tau)$).

4.3.2 Description of the G-CSF model

As it can be seen from the previous equations, many of the parameters in the system depend on the G-CSF concentration $G(t)$. Indeed, G-CSF regulates the system in several different ways and, in particular, it is known to regulate the neutrophil production through a negative feedback mechanism.

The model for G-CSF is similar to the one used in Colijn et al. (2007). It is a two-compartment model that accounts for subcutaneous G-CSF injections. The model is illustrated in Fig. 4.2. The notation is as follows: X denotes the tissue levels of G-CSF (units $\mu g/kg(\text{body weight})$) and G denotes the circulating G-CSF concentration (units $\mu g/mL$). Note that instead of using concentrations for both tissue and blood

compartment, we used per body weight levels for the tissue compartment. Since it is easier to express the input $I(t)$ in terms of quantity, this allows us to get rid of the parameter representing the volume of tissue compartment. Of course, the corresponding terms need to be scaled accordingly by the volume of the blood compartment V_B in order to make units of G and X agree in both equations. G-CSF is injected into the tissue compartment and enters the circulation from there. It is eliminated through saturable and unsaturable mechanisms. The saturable mechanism involves the G-CSF receptors on neutrophils whereas the unsaturable process mainly involves kidneys (Vainstein et al. (2005)). From Fig. 4.2, one can write down the dynamic equation for the G-CSF

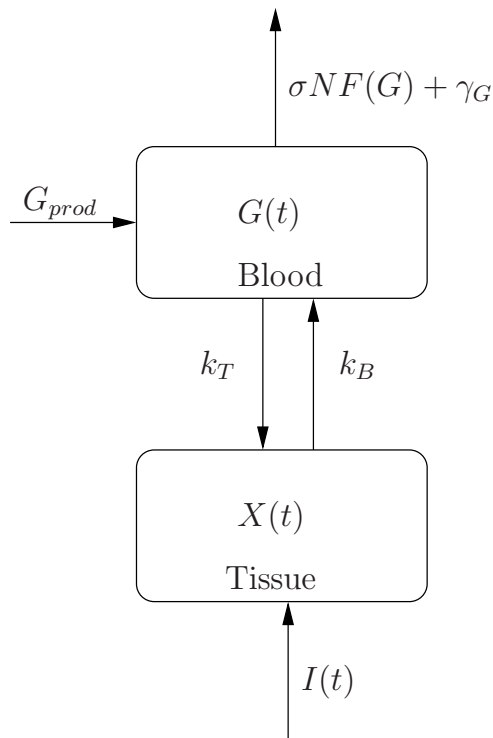


Fig. 4.2 A two-compartment model for subcutaneous administration of G-CSF. $I(t)$ is a step function representing injection of exogenous G-CSF into the tissues. $X(t)$ and $G(t)$ are respectively the amount of G-CSF in tissues ($\mu\text{g}/\text{kg}$) and the blood G-CSF concentration ($\mu\text{g}/\text{ml}$). k_T and k_B are rate constants for exchange between the blood and tissue compartments. G-CSF clearance rate is given by $\sigma NF(G) + \gamma_G$. See the text for further details.

compartment:

$$\frac{dX}{dt} = I(t) + k_t V_B G - k_B X \quad (4.14)$$

$$\frac{dG}{dt} = G_{prod} + \frac{k_B X}{V_B} - k_T G - (\gamma_G + \sigma W F(G))G. \quad (4.15)$$

The first equation represents the rate of change of G-CSF in tissues. $I(t)$ is the input from exogenous G-CSF given subcutaneously, V_B is the volume of the blood compartment and k_T and k_B are rate constants for exchange between the blood and tissue compartments. The rate of change of G-CSF concentration in blood is expressed in the second equation, where G_{prod} is the fixed G-CSF production and the clearance is given by $\gamma_G G + \sigma W F(G)G$.

Next, we derive expressions for G-CSF clearance and the input function $I(t)$ that models subcutaneous injections.

G-CSF clearance

A number of mathematical models of G-CSF clearance have been used in the literature. Some authors used Michaelis-Menten kinetics to model the combination of saturable and non-saturable clearance (Kuwabara et al. (1994); Hayashi et al. (2001); Ostby et al. (2003)). Alternatively, one could model the unsaturable clearance by a first-order process and the saturable G-CSF clearance by directly treating the binding of G-CSF receptors (Vainstein et al. (2005)). The model we propose here is of the second type.

First, the unsaturable clearance process could be modeled by a first-order process $\gamma_G G$, where γ_G is the rate of degradation of G-CSF by the kidneys. To this, we add an expression for the saturable G-CSF clearance. Indeed, G-CSF is also removed from the circulation by binding to free receptors on neutrophils. Let $F(G)$ be the fraction of bound G-CSF receptors, W be the neutrophil number and σ be a binding coefficient of G-CSF to its receptors. Thus, the number of G-CSF molecules removed from the circulation through the saturable clearance is given by $\sigma W F(G)$, where

$$F(G) = \frac{G^2}{G^2 + k}. \quad (4.16)$$

The reader is referred to the Appendix for further details on the derivation of the function

$F(G)$.

Input function $I(t)$

In this study, we consider subcutaneous administration of rhG-CSF, which has been shown to lead to a higher increase in neutrophil count and a longer duration than for intravenous administration (Hayashi et al. (1999)). To model a bolus subcutaneous injection (a high quantity of drug injected rapidly in the tissue), we used a step function of amplitude a and duration s that is turned on at $t = t_{on}$. More precisely,

$$I(t) = a * [H(t - t_{on}) * (1 - H(t - (t_{on} + s)))], \quad (4.17)$$

where $H(t)$ is the heaviside function defined as

$$H(t) = \begin{cases} 0 & t \leq 0 \\ 1 & t > 0. \end{cases}$$

The total quantity given in the bolus injection is easily computed as $a * s$.

4.4 Numerical simulations

We use a numerical solver for delay differential equations (dde) called `ddesd` (Shampine (2005)) that runs under `matlab`. For all simulations, we set the maximum time step to 0.01. Recall that the full model is given by the Equations (4.10)-(4.15). We first make some simplifying assumptions. The computation of $\bar{\tau}_n$ requires integrating the aging velocity over time until the area under the curve is equal to τ_n ($\tau_n = \int_0^{\bar{\tau}_n} V_n(G(w)) dw$). It involves finding the upper bound of the integral, which depends on the shapes of $G(t)$ and $V_n(G)$ and on the value at which we start integrating (at the beginning of the phase ($a = 0$), at the current time t , etc.). For example, one could also define $\tau_n = \int_{t-\bar{\tau}_n}^t V_n(G(w)) dw$. For this reason, we decided to simplify the problem and to assume that $\bar{\tau}_n$ at time t is given by $\bar{\tau}_n = \tau_n/V_n(G(t))$. This represents the instantaneous value of $\bar{\tau}_n$ and it will change as t changes. It means that if V_n was kept constant, it will take τ_n/V_n days to go through the proliferative phase. For similar reasons, we simplify the computation of $\exp(-\int_0^{\tau_s} \gamma_s(G(t)) dt)$, $\exp(-\int_0^{\tau_p} \gamma_p(G(t)) dt)$ and

$\exp\left(-\int_0^{\bar{\tau}_n} \gamma_n(G(t)) dt\right)$ by using, respectively, $e^{-\gamma_s \tau_s}$, $e^{-\gamma_p \tau_p}$ and $e^{-\gamma_n \bar{\tau}_n}$.

Often in discussing our results we will talk as if discussing an individual with cancer, or an individual receiving chemotherapy. The reader will appreciate that this only a literary device, and we are really talking about the model with a set of parameters appropriate to a given condition.

Thus, we numerically integrate the mathematical model and study how the model behaves in four different situations. First, in Section 4.4.1, we perform simulations of the system without G-CSF treatment. Next, we look at the effects of daily G-CSF (Filgrastim) on cancer patients (Section 4.4.2) and following chemotherapy (Section 4.4.3). Finally, we simulate the effects of Pegfilgrastim on the model in Section 4.4.4.

4.4.1 Simulation without G-CSF treatment

First, we integrate the system assuming no exogenous G-CSF is given. Since we have delayed variables, we need to specify a history function on the interval $[-\max(\tau_s, \tau_p, \tau_n), 0]$. For simplicity, we chose constant initial functions and simulated the system for several different initial values (ranging from 0 to three times the steady state values for each state variable). We found that for these initial functions, the system settles down to a steady state after a transient of about 100 days. Let (S_*, P_*, N_*, W_*) denote the steady state solution of stem cells, proliferative neutrophil precursors, non-proliferative neutrophil precursors and circulating neutrophils. Using the parameters listed in Table 4.1, numerical simulations yield values of $S_* = 3.1 \times 10^6$ cells/kg, $P_* = 0.46 \times 10^6$ cells/kg, $N_* = 8.45 \times 10^9$ cells/kg and $W_* = 2.35 \times 10^8$ cells/kg. Values for normal subjects reported in the literature vary from one study to the another. In Bernard et al. (2003), the estimate for the stem cell numbers S_* is 1.1×10^6 cells/kg but this is an imperfect estimate for many reasons, primarily because of the lack of precision in defining and experimentally determining which cells are truly stem cells. The normal number of non-proliferative neutrophil precursors (N_*) ranges between 4.0 to 10.0×10^9 cells/kg (Vainstein et al. (2005)) and is estimated at 5.59×10^9 cells/kg in Dancey et al. (1976). Finally, Bernard et al. (2003) estimated a normal blood neutrophil count W_* of 6.9×10^8 cells/kg (range between 5.0 to 10.0×10^8 cells/kg) whereas Vainstein et al. (2005) reported an average of 3.0×10^8 cells/kg (range between 2.0 and 5.0×10^8 cells/kg). Despite the apparent discrepancy for the stem cell numbers, our steady state values are similar to

those reported in the literature.

We can also solve the system at steady state and get analytical expressions for the equilibrium values of S_* , P_* , N_* and W_* . See Appendix 4.7.4 for the analytical derivation and a proof of the uniqueness of a positive steady state.

4.4.2 Simulating G-CSF (filgrastim) treatment

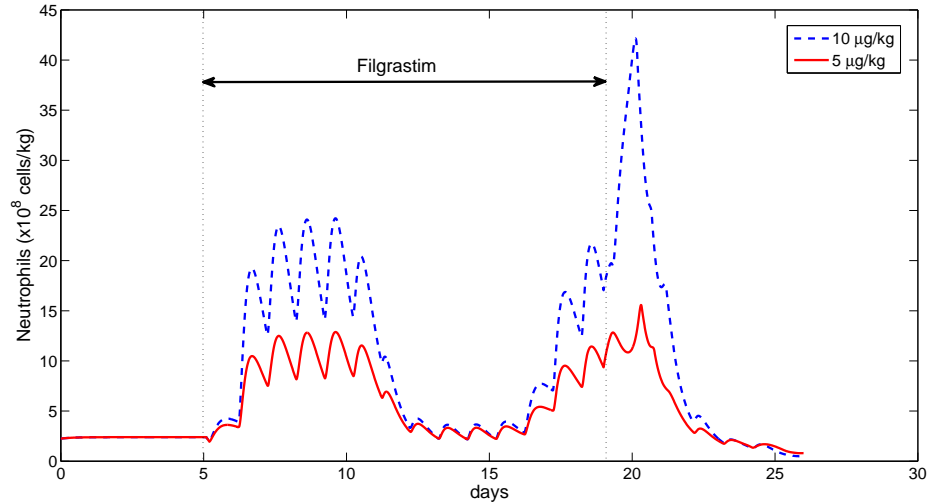


Fig. 4.3 Effects of varying G-CSF dose. Simulation of daily filgrastim administration in the model (before chemotherapy) during a period of 14 days for two dosages: $5\mu\text{g}/\text{kg}$ (blue) and $10\mu\text{g}/\text{kg}$ (red). Parameters used are listed in Table 4.1.

In this section, we use our model to study the effects of daily filgrastim administration. Since we are considering only nonmyeloid malignancies, we assume the same set of parameters for normal and cancer subjects. Simulations of the model for daily doses of $5\mu\text{g}/\text{kg}$ and $10\mu\text{g}/\text{kg}$ during 14 days are shown in Fig. 4.3. We used constant initial functions corresponding to the steady state solutions obtained in Section 4.4.1. One can see that neutrophils increase to 7-fold ($5\mu\text{g}/\text{kg}$) and 17-fold ($10\mu\text{g}/\text{kg}$) during daily G-CSF treatment, in agreement with results of Chatta et al. (1994). The aging velocity $V_n(t)$ and the amplification factor $A(t)$ are also increased under treatment, as explained in Section 4.7.3.

4.4.3 Simulating Filgrastim effects following chemotherapy

The use of cytotoxic drugs is considered as a standard treatment for cancer. There are many chemotherapeutic agents and several of them have been shown to induce apoptosis in cancer cells as well as in healthy cells (see Hannun (1997) for a review). Moreover, the apoptosis induced by cytotoxic agents can be inhibited by hematopoietic growth factors, such as G-CSF (Lotem and Sachs (1992)). In this section, we use the model to study the effects of daily G-CSF (filgrastim) on subjects suffering from nonmyeloid malignancies who have undergone chemotherapy. After presenting the numerical method used for simulation in Section 4.4.3, we briefly review previous clinical attempts in optimizing G-CSF treatment schedules following chemotherapy in Section 4.4.3. Then, we use our model to study the effects of the starting day of G-CSF treatment following chemotherapy (Section 4.4.3) and of the duration of G-CSF treatment (Section 4.4.3).

Numerical method

From a modeling point of view, the effects of chemotherapy and G-CSF treatment are mimicked through the functions $A(G)$, $V_n(G)$, $\gamma_s(G)$, $\gamma_p(G)$ and $\gamma_n(G)$. As explained in Section 4.7.3, G-CSF increases the amplification factor, decreases the transit time in the postmitotic pool (increases aging velocity V_n) and decreases the apoptosis rates in the stem cells (γ_s) and in the neutrophil precursor cells (γ_N and γ_P).

To numerically simulate the effects of G-CSF following chemotherapy, we start from the stable steady state found in Section 4.4.1 that represents cancer. Then, we increase the values of γ_s , γ_p and γ_n to their maximum values γ_i^{max} ($i = s, p, n$) to mimic the effects of chemotherapy. The administration of exogenous G-CSF is explicitly expressed by changing the input function $I(t)$, which then affects the amplification $A(G)$, the aging velocity $V_n(G)$ and the apoptosis rates $\gamma_s(G)$, $\gamma_p(G)$ and $\gamma_n(G)$. The parameters used after chemotherapy are the same as in healthy/cancer subjects. Finally, note that since it is recommended that G-CSF is to be started at least 24 hours after chemotherapy, we gradually decrease the apoptosis rates between the end of chemotherapy and the beginning of G-CSF treatment. We use decreasing linear functions of the type $\gamma_i(t) = (\gamma_i^{min} - \gamma_i^{max})\frac{t}{8} + \gamma_i^{max}$ for $i = s, p, n$. The factor 8 in the slope of the linear functions was chosen because a study in monkeys (Meisenberg et al. (1992)) reported an average period of 8 days for recovery of the ANC following chemotherapy.

Previous studies

In this section, we review previous clinical attempts to optimize filgrastim administration following chemotherapy.

Typically, a rapid rise in the neutrophil count is observed after G-CSF administration, followed by a neutrophil decrease to low ANC values. After this ANC nadir, the neutrophil levels then increase. Treatment protocols prescribe daily filgrastim (starting dose of $5\mu\text{g}/\text{kg}$) beginning at least 24 hours after chemotherapy. It should be administered daily for up to 14 days or until the ANC has reached normal levels following the neutrophil nadir.

The use of G-CSF has been proven to be of great utility in reducing chemotherapy-induced neutropenia. Nevertheless, it is not clear what would be the best schedule for giving G-CSF following chemotherapy. A few studies have considered alternative G-CSF regimens in order to find optimal G-CSF timing (Morstyn et al. (1989), Meisenberg et al. (1992), Butler et al. (1992), Fukuda et al. (1993), Koumakis et al. (1999)). However, the results and conclusions vary from one study to another. There are basically two main lines of thought concerning the timing of G-CSF administration. Some authors consider that the duration of neutropenia and the neutrophil nadir are not significantly different whether G-CSF is given as early as 24 h or even as late as 8 days after chemotherapy (Meisenberg et al. (1992), Morstyn et al. (1989)). However, others have concluded that it is preferable to start G-CSF administration early after chemotherapy treatment because it reduces the number of infections and hospitalization days. Next, we briefly discuss the main results of studies based on these two premises. In their study on monkeys, Meisenberg et al. (1992) showed that beginning daily filgrastim ($5\mu\text{g}/\text{kg}$) on either days 1, 3, 5 or 7 after chemotherapy all reduce neutropenia. They demonstrated that the duration of G-CSF treatment could be reduced considerably by delaying G-CSF initiation. They also observed that early G-CSF (1 day after chemotherapy) led to a more rapid recovery of myeloid progenitor cells and an earlier onset of neutropenia than delayed treatment.

Morstyn et al. (1989) also studied the effects of delaying filgrastim treatment following chemotherapy and of reducing its duration of administration. Data in their paper (reproduced in Fig. 4.4) suggests that the amplitude in the ANC levels in response to G-CSF could vary depending on the starting day of G-CSF administration. In particular,

maximal neutrophil levels are higher when starting filgrastim treatment on the day following chemotherapy and lower when starting 7 days after chemotherapy. Morstyn et al. (1989) demonstrated that starting G-CSF 7 days after chemotherapy still has the effect of rapidly raising the ANC levels, although the neutrophil response is typically of smaller amplitude (see Fig. 4.4). They also concluded that it was not necessary to continue G-CSF for more than 7 days.

In contrast to these studies, Butler et al. (1992) administered G-CSF starting on days 4 or 11 during intensive chemotherapy for breast cancer. They found that patients who were given G-CSF on day 4 had fewer days of neutropenia, hospitalization and antibiotic days while having similar duration the G-CSF treatment. These results are in agreement with another study by Fukuda et al. (1993), who also showed that early G-CSF administration following chemotherapy was more beneficial than late administration, when the number of neutropenic days and the depth of the nadir were considered. Finally, Koumakis et al. (1999) compared various timing schedules of G-CSF treatment following chemotherapy. They were interested in investigating the dependence of the optimal time (preemptive vs. supportive) of G-CSF initiation on criteria such as incidence of febrile neutropenia, antibiotic use, duration and cost of G-CSF administration. Preemptive treatment involves starting G-CSF shortly after chemotherapy whereas in supportive therapy, G-CSF is started later and only when neutropenia occurs. The authors concluded that G-CSF administration shortens neutropenia regardless of the treatment starting day and that no significant difference was observed among early- and late- treatment groups. However, the incidence of antibiotic use and febrile episodes was less when G-CSF was started early (1 or 2 days after chemotherapy). For these reasons, they recommended preemptive rather than therapeutic administration of G-CSF for subjects receiving chemotherapy.

In the next section we use our model to study the timing of filgrastim administration with respect to the starting day of administration and the duration of treatment.

Effects of varying the starting day of filgrastim treatment

As discussed above, it has been suggested that delayed initiation of filgrastim could successfully reduce neutropenia while being cost-effective. Using our mathematical model, we found that changing the starting day of filgrastim administration could result in

important qualitative changes in the ANC levels. Fig. 4.5 shows the effects of starting filgrastim 1 day and 8 days after chemotherapy. Note that, as in Morstyn et al. (1989), our model leads to very different responses in the ANC levels. Early administration of filgrastim results in a large response in the neutrophil levels, followed by a decrease to low ANC. Filgrastim was simulated to stop when the neutrophil levels were back to normal following this nadir. Conversely, initiation of filgrastim 8 days after chemotherapy lead to a very different qualitative response. Neutrophil levels increased but remained relatively stable around normal levels during G-CSF treatment without falling to very low values (see Fig. 4.5). Starting G-CSF one week after chemotherapy leads to a reduced

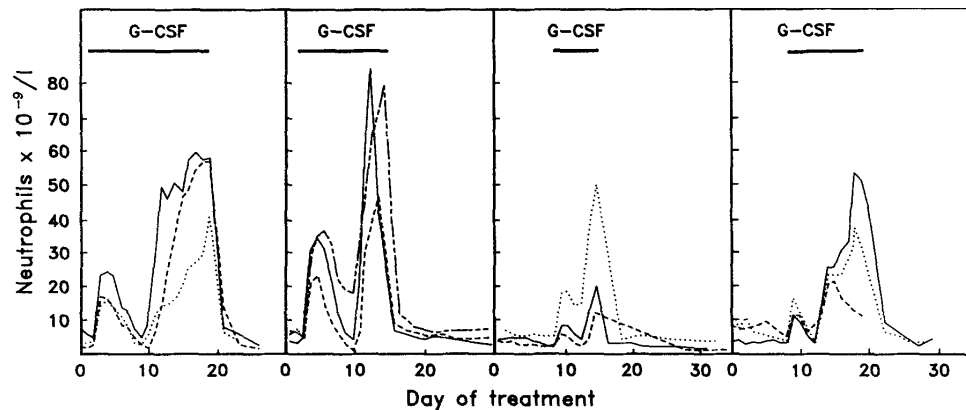


Fig. 4.4 Data from Morstyn et al. (1989) showing the effects of varying the time and duration of filgrastim administration on neutrophil levels in relation to melphalan therapy. Each of the 4 panels show data from 4 patients. G-CSF is started on day 1 after chemotherapy in the first two panels and on day 7 in the last two panels.

maximum ANC during G-CSF treatment (about half of the maximum ANC value when starting G-CSF the day following chemotherapy) (see Fig. 4.6). Interestingly, delaying filgrastim of one week also coincides with higher neutrophil nadir during filgrastim treatment (approximately twice the nadir value compared to starting treatment on day one).

These results are in agreement with those reported in Morstyn et al. (1989). It suggests that late G-CSF administration following chemotherapy should be efficient in reducing the neutropenic period, provided that neutropenia does not occur prior to the start of treatment. Since the ANC increases rapidly after filgrastim administration, this suggests

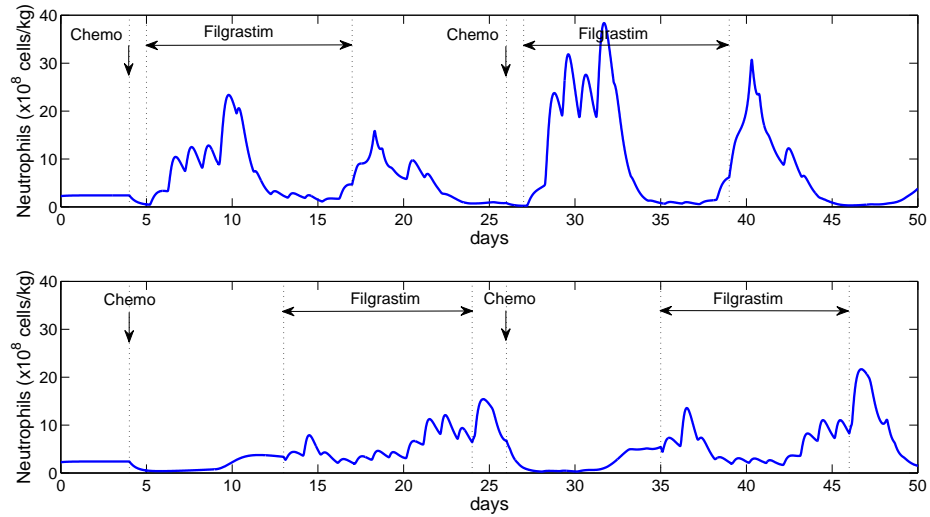


Fig. 4.5 Simulation of 2 cycles of chemotherapy and daily filgrastim ($5\mu\text{g}/\text{kg}$). Top panel: Filgrastim is administered daily, starting the day following chemotherapy treatment until the neutrophil levels reach normal values following the expected nadir. Bottom panel: Filgrastim is started 8 days after chemotherapy treatment for a period of 11 days. Changing the starting day of treatment may lead to different responses in the neutrophil count.

that filgrastim could be efficiently used as supportive treatment, i.e. starting G-CSF only at the onset of neutropenia. Moreover, this could result in a more stable ANC response and avoid the typical decrease in neutrophil count. However, we do not take into account the use of antibiotics in this model, which is a criteria that was in favor of a preemptive treatment in the study by Koumakis et al. (1999). Also, in a clinical setting, there are several factors to consider when administering G-CSF to patients, such as the type of cancer, the intensity of the chemotherapy, the age and general health of the subject, the history of febrile neutropenic episodes, etc. All these factors can influence the response to filgrastim treatment. Therefore, our results should be looked at from a qualitative point of view. Our model suggests that two different types of response (large amplitude followed by low nadir and a relatively stable ANC) can be obtained by filgrastim administration. We believe that this may be due to the existence of multiple stable solutions in the system (see Section 4.5).

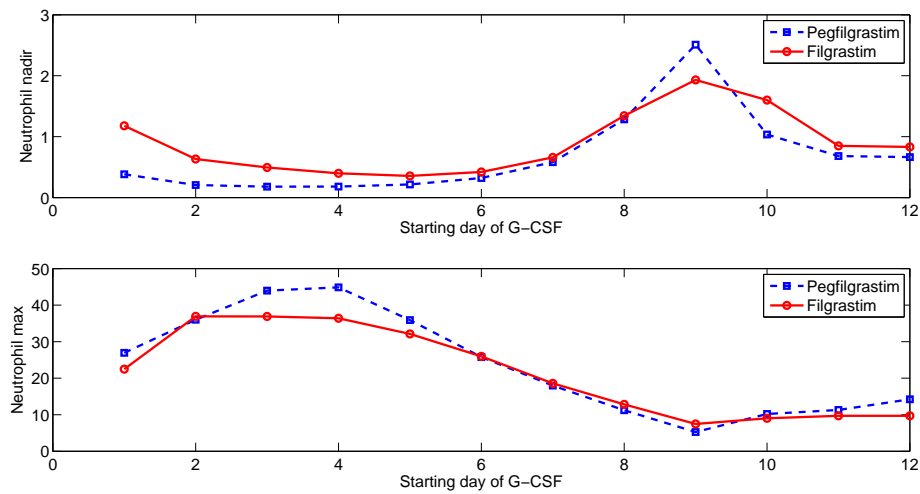


Fig. 4.6 Minimum and maximum neutrophil values during G-CSF treatment for both filgrastim ($5\mu\text{g}/\text{kg}/\text{day}$) and pegfilgrastim ($100\mu\text{g}/\text{kg}$) with respect to the starting day of G-CSF treatment following chemotherapy. Neutrophil levels are in $\times 10^8$ cells/kg.

Effects of varying the duration of filgrastim treatment

In this section, we study the effects of varying the duration of filgrastim treatment. Since clinical guidelines suggest starting filgrastim on day 1 and stopping its administration when the neutrophil levels are back to normal values following the expected nadir, we chose to always simulate the start of filgrastim on the day following chemotherapy and only vary the end of G-CSF treatment. Fig. 4.7 shows the simulation when filgrastim is

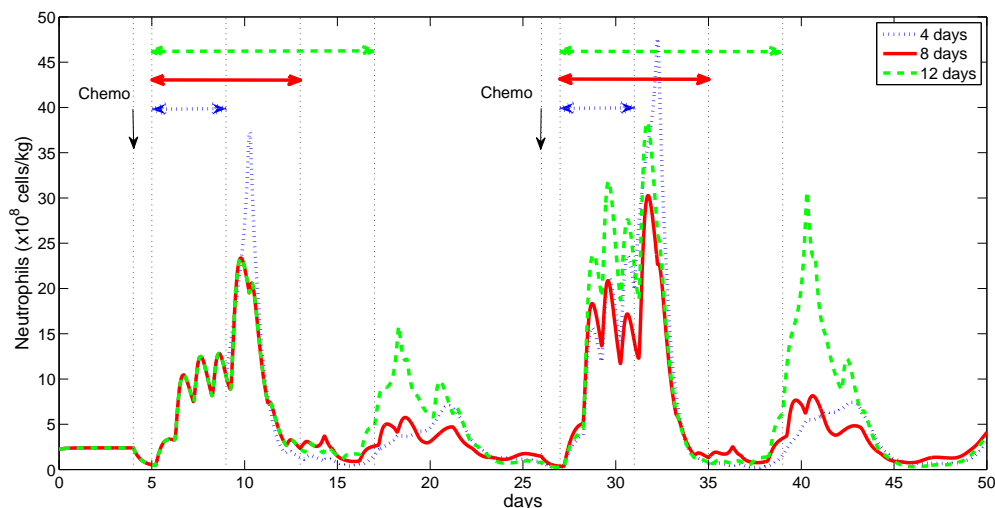


Fig. 4.7 Effects of varying the duration of filgrastim treatment. Simulation of daily filgrastim ($5 \mu\text{g}/\text{kg}$) started on day 1 after chemotherapy. Top panel: Filgrastim is given for 4 days and stopped when the ANC is still increasing. Middle panel: Filgrastim is given for 8 days and stopped just before the nadir. Bottom panel: The duration of filgrastim is 12 days and filgrastim is stopped when neutrophil levels have reached normal ANC after the expected nadir.

given for 4, 8 and 12 days. When starting treatment on day 1, one can see that a rapid rise in neutrophil occurs, followed by the decrease and a second increase in ANC. The amplitude of this second increase as well as the depth of the expected nadir vary with the length of treatment. For each duration of filgrastim from 1 to 14 days, we computed the nadir and maximum neutrophil counts of the second ANC increase over 2 cycles of chemotherapy (see Fig. 4.8). We found that the longer the treatment, the higher are the maximum neutrophil levels. More interestingly, depths of the nadir are similar for treatment duration of more than 8 days. With this model, administering filgrastim for 8

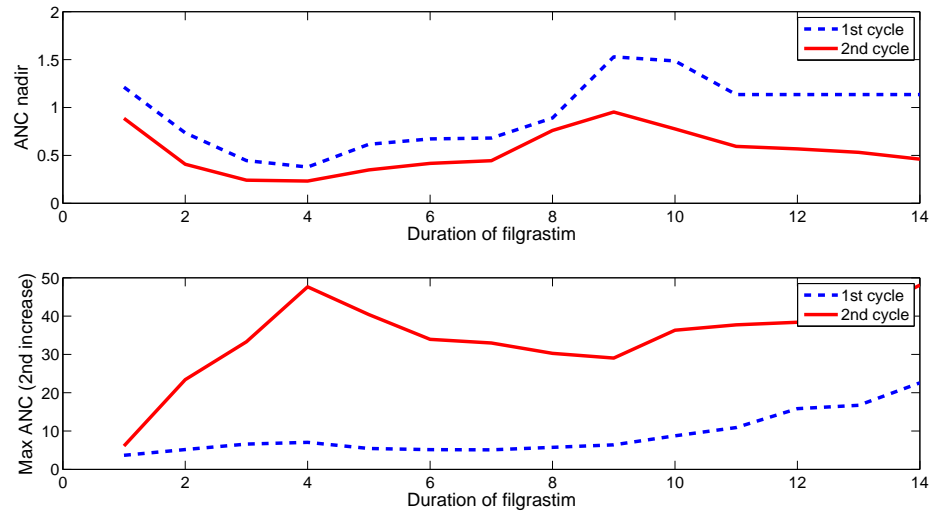


Fig. 4.8 Effects of the duration of daily filgrastim ($5\mu\text{g}/\text{kg}$) over 2 cycles of chemotherapy (3 weeks between chemotherapy treatment). Filgrastim is started on day 1. Top panel: Values of the chemotherapy-induced nadir with respect to the duration of treatment. Bottom panel: Maximum neutrophil levels reached following the expected nadir. Neutrophil levels are in $\times 10^8$ cells/kg.

days correspond to stopping it just before the expected neutrophil nadir whereas ending G-CSF when ANC are back to a normal after the nadir corresponds to a duration of 12 days of treatment. Therefore, our simulations suggest that the duration of filgrastim therapy could be reduced by stopping treatment when the nadir is reached, instead of waiting for the ANC to get back to normal levels.

It is worth noting that only one day of filgrastim given the day following chemotherapy leads to a reduced increase of the ANC and a higher neutrophil nadir, as shown in Fig. 4.9. As in the case of delayed treatment discussed above, the ANC response remains relatively stable around normal values, without falling down to very low neutrophil levels. We make the hypothesis that this reflects the existence of another stable solution in the system. From a mathematical point of view, many factors influence the response of the model, among which the historical values of all variables (stem cells, precursors, neutrophils) as well as the choice of parameters. Therefore, even though our model predicts the existence of such solution and suggests that only one day of filgrastim could be successful in managing chemotherapy-induced neutropenia, further investigation would be needed since, to our knowledge, no data on this is available in the literature. As one

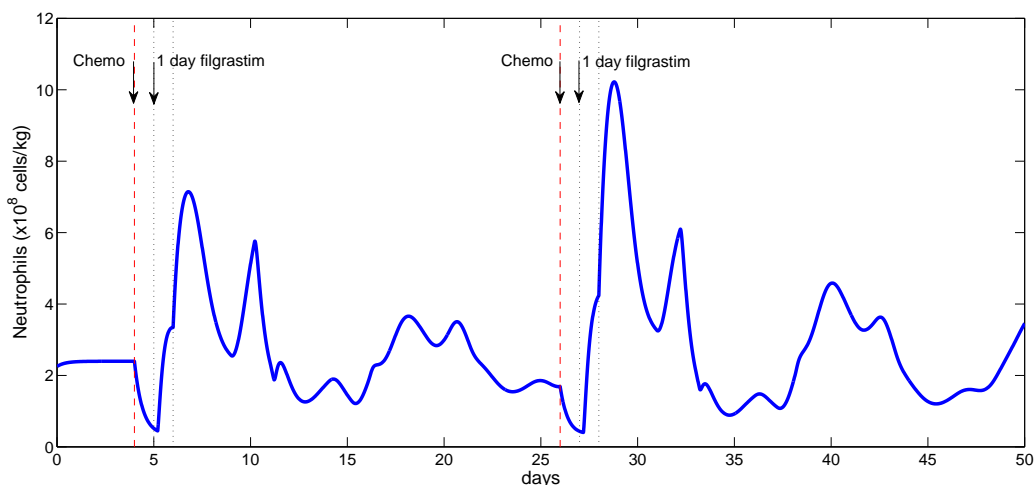


Fig. 4.9 Simulation of filgrastim ($5\mu\text{g}/\text{kg}$) given only for one day the next day after chemotherapy. Two cycles of chemotherapy (3 weeks between chemotherapy treatment) are shown. ANC levels remain close to normal values and no deep nadir occurs. Neutrophil levels are in $\times 10^8$ cells/kg.

can see in Fig. 4.8, the nadirs and maximum values with respect to the duration of treatment have similar behaviour for both cycles, except that the nadirs are lower and maximums are higher for the second cycle. We do not have a clear explanation for that difference. However, since we are mainly interested in the dynamical properties of the model, we believe that this quantitative aspect is of less importance and focus on the fact that the same types of variations in nadirs and maximum values hold for both cycles.

4.4.4 Simulation of Pegfilgrastim responses following chemotherapy

In this section, we study the effects of pegfilgrastim administration following chemotherapy. Recall that clinical guidance for pegfilgrastim calls for a 6 mg dose no earlier than 24 hours following the chemotherapy treatment. Using the parameters listed in Table 4.1, we integrated the model and looked at the effects of a bolus subcutaneous administration of $100 \mu\text{g}/\text{kg}$ (corresponding to the standard 6 mg dose for a 60 kg subject). As with filgrastim, we found that modifying the starting day of the treatment

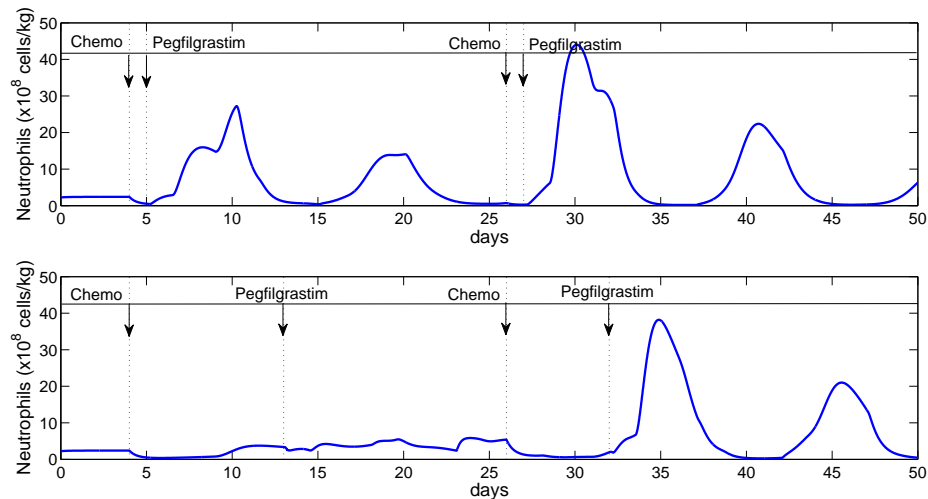


Fig. 4.10 Effects of changing the starting day of pegfilgrastim treatment on the neutrophil count. Top panel: Pegfilgrastim ($100\mu\text{g}/\text{kg}$) is given 1 day after chemotherapy. Bottom panel: Pegfilgrastim ($100\mu\text{g}/\text{kg}$) is given 8 days (first cycle) and 5 days (2nd cycle) after chemotherapy.

may change the qualitative response of the ANC levels. This was expected since a number of studies have shown that pegfilgrastim has the same effects as filgrastim for

treating neutropenia (Holmes et al. (2002), Green et al. (2003), Molineux et al. (1999)). Our model agrees with that. In the first panel of Fig. 4.10, pegfilgrastim is given 1 day after the chemotherapy treatment, resulting in a large ANC response. In the second panel, pegfilgrastim is administered 8 days (first cycle) and 5 days (second cycle) after the chemotherapy treatment. The ANC increase is of less amplitude in the first cycle. Thus, as for filgrastim, the model predicts that delaying G-CSF administration may result in different qualitative behaviours (see Fig. 4.6 for the minimum and maximum values with respect to the starting day of G-CSF) and potentially abolish the nadir typically observed after the large ANC rise.

4.5 Bifurcation and multistability

Numerical results from Section 4.4 suggest that different types of qualitative behaviours can be observed when performing simulations of the mathematical model. By varying the starting day or duration of G-CSF treatment following chemotherapy, the model displayed either a large ANC response followed by low nadir or a smaller ANC increase that remains relatively stable. We hypothesize that this is due to coexistence of multiple stable solutions (multistability) in the system. Multistability (or bistability in the case of two coexisting stable solutions) has been shown to explain different types of biological responses (Angeli et al. (2004), Ferrell (2002), Ozbudak et al. (2004)). In particular, it has been invoked to explain the establishment of mutually exclusive phases and oscillatory behaviour in cell cycle (Pomerening et al. (2003), Sha et al. (2003)), properties of mitogen-activated protein kinase cascades in animal cells (Ferrell and Machleder (1998), Bagowski and Ferrell (2001), Bhalla et al. (2002)), cell cycle regulatory circuits in *Xenopus* and *Saccharomyces cerevisiae* (Cross et al. (2002), Pomerening et al. (2003)) as well as switch-like biochemical responses in the *lac* operon and *trp* operon (Yildirim and Mackey (2003), Yildirim et al. (2004), Santillan and Mackey (2004), Santillan et al. (2007)). It has also been suggested that bistability could account for oscillations triggered by G-CSF in non-cycling forms of neutropenia (Foley et al. (2006)). In this section, we study some dynamical aspects of the mathematical model in order to validate the existence of multistability.

The fact that we obtained different qualitative responses in our simulations is an indication that the system undergo a bifurcation. A bifurcation occurs when a small

change in parameter values (bifurcation parameters) causes a sudden qualitative change in the long-term dynamical behaviour of the system (the reader is referred to Beuter et al. (2003) and Strogatz (2000) for more details on bifurcation theory in dynamical systems). To better analyze the dynamical properties of the model, we first choose a relevant bifurcation parameter among all the parameters of the model. Since we are interested in the effects of G-CSF, we consider only the main part of the model (variables S, P, N , and W , see Fig. 4.1) and take G-CSF concentration G as the bifurcation parameter. Recall that the effects of G-CSF are modeled through the functions $A(G), V_n(G), \gamma_S(G), \gamma_p(G)$ and $\gamma_N(G)$.

We attempted to compute a bifurcation diagram for the neutrophil level solutions with respect to G-CSF concentration G . We used `DDEBiftool`, a `matlab` package for bifurcation analysis of delay differential equation with constant or state-dependent delays. Although the computation of steady state solutions was successful, numerical problems occurred when computing branches of periodic solutions. In fact, the system is very complex and it appears that several branches of periodic solutions (many of which are unstable) coexist. Moreover, numerical instabilities made the computation difficult. Nevertheless, we were able to explore some dynamical aspects of the DDE model by numerically integrating the main part of the model and varying G (again considered as a parameter as explained above). We found that for low concentration of G-CSF after chemotherapy, oscillatory behaviour is observed, indicating the existence of a locally stable periodic solution. Also, for large values of G-CSF concentration, solutions settled down a locally stable steady state. More interestingly, we were able to illustrate the bistable nature of the system by keeping a fixed value of G and varying only the initial function (history). We obtained two qualitatively different responses as shown in Fig. 4.11: a stabilization toward a locally stable steady state (top panel) and sustained oscillations (bottom panel). This shows that two coexisting stable solutions exist and may provide an explanation for the different qualitative behaviours observed in Section 4.4. In fact, changing the starting day of G-CSF after chemotherapy is equivalent to changing the past values of the state variables (initial functions).

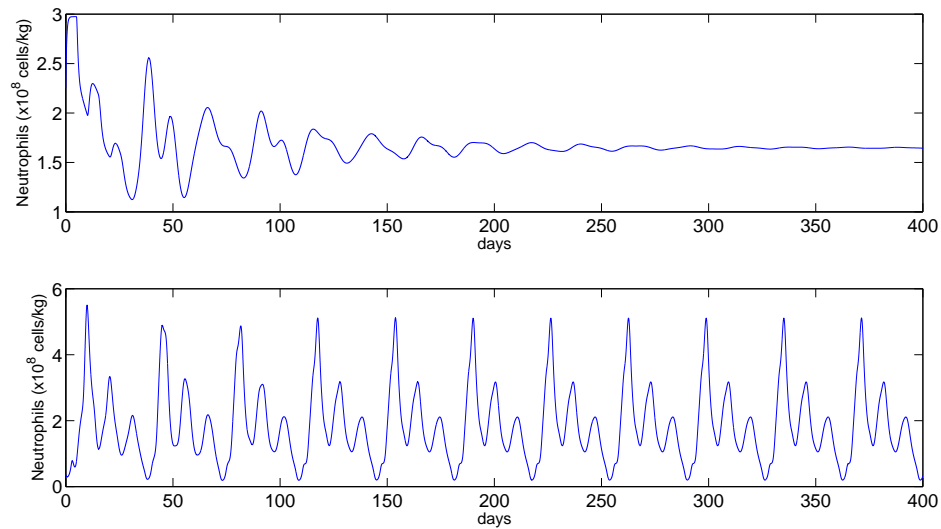


Fig. 4.11 Bistable behaviour in the model. Simulation of the DDE model for a fixed value of $G = 0.9$. The initial functions (history) of the variables S , P , N , and W are different for each panel. Top panel: the solution settles down to a steady state. The constant initial function corresponding to steady state solutions of Section 4.4.1 was used. Bottom panel: sustained oscillations are present, indicating the existence of a stable periodic orbit. The initial function was the oscillatory solution obtained when using $G = 0.8$ and starting with constant steady state values. Parameters used are the same as in Table 4.1 except that $b_i = 10$ ($i = A, v, s, p, n$) to avoid numerical instabilities.

4.6 Discussion

We have developed a mathematical model of white blood cell production to study schedules of G-CSF treatment following chemotherapy. The model incorporates explicitly the effects of G-CSF, namely a decrease in postmitotic transit time, an enhanced amplification, and effects on apoptosis rates. Experimental data for two recombinant forms of G-CSF, filgrastim and pegfilgrastim, were successfully reproduced with the mathematical model.

Through numerical simulations, we studied the effects of varying the starting day of G-CSF administration following chemotherapy for both filgrastim and pegfilgrastim. We found that this could result in two qualitatively different responses: a large neutrophil increase followed by a deep nadir (early treatment) or a smaller ANC increase that remains relatively stable and does not go to very low levels (delayed treatment). We showed that this can apparently be explained by the coexistence of two stable solutions in the system (oscillations and steady state). In fact, the model dynamics are very rich and the outcome of numerical simulations depend on several factors (parameter values, initial function, etc.). Similarly, several aspects also influence responses to G-CSF therapy in clinical practice (age, chemotherapy regimen and intensity, type of cancer, ...). As a result, there are great variations in the ANC among individuals and also from one cycle to another for the same patient. Therefore, the reader should consider our results from a qualitative point of view and focus on the fact that changing the starting day of G-CSF could lead to different behaviours and potentially abolish the neutrophil nadir.

We also studied the effects of the duration of filgrastim treatment. Contrary to clinical guidance, which suggests administering filgrastim until ANC levels are back to normal following the expected nadir, our simulations predict that stopping it just before the nadir would have similar effects while reducing the amount of drug.

Earlier modeling work on alternative G-CSF schedules for cyclical neutropenia (Foley et al. (2006) and Colijn et al. (2007)) also suggested that different treatment regimens can lead to significantly different responses. Our results substantiate this and propose practical strategies for reducing the cost of G-CSF treatment following chemotherapy. Moreover, our model could easily be used for exploring other issues concerning G-CSF treatment. Indeed, it is easy to change the dose and the frequency of treatment in the model. One could think of other interesting treatment regimens that could be studied,

such as the effects of administering G-CSF every other day, instead of everyday for example. The model could also be used for assessing different mechanisms of action of G-CSF. For instance, it has been shown that G-CSF increases the amplification factor for the neutrophils precursors (Lord et al. (1989)). However, it is not clear whether this is due to a real increase in the number of cell divisions, a decrease in the apoptosis rate in the precursors or a combination of both. In this study, we assume both mechanisms were affected by G-CSF. Since our model accounts for these two effects separately, one could study in more detail the impact of each mechanism. In conclusion, despite the great variability among individuals, we believe that the model can provide interesting insights on the effects of G-CSF treatment following chemotherapy and help to better understand the dynamical nature of the underlying system.

4.7 Appendix

4.7.1 Derivation of the model

We show the derivation of the DDE model. First, we briefly present a generic equation for a PDE model and then present how such a model can be expressed as delay differential equations. For a full derivation, see the review by Foley and Mackey (2008).

Let $x(t, a)$ be the the cell density at time t and age a . The general form of equation for the cell density $x(t, a)$ of this model is

$$\frac{\partial x}{\partial t} + V(G(t)) \frac{\partial x}{\partial a} = -\gamma(G(t))x \quad t > 0, a \in [0, \tau],$$

with some boundary condition $x(t, 0) = H(t)$ and initial condition $x(0, a) = \phi(a)$. By integrating with respect to the age variable and using the method of characteristics to find an expression for $x(t, \tau)$, one obtains the following delay differential equation (DDE):

$$\frac{dX}{dt} = V(G(t)) \left[H(t) - H(t - T_\tau) \exp \left(- \int_0^{T_\tau} \gamma(G(w)) dw \right) \right] - \gamma(G(t))X(t),$$

where $X(t) = \int_0^\tau x(t, a) da$ is the total number of cells at time t . Note that if the death

rate γ is a constant, the equation reduces to

$$\frac{dX}{dt} = V(G(t)) [H(t) - H(t - T_\tau)e^{-\gamma T_\tau}] - \gamma X(t).$$

We now apply this technique to equations (4.1)-(4.5) to express the model as delay differential equation for the total population numbers $S(t)$, $P(t)$, $N(t)$ and $W(t)$. First, we integrate equation (4.2) for $s(t, a)$ with $s(t, 0) = 2m(t, \tau_s)$ and $\lim_{a \rightarrow \infty} s(t, a) = 0$. We obtain

$$\begin{aligned} \frac{dS}{dt} + \lim_{a \rightarrow \infty} s(t, a) - s(t, 0) &= -[\beta(S(t)) + \delta(W(t))]S(t). \\ \implies \frac{dS}{dt} &= 2m(t, \tau_s) - [\beta(S(t)) + \delta(W(t))]S(t). \end{aligned} \quad (4.A.1)$$

In order to get an expression for $m(t, \tau_s)$, we have to solve equation (4.1)

$$\frac{\partial m}{\partial t} + \frac{\partial m}{\partial a} = -\gamma_s(G(t))m \quad t > 0, a \in [0, \tau_s],$$

with $m(t, 0) = \beta(S(t))S(t)$. We obtain

$$\begin{aligned} m(t, \tau_s) &= m(t - \tau_s, 0) \exp\left(\int_0^{\tau_s} -\gamma_s(G(t)) dt\right) \\ &= \beta(S(t - \tau_s))S(t - \tau_s) \exp\left(\int_0^{\tau_s} -\gamma_s(G(t)) dt\right). \end{aligned}$$

Substituting $m(t, \tau_s)$ in equation (4.A.1) yields the equation for $S(t)$:

$$\frac{dS}{dt} = 2\beta(S_{\tau_s})S_{\tau_s} \exp\left(\int_0^{\tau_s} -\gamma_s(G(t)) dt\right) - [\beta(S) + \delta(W)]S. \quad (4.A.2)$$

Using constant apoptosis rate, the equation becomes

$$\frac{dS}{dt} = 2\beta(S_{\tau_s})S_{\tau_s}e^{-\gamma_s\tau_s} - [\beta(S) + \delta(W)]S. \quad (4.A.3)$$

We use the notation $S_{\tau_s} := S(t - \tau_s)$ and $G_{\tau_s} := G(t - \tau_s)$. More generally, a subscript on a variable denotes the delay in this variable.

Next, we derive an expression for the proliferative population of precursors cells $P(t)$ by

solving the partial differential equation (4.3) with boundary condition $p(t, 0) = \delta(W(t))S(t)$. Integrating with respect to a leads to

$$\frac{dP}{dt} + p(t, \tau_p) - p(t, 0) = -\gamma_p(G(t))P(t). \quad (4.A.4)$$

The value of $p(t, \tau_p)$ is found by solving the partial differential equation with the method of characteristics presented in Foley and Mackey (2008). We directly obtain

$$p(t, \tau_p) = \delta(W_{\tau_p})S_{\tau_p} \exp\left(-\int_0^{\tau_p} \gamma_p(G(t)) dt\right).$$

Substituting in equation (4.A.4), we get the following delay differential equation for the proliferative neutrophil precursors:

$$\frac{dP}{dt} = -\gamma_p(G)P + \delta(W)S - \delta(W_{\tau_p})S_{\tau_p} \exp\left(-\int_0^{\tau_p} \gamma_p(G(t)) dt\right). \quad (4.A.5)$$

Similarly, we derive an equation for the non-proliferative precursors cells $N(t)$ with $n(t, 0) = A(G(t))p(t, \tau_p)$ and obtain

$$\frac{dN}{dt} + V_n(G(t))[n(t, \tau_n) - n(t, 0)] = -\gamma_n(G(t))N(t). \quad (4.A.6)$$

The value of $n(t, \tau_n)$ is given by

$$\begin{aligned} n(t, \tau_n) &= n(t - \bar{\tau}_n, 0) * e^{-\gamma_n \bar{\tau}_n} \\ &= A(G_{\bar{\tau}_n})\delta(W_{\tau_p})S_{\tau_p} \exp\left(-\int_0^{\tau_p} \gamma_p(G(t)) dt - \int_0^{\bar{\tau}_n} \gamma_n(G(t)) dt\right), \end{aligned}$$

with $\bar{\tau}_n$ satisfying

$$\tau_n = \int_{t-\bar{\tau}_n}^t V_n(G(w)) dw.$$

Substituting in equation (4.A.6), we obtain a delay differential equation for the

non-proliferative neutrophil precursors:

$$\begin{aligned} \frac{dN}{dt} = & -\gamma_n(G)N + V_n(G)\delta(W_{\tau_p})S_{\tau_p} \exp\left(-\int_0^{\tau_p} \gamma_p(G(t)) dt\right) * \\ & * \left[A(G) - A(G_{\bar{\tau}_n}) * \exp\left(-\int_0^{\bar{\tau}_n} \gamma_n(G(t)) dt\right) \right] \end{aligned} \quad (4.A.7)$$

Finally, we derive an equation for the circulation white blood cell population $W(t)$ by solving equation (4.5) with $w(t, 0) = n(t, \tau_p)$ and $\lim_{a \rightarrow \infty} w(t, a) = 0$. Integrating with respect to a gives

$$\begin{aligned} \frac{dW}{dt} + [\lim_{a \rightarrow \infty} w(t, a) - w(t, 0)] &= -\gamma_w W(t) \\ \implies \frac{dW}{dt} &= n(t, \tau_n) - \gamma_w W(t). \end{aligned}$$

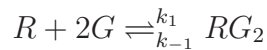
Substituting the value of $n(t, \tau_n)$ leads to the governing equation for white blood cells:

$$\frac{dW}{dt} = -\gamma_w W + A(G_{\bar{\tau}_n})\delta(W_{\tau_p})S_{\bar{\tau}_p} \exp\left(-\int_0^{\tau_p} \gamma_p(G(t)) dt - \int_0^{\bar{\tau}_n} \gamma_n(G(t)) dt\right). \quad (4.A.8)$$

Notice that we have not derived an equation for the proliferative stem cell compartment $m(t, a)$ because it was not necessary to do so. Indeed, it can be seen from Fig. 4.1 that the dynamics of this compartment is included in a loop and hence, in the equation for the resting stem cells $s(t, a)$. We only solved the pde (4.1) to get the value of $m(t, \tau_s)$ when solving for the resting stem cells $S(t)$.

4.7.2 Derivation of the fraction of bound G-CSF receptors ($F(G)$)

We define an expression for the fraction $F(G)$ of G-CSF receptors that are bound. To do so, we consider more closely the process of binding of G-CSF to its receptor. On a single neutrophil, there are between 200 to 1000 binding sites. Each binding sites contain a G-CSF receptor, which can bind to two G-CSF molecules (Layton and Hall (2006)). We assume that two G-CSF molecules bind simultaneously. This could be represented by the following submodel:



where R are G-CSF receptors, G is G-CSF, RG_2 is the bound complex and k_1 and k_{-1} and binding rate constants. From the law of mass action,

$$\frac{d[RG_2]}{dt} = k_1[R][G]^2 - k_{-1}[RG_2], \quad (4.A.9)$$

where the brackets denote concentrations. At steady state, $\frac{d[RG_2]}{dt} = 0$ and therefore, $k_1[R][G]^2 = k_{-1}[RG_2]$. To simplify, let us scale out one parameter and define $k = k_{-1}/k_1$. Also, let T be the total number of receptors (free and bound in the complex RG_2):

$$T = R + RG_2.$$

Thus, we obtain

$$\begin{aligned} & [R][G]^2 &= k[RG_2] \\ \implies & [T - RG_2][G]^2 &= k[RG_2] \\ \implies & [T][G]^2 &= [RG_2]([G]^2 + k) \\ \implies & \frac{[RG_2]}{[T]} &= \frac{[G]^2}{[G]^2 + k}. \end{aligned}$$

Hence, the fraction of bound G-CSF receptors ($\frac{[RG_2]}{[T]}$) is given by

$$F(G) = \frac{G^2}{G^2 + k}. \quad (4.A.10)$$

Therefore, the expression for clearance of G-CSF is $(\gamma_G + \sigma WF(G))G$.

4.7.3 Parameter estimation

We present the parameter estimation for the main compartment as well as the G-CSF compartment (for both filgrastim and pegfilgrastim).

Parameter estimation for the main compartment

In this section, we estimate the parameters of the main part of the model using experimental data and other information from the literature. A list of the parameters is

presented in Table 4.1. Since we are interested in studying the effects of G-CSF following chemotherapy, we need to be able to mimic the three following situations with the mathematical model:

1. *Cancer*: This set of parameters represents the characteristics of people suffering from cancer prior to chemotherapy. We do not look at a specific type of cancer, but we do consider only nonmyeloid types of cancer. The parameters used for this category are the same as for healthy subjects.
2. *Chemotherapy*: The effects of myelosuppressive anti-cancer drugs are often associated with a significant incidence of severe neutropenia. We mimic chemotherapy by increasing the apoptosis rates γ_s , γ_p and γ_n (Hannun (1997)) and keeping all the other parameters fixed.
3. *G-CSF*: G-CSF is used for treating chemotherapy-induced neutropenia. The effects of G-CSF are included explicitly in the model through the functions $A(G)$, $V_n(G)$, $\gamma_s(G)$, $\gamma_p(G)$ and $\gamma_n(G)$.

Age at the end of different phases τ_i The age at the end of a given phase will not be dependent on the G-CSF concentration. To mimic the decrease or increase in the time spent in the proliferative or non-proliferative phase, we increase or decrease the aging velocity.

- τ_s : In Bernard et al. (2003), τ_s was estimated to lie between 1.4 and 4.2 days. We use the same value of 2.8 days as in Bernard et al. (2003).
- τ_p : From Israels and Israels (2002), cells spend about 6 days in the mitotic pool under normal physiological state whereas in Mackey and Dormer (1982), they estimated 3.27 days. We take $\tau_p = 5$ days.
- τ_n : The transit time through the postmitotic pool under normal physiological conditions (no exogenous G-CSF) is between 6 and 8.4 days (Israels and Israels (2002), Price et al. (1996), Roskos et al. (2006)). We take $\tau_n = 6$ days. Under G-CSF treatment, τ_n varies from 2.9 days ($4.3\mu\text{g}/\text{kg}$) to 4.3 days ($0.4\mu\text{g}/\text{kg}$) (Price et al. (1996)) and we account for this decrease by changing the aging velocity $V_n(G)$.

Aging velocities for the non-proliferative phase $V_n(G)$ We use the following bounded function for modeling the aging velocity:

$$V_n(G) = (V_{max} - 1) \frac{G}{G + b_v} + 1,$$

where V_{max} is the maximum velocity and the parameter b_v controls how fast the velocity is increasing. Notice that for $G = 0$, the velocity is 1, so that it takes τ_n days to go through the phase. We set V_{max} to τ_n , so that the minimum transit time for the postmitotic pool is one day (Lord et al. (1989)). In order to determine the value of the parameter b_v , we simulated G-CSF (filgrastim and pegfilgrastim) administration in the system and fitted the model to data from Green et al. (2003) using a nonlinear least squares approach (see Fig. 4.12). We also ensured that the aging velocity doubles under G-CSF. Indeed, from Price et al. (1996), we have that the time spent in the postmitotic pool is reduced from 6.4 days (no G-CSF) to 2.9 days ($5 \mu\text{g}/\text{kg}$ G-CSF/day). Using $b_v = 0.001$ for filgrastim and $b_v = 0.08$ for pegfilgrastim, we obtain that $\bar{\tau}_n$ (time spent in postmitotic pool) ranges between 2.9 and 6 days.

Apoptosis rates γ_i There are 4 apoptosis rates to consider. Three of them (γ_s, γ_p and γ_n) vary in response to G-CSF and chemotherapy, whereas we assume that the death rate from the circulating neutrophils γ_w remains unchanged during chemotherapy and G-CSF treatment. We take $\gamma_w = 2.4 \text{ days}^{-1}$ as in Bernard et al. (2003). Next, we look at the three other apoptosis rates for cancer subjects, under chemotherapy and G-CSF treatment.

- *Cancer*: To simulate nonmyeloid cancer with the model, we use the same values as for healthy individuals. We take $\gamma_s = 0.07 \text{ days}^{-1}$ (Bernard et al. (2003)). In Mackey et al. (2003), they estimated γ_p to vary between 0.27 and 0.31 days^{-1} (average 0.28 days^{-1}). We take $\gamma_p = 0.27 \text{ days}^{-1}$. Finally, we assume that the death rate for the proliferative and non-proliferative precursors are the same ($\gamma_n = 0.27 \text{ days}^{-1}$).
- *Chemotherapy*: It has been shown that myelosuppressive chemotherapy induces apoptosis in cells (Hannun (1997)). Moreover, it has been reported that chemotherapy may induce oscillations in the blood neutrophil count (Kennedy (1970)). Thus, we chose the death rate values so that the model displays oscillations

(the minimal value so that we get oscillations). Indeed, increasing the apoptosis in the model destabilizes the system and triggers oscillations (see later). However, we need to be careful not to increase the death rates too much because it leads to failure in the system (number of proliferative cells goes below zero). Since the apoptosis rates are maximal under chemotherapy, we denote the parameters by the superscript "max". We take $\gamma_s^{max} = 0.2 \text{ days}^{-1}$, $\gamma_p^{max} = 0.45 \text{ days}^{-1}$ and $\gamma_n^{max} = 0.45 \text{ days}^{-1}$.

- *G-CSF*: As mentioned said above, G-CSF inhibits the chemotherapy-induced apoptosis. Therefore, we will mimic the action of G-CSF following chemotherapy by decreasing the apoptosis rates γ_S, γ_p and γ_N as a function of G-CSF. We use the following decreasing bounded functions:

$$\gamma_s(G) = (\gamma_s^{max} - \gamma_s^{min}) \frac{b_s}{G + b_s} + \gamma_s^{min}, \quad (4.A.11)$$

$$\gamma_p(G) = (\gamma_p^{max} - \gamma_p^{min}) \frac{b_p}{G + b_p} + \gamma_p^{min}, \quad (4.A.12)$$

$$\gamma_n(G) = (\gamma_n^{max} - \gamma_n^{min}) \frac{b_n}{G + b_n} + \gamma_n^{min}. \quad (4.A.13)$$

where γ_i^{min} and γ_i^{max} are respectively the minimum and maximum values for the apoptosis rates ($i = s, p, n$) and the b_i are parameters that control the steepness of the function. We use minimum values γ_i^{min} to be the same as the cancer (healthy) values and the maximum values to be the same as the chemotherapy values. The parameters b_s, b_p and b_n have an important effect on the model's response to G-CSF administration. A low value of b_i means that the death rate will remain near its maximum value γ_i^{max} longer, whereas high values of b_i lead to a more rapid decrease toward its minimum value γ_i^{min} . Moreover, since the pharmacokinetic properties of filgrastim and pegfilgrastim are different, values differ depending on the type of G-CSF recombinant form. We used data from Green et al. (2003) to fit values (using a least squares approach as before) and obtain $b_s = 0.01$ and $b_p = b_n = 0.05$ for filgrastim and $b_s = 0.01$ and $b_p = b_n = 1$ for pegfilgrastim (see Fig. 4.12).

Amplification factor $A(G)$ A study by Lord et al. (1989) reported an extra 3.2 amplification divisions in neutrophil development with added G-CSF. This corresponds to

a number of effective divisions (N_E), i.e. it includes the effects of apoptosis in the mitotic compartment. However, the apoptosis rate γ_p is included explicitly in our model, and therefore we are interested in the absolute number of divisions (N_A). Using the relation $N_A = N_E e^{-\gamma_p \tau_p}$ and parameters listed in Table 4.1, we obtain that 3.2 effective divisions correspond to 5.1 absolute cell divisions. Roskos et al. (2006) estimated an maximum amplification factor of 4 extra effective divisions, corresponding to 5.8 extra cell divisions. We use a simple bounded function to model the amplification factor as a function of G :

$$A(G) = (A_{max} - A_{min}) \frac{G}{G + b_A} + A_{min}. \quad (4.A.14)$$

In Bernard et al. (2003), they estimated that 15.2 cell divisions occur in the mitotic compartment. We use $A_{min} = 2^{16} \times 10^2$ and $A_{max} = 2^{21} \times 10^2$ so that it leads to relevant steady states values for the neutrophil number. The parameter b_A influences how fast the amplification is increased under G-CSF. The smaller b_A , the faster A increases. We simulated daily filgrastim administration ($5\mu\text{g}/\text{kg}$) as well as a bolus $100\mu\text{g}/\text{kg}$ of pegfilgrastim and fitted the model to data from Green et al. (2003). We obtained values of $b_A = 0.35$ (filgrastim) and $b_A = 1.05$ (pegfilgrastim) (see Fig. 4.12). With these values, the amplification ranges between $2^{16} \times 10^2$ (655) to $2^{18.3} \times 10^2$ (3700). For daily doses of $10\mu\text{g}/\text{kg}$ of filgrastim, amplification goes up to approximately 4500×10^2 (18.8 divisions). This is less than the estimate of 3.2 extra effective cell divisions reported in Lord et al. (1989), but we consider this is reasonable. Lower values of b_A lead to higher ANC responses.

Differentiation rate from stem cell $\delta(W)$ We use $\delta(W) = f_0 \frac{\theta_1}{\theta_1 + W}$ as in Colijn and Mackey (2005a) with $f_0 = 0.40 \text{ days}^{-1}$ and $\theta_1 = 0.36 \times 10^8 \text{ cells}/\text{kg}$. This is a monotone decreasing function, accounting for the negative feedback loop in the system (if W decreases, then $\delta(W)$ increases, leading to an increase in differentiation and eventually an increase in W).

Reentry into stem cell proliferative phase $\beta(S)$ We assume that $\beta(S)$ does not depend on G-CSF and we take the decreasing Hill function $\beta(S) = k_0 \frac{\theta_2^2}{\theta_2^2 + S^2}$ as in Colijn and Mackey (2005a). Values of k_0 and θ_2 are 8.0 days^{-1} and $0.3 \times 10^6 \text{ cells}/\text{kg}$.

Parameter Name	Value Used	Unit	Sources
<i>Stem cell compartment</i>			
S_*	1.1 (0.0001-1.1)	$\times 10^6$ cells/kg	Mackey (2001)
γ_s	0.05 (0.01-0.20)	days ⁻¹	Bernard et al. (2003)
γ_s^{min}	0.05	days ⁻¹	calculated
γ_s^{max}	0.20	days ⁻¹	calculated
b_s	0.01	-	calculated
τ_s	2.8 (1.4 - 4.2)	days	Bernard et al. (2003)
k_0	8.0 (2.0-10.0)	days ⁻¹	Colijn and Mackey (2005a)
θ_2	0.3	$\times 10^6$ cells/kg	Colijn and Mackey (2005a)
f_0	0.40	days ⁻¹	Colijn and Mackey (2005a)
θ_1	0.36 (0.1-2.0)	$\times 10^8$ cells/kg	Colijn and Mackey (2005a)
<i>Prolif. precursors compartment</i>			
P_*	2.11	$\times 10^9$ cells/kg	Dancey et al. (1976)
γ_p	0.27	days ⁻¹	Mackey et al. (2003)
γ_p^{min}	0.27	days ⁻¹	Mackey et al. (2003)
γ_p^{max}	0.45	days ⁻¹	calculated
b_p (filgrastim)	0.05	-	fit
b_p (pegfilgrastim)	1	-	fit
τ_p	5	days	Israels and Israels (2002)
A_{max}	20972	100	Bernard et al. (2003)
A_{min}	655	100	Bernard et al. (2003)
b_A (filgrastim)	0.35	-	fit
b_A (pegfilgrastim)	1.05	-	fit
<i>Non-prolif. precursors compartment</i>			
N_*	5.59	$\times 10^9$ cells/kg	Dancey et al. (1976)
γ_n	0.27	days ⁻¹	Mackey et al. (2003)
γ_n^{min}	0.27	days ⁻¹	Mackey et al. (2003)
γ_n^{max}	0.45	days ⁻¹	calculated
b_n (filgrastim)	0.05	-	fit
b_n (pegfilgrastim)	1	-	fit
τ_N	6 (3.27-8.4)	days	Price et al. (1996)
V_{max}	6	-	calculated
b_v (filgrastim)	0.001	-	fit
b_v (pegfilgrastim)	0.08	-	fit
<i>Neutrophils compartment</i>			
W_*	6.9 (4.0 - 10.0)	$\times 10^8$ cells/kg	Abkowitz et al. (1988); Beutler et al. (1995)
γ_w	2.4 (2.2-2.5)	days ⁻¹	Bernard et al. (2003)
<i>G-CSF compartment</i>			
X_*	0.1	$\mu\text{g}/\text{kg}$	Colijn et al. (2007)
G_*	0	$\mu\text{g}/\text{ml}$	Colijn et al. (2007)
V_B	76	mL/kg	Hayashi et al. (2001), Colijn et al. (2007)
G_{prod}	7.2×10^{-29}	$\mu\text{g}/(\text{ml}*\text{day})$	Vainstein et al. (2005)
<i>Filgrastim</i>			
k_T	1.68	day ⁻¹	Hayashi et al. (2001), Colijn et al. (2007)
k_B	9.84	day ⁻¹	Colijn et al. (2007)
σ	0.72	kg/day	Stute et al. (1992); Kearns et al. (1993a); Colijn et al. (2007)
γ_G	3.36	day ⁻¹	fit
a	1200	$\mu\text{g}/(\text{kg}*\text{day})$	(calculated)
s	0.0083	day	(calculated)
t_{on}	0.0083	day	(calculated)
k	10	-	fit
<i>Pegfilgrastim</i>			
k_T	0	day ⁻¹	Roskos et al. (2006)
k_B	0.32	day ⁻¹	fit
σ	0.01	kg/day	fit
γ_G	1.4	day ⁻¹	fit
a	12048	$\mu\text{g}/(\text{kg}*\text{day})$	(calculated)
s	0.0083	day	(calculated)
t_{on}	0.0083	day	(calculated)
k	0.01	-	fit

Table 4.1 Parameters of the model (steady state values).

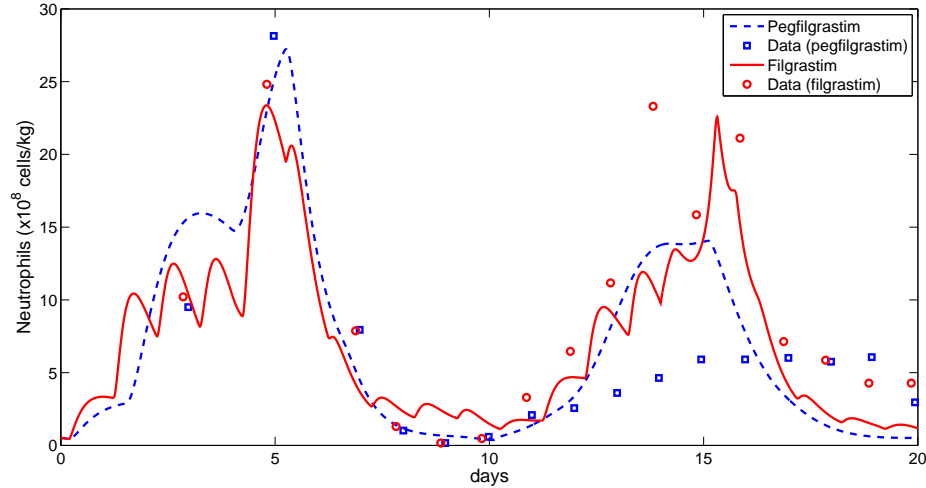


Fig. 4.12 Simulation of daily filgrastim ($5\mu\text{g}/\text{kg}$) and pegfilgrastim ($100\mu\text{g}/\text{kg}$) on cancer patients. Data (squares and circles) are taken from Green et al. (2003). Filgrastim was given for a period of 14 days. Parameters used are listed in Table 4.1.

Parameter estimation for the G-CSF compartment (Filgrastim)

In this section, we present the parameters used for modeling the effects of filgrastim administration with the G-CSF model presented in Fig. 4.2. Most of the pharmacokinetic parameters were taken from published studies on G-CSF kinetics, whereas the remaining ones were calculated or estimated using experimental data taken in the literature.

The values of the parameters are presented in Table 4.1. The rate constants $k_T = 0.07 \text{ hour}^{-1}$ (1.68 day^{-1}) and $\sigma = 0.03 \text{ kg}/\text{hour}$ ($0.72 \text{ kg}/\text{day}$) as well as the volume of blood $V_B = 76 \text{ ml}/\text{kg}$ are the same as in Colijn et al. (2007). The value of the endogenous production rate of G-CSF G_{prod} was taken from Vainstein et al. (2005) who estimated it as $4.83 \text{ pM}/\text{hour}$ ($7.259 \times 10^{-28} \mu\text{g}/(\text{ml blood}) \cdot \text{day}$). To estimate the values of the constant k , γ_G and k_B , we fitted our model to the digitized data from Morstyn et al. (1989), which shows G-CSF blood levels following a bolus subcutaneous injection of $10\mu\text{g}/\text{kg}$ (see Fig. 4.13) in patients who had histologically proven metastatic malignancy. We minimized the mean square error (MSE) of our model with respect to the wanted parameters using `fminsearch` in `matlab`, which implements the Nelder-Mead simplex (direct search) method for multidimensional unconstrained nonlinear minimization.

Despite the fact that this method only minimizes functions locally and that our MSE function has several local minima, this method gave good results because we had good initial guesses to supply to the function. More sophisticated numerical methods that are designed for globally optimizing functions, such as simulated annealing, were tried but the results were not better while the computation time was much higher.

We estimated the value of k to be 10 and the value of γ_G to be 0.14 hour^{-1} (3.36 day^{-1}). In Vainstein et al. (2005), they took γ_G to be 0.06 hour^{-1} although their value could vary between 0.01 and 0.5 hour^{-1} . In Hayashi et al. (2001), they estimated $k_B = 0.10 \text{ hour}^{-1}$ whereas Colijn et al. (2007) used $k_B = 0.25 \text{ hour}^{-1}$. For our study, it was necessary to use a higher value ($k_B = 0.41 \text{ hour}^{-1} = 9.84 \text{ day}^{-1}$) in order to reach to observed levels of G-CSF following a $10\mu\text{g}/\text{kg}$ injection from the experimental data (Morstyn et al. (1989)). As explained above, the exogenous input function $I(t)$ was modeled by a step function. For the purpose of fitting data from Morstyn et al. (1989), we used $a = 50\mu\text{g}/(\text{kg}\cdot\text{hour})$ ($a = 1200\mu\text{g}/(\text{kg}\cdot\text{day})$), $s = 0.2 \text{ hours}$ ($s = 0.0083 \text{ days}$) and $t_{on} = 0.2 \text{ hours}$ ($t_{on} = 0.0083 \text{ days}$), which is equivalent to a bolus injection of $10\mu\text{g}/\text{kg}$. Fig. 4.13 shows a numerical simulation of the model using parameters in Table 4.1.

Parameter estimation for the G-CSF compartment (Pegfilgrastim)

The two-compartment model presented in Fig. 4.2 is used for modeling both filgrastim and pegfilgrastim administrations. However, since the pharmacokinetic properties of these two recombinant forms of G-CSF are different, some parameters need to be changed. Recall that filgrastim is cleared from the body by two mechanisms: renal clearance (the main degradation route) and neutrophil-mediated clearance (Zamboni (2003)). However, pegfilgrastim, which has a larger molecular weight, is less easily cleared by the kidneys. The predominant route of elimination for pegfilgrastim is thus by binding to neutrophil receptors. From a modeling point of view, we make the following modifications:

- Decrease the clearance parameter γ_G associated with renal clearance.
- Decrease the rates k_T and k_B between the tissue and blood compartments. Since Pegfilgrastim is a larger molecule, we assume a slower absorption into the blood (Molineux et al. (1999)) and thus we decrease k_B . In their model, Roskos et al. (2006) included a time lag to account for this delayed absorption. Moreover, we assume $k_T = 0$ as in Roskos et al. (2006).

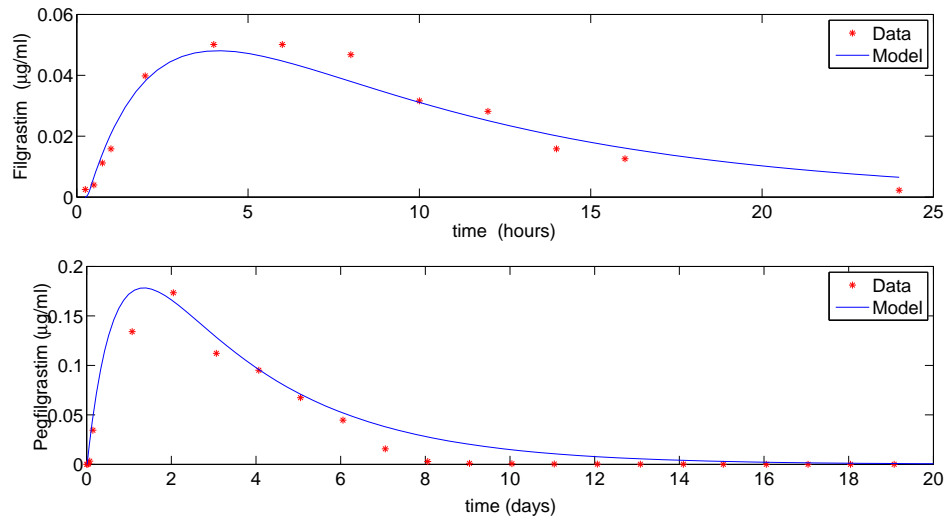


Fig. 4.13 Simulation of bolus subcutaneous injection using the G-CSF model (4.15). Top panel: Filgrastim administration ($10 \mu\text{g}/\text{kg}$). The model (solid line) is compared to data from Morstyn et al. (1989) (stars). Parameters used are listed in Table 4.1. Bottom panel: Simulation of an injection of $100 \mu\text{g}/\text{kg}$ of Pegfilgrastim using the G-CSF model (solid line). The parameters used are $N = 5.6 \times 10^8 \text{ cells}/\text{kg}$, $\gamma_G = 1.4 \text{ day}^{-1}$, $k_T = 0 \text{ day}^{-1}$, $k_B = 0.32 \text{ day}^{-1}$, $\sigma = 0.01 \text{ kg}/\text{day}$ and $k = 0.01$. All other parameters are the same as in Table 4.1. Data from Zamboni (2003) are shown in red stars.

- Modify the parameter k in the function $F(G)$ (fraction of bound receptors). Recall that if we decrease the value of k , this implies that a smaller G-CSF concentration is needed for obtaining the same fraction of bound receptors.
- Modify the binding coefficient σ to account for the delayed absorption of the drug.

To estimate these parameters, we used data from Zamboni (2003) and fitted the model equations (4.15) using the same least square approach as for filgrastim (see above). We used a constant neutrophil value of $N = 5.6 \times 10^8$ cells/kg based on ANC data reported in Zamboni (2003). We obtained the estimated values $\gamma_G = 1.4 \text{ day}^{-1}$, $k_B = 0.32 \text{ day}^{-1}$ and $k = 0.01$ and $\sigma = 0.01 \text{ kg/day}$. Fig. 4.13 shows integration of the model compared to clinical data from Zamboni (2003).

4.7.4 Analytical derivation of steady state values

In this section, we derive analytically the expressions for the steady states and show that there exists a unique positive equilibrium value. First, one needs to solve the following system of equations:

$$\begin{aligned} \frac{dS}{dt}|_* &= 0, & \frac{dN}{dt}|_* &= 0, & \frac{dG}{dt}|_* &= 0, \\ \frac{dP}{dt}|_* &= 0, & \frac{dW}{dt}|_* &= 0, & \frac{dX}{dt}|_* &= 0, \end{aligned}$$

where $|_*$ denotes that the equation are evaluated at steady state values $(S_*, P_*, N_*, W_*, G_*, X_*)$. Note that at equilibrium, delayed variables remain constant (for example, $S(t - \tau_s)_* = S_*$). Assuming, $G_* = 0$ and $X_* = 0$, we first obtain expressions for the steady state values S_* and W_* :

$$\frac{dS}{dt}|_* = 0 \implies \beta(S_*)(2e^{-\gamma_s \tau_s} - 1) = \delta(W_*) \quad (S_* \neq 0), \quad (4.A.15)$$

$$\frac{dW}{dt}|_* = 0 \implies \gamma_w W_* = A_* \delta(W_*) S_* e^{-\gamma_p \tau_p - \gamma_N \tau_N}. \quad (4.A.16)$$

We ignore the trivial zero solution and consider only positive solutions. Solving Equation (4.A.15) for S_* in terms of W_* yields:

$$S_* = \theta_2 \sqrt{\frac{k_0(2e^{-\gamma_s \tau_s} - 1)}{\delta(W_*)} - 1}. \quad (4.A.17)$$

Substituting into Equation (4.A.16), we obtain

$$W_* = \frac{A_* \delta(W_*)}{\gamma_w} \left[\theta_2 \sqrt{\frac{k_0(2e^{-\gamma_s \tau_s} - 1)}{\delta(W_*)} - 1} \right] e^{-\gamma_p \tau_p - \gamma_N \tau_N^*}. \quad (4.A.18)$$

One can find a sufficient condition under which the system has a unique positive steady state solution (a similar proof as in Bernard et al. (2003)). Let the right-hand side of the previous equation be $H(W_*)$ and $r = 2e^{-\gamma_s \tau_s} - 1$. We only need to prove that $\frac{dH}{dW_*}$ is negative. Then, by the fixed point theorem, we conclude that there exists a unique positive steady state. The derivative of $H(W_*)$ with respect to W_* is

$$\frac{dH}{dW_*} = \frac{A_* \theta_2 \delta'(W_*) e^{-\gamma_p \tau_p - \gamma_N \tau_N^*}}{2\gamma_w} \left(\sqrt{\frac{k_0 r}{\delta(W_*)} - 1} \right) * \left(2 - \frac{1}{1 - \delta(W_*)/(k_0 r)} \right). \quad (4.A.19)$$

Since all parameters have positive values and $\delta'(W_*)$ is negative by definition ($\delta(W)$ is a decreasing function), we have that $H'(W_*)$ is negative if and only if the term $\left(2 - \frac{1}{1 - \delta(W_*)/(k_0 r)} \right)$ is positive. This is equivalent to showing

$$\frac{1 - 2\delta(W_*)/(k_0 r)}{1 - \delta(W_*)/(k_0 r)} > 0. \quad (4.A.20)$$

Sufficient conditions for this to hold are $\delta(W_*) < \frac{k_0 r}{2}$ and $r > 0$ ($r = 0.97$ using the parameter values in Table 4.1). Also, from definition of $\delta(W)$, we have that $f_0 > \delta(W)$ for all W . Therefore, a sufficient condition under which there exists one and only one positive steady state solution for W_* is

$$f_0 < \frac{k_0(2e^{-\gamma_s \tau_s} - 1)}{2}. \quad (4.A.21)$$

A unique solution for W_* implies a unique nonzero positive solution for S_* from Equation

(4.A.17). Finally, given values of S_* and W_* , one obtains values for N_* and P_* from the following relationships:

$$\frac{dN}{dt}\Big|_* = 0 \quad \Longrightarrow \quad P_* = \frac{1}{\gamma_p} [\delta(W_*)S_*(1 - e^{-\gamma_p \tau_p})], \quad (4.A.22)$$

$$\frac{dP}{dt}\Big|_* = 0 \quad \Longrightarrow \quad N_* = \frac{1}{\gamma_N} [V_{n*}\delta(W_*)S_*e^{-\gamma_p \tau_p} A_*(1 - e^{-\gamma_N \bar{\tau}_{N*}})]. \quad (4.A.23)$$

Using $(X_*, G_*) = (0, 0)$ and values from Table 4.1 for solving Equations (4.A.17), (4.A.18), (4.A.22) and (4.A.23), one obtains the same steady states values as in the numerical simulations.

Chapter 5

Conclusion

5.1 Discussion

We have reviewed different methods used to model hematological processes and explained how dynamical diseases can provide insight into hematopoietic regulatory mechanisms and help to better understand how clinical treatment can affect their dynamics. In particular, we showed that the administration of granulocyte-colony stimulating factor (G-CSF) may lead to qualitatively different responses. Even though G-CSF is widely used clinically for treating different types of neutropenia, it is not clear if there is an optimal way of giving it. In this thesis, we have studied alternative G-CSF treatment strategies for cyclical neutropenia and chemotherapy-induced neutropenia using a modeling approach and a combination of analysis and computer simulations.

As discussed in Chapter 2, each model has its positive and negative aspects and takes into account more or less detail of the underlying system. The choice of the level of detail is often directed by the question we want to address and by the type of analysis we want to be able to perform with the model. Mathematical modeling is a process that is in constant evolution and the work in this thesis illustrates this. Indeed, the idea of using a mathematical approach to study different G-CSF administration schemes originates from a previous study by Foley et al. (2006). In this work, the authors used a two-dimensional DDE model that includes neutrophils and stem cells. To mimic the effects of G-CSF on cyclical neutropenic dogs, five relevant parameters were changed: the amplification and apoptosis rates, the transit times in the proliferative and differentiating phases and a parameter θ_1 that was part of a negative feedback function. Two sets of parameters (one

for CN and another one for G-CSF) were taken into account and simulating G-CSF effects was carried out by switching from one set of parameters to the other. G-CSF effects were also implicitly included in the feedback function. Although this model assumed several simplifications, it had the advantage of grasping the essential features of cyclical neutropenia and G-CSF treatment while being simple enough to perform complete bifurcation analysis. Interestingly, simulations and analysis revealed that the system was bistable and that varying the time of initiation of G-CSF treatment could affect the dynamical behaviour of the system and potentially abolish oscillations. The fact that different behaviours could be obtained when varying the G-CSF administration schedule motivated the two new models presented in this thesis. In Chapter 3, we were also interested in the treatment of cyclical neutropenia with G-CSF and wanted to see whether the bistability found earlier in the system was still present in a more elaborate model. Since oscillations are also present in platelets and red blood cell precursors in cyclical neutropenia, we used a DDE model for the full hematopoietic system (red blood cells, white blood cells and platelets), coupled with an ODE pharmacokinetic model for G-CSF administration. The addition of this two-compartment model for subcutaneous injections of G-CSF made the model more realistic by taking into account the time needed for G-CSF to go from the tissue compartment to the blood as well as its degradation rate. In the earlier version, G-CSF was assumed to be effective immediately when administered (when the G-CSF parameter set was turned on) and to disappear instantaneously when the G-CSF parameters were turned off. Another improvement of the present model was that we used linear functions to go from the untreated to the G-CSF treated state instead of an on-off switch. Three parameters were modified to mimic the effects of treatment: the amplification in the proliferating neutrophil precursors, the rate of apoptosis in the proliferating hematopoietic stem cells (HSC), and the maximal rate of differentiation from the HSCs into the neutrophil line. The model parameters were successfully fit to experimental data for seven cyclical neutropenic dogs before and during treatment. Numerical simulations, which were performed for each dog, showed that changing the time of treatment initiation and/or the period of treatment could result in satisfactory long-term outcomes and may require less G-CSF than usual. Different types of responses were observed (small and large amplitude oscillations), suggesting the existence of multiple stable solutions. Since G-CSF is also often used for treating neutropenia after chemotherapy treatment, we

were interested in studying the effects of G-CSF on the dynamics of granulopoiesis in this situation. In Chapter 4, we developed a new DDE model for neutrophil production, which is coupled to a two-compartment pharmacokinetic model for G-CSF, similar to the one proposed in Chapter 3. It differs from the previous model by making explicit the effects of G-CSF rather than having some effects included implicitly in the feedback functions. More precisely, amplification, transit time for the postmitotic phase and apoptosis rates were modeled using simple bounded functions that depend on G-CSF blood concentration. The proliferative and non-proliferative phases of neutrophil precursors were considered separately and the apoptosis was no longer implicitly included in the amplification for the neutrophil mitotic precursors compartment. Moreover, the clearance of G-CSF was modeled so that it takes into account the neutrophil-mediated clearance process instead of only the clearance from the kidney (as in Chapter 3). All these refinements made the model more realistic with respect to G-CSF administration. Parameters of the model were obtained for both filgrastim and pegfilgrastim, two recombinant forms of G-CSF that are used clinically for treatment of chemotherapy-induced neutropenia. The goal was to study different treatment strategies through numerical simulations of the model. We found that varying either the starting day of G-CSF treatment or its duration could result in two qualitatively different responses: a large neutrophil increase followed by a deep nadir or a smaller ANC increase that remains relatively stable and does not go to very low levels. We showed that this could be explained by the very rich dynamics of the system and the presence of multistability.

In summary, our results suggest that hematopoiesis in general, and granulopoiesis in particular, have inherent dynamical properties and that G-CSF administration can affect these dynamics. We believe that these dynamical properties could be exploited to design more efficient G-CSF treatment strategies for CN and chemotherapy-induced neutropenia, presumably leading to financial savings and fewer side effects. However, our results are based on mathematical modeling and numerical simulations. Although this approach allows one to explore a wide range of potential treatment regimens in a systematic way, experimental data on such alternative G-CSF administration schemes would be needed to better validate our modeling results. Indeed, despite the improvements made to the earlier model used in Foley et al. (2006) regarding G-CSF administration, our models represent approximations to reality. In real life, there is a great variability in and between patients and several factors may influence treatment.

5.2 Future work

The model presented in Chapter 4 could be used to study different mechanisms of granulopoiesis and of G-CSF administration. In particular, we assumed G-CSF was acting on both the apoptosis rate and the amplification factor in the proliferative phase of neutrophil precursors. Since both effects are modeled separately, we could study in more detail the precise effects of each factor.

As mentioned above, clinical data for alternative treatment schedules with G-CSF are needed to validate our results and make further model improvements. If such data were available, the individualized approach presented in Chapter 3 could be interesting to implement since it fits the model to data before and during treatment for a given subject. Numerical simulations for this subject could then predict the possible outcomes of different treatment schemes.

In conclusion, hematopoiesis and G-CSF effects are not yet fully understood and several aspects are still being studied. Clinical findings and future studies will provide new insights and help to better understand the system. The models presented here would then have to be modified accordingly, as this is part of the evolutionary process of mathematical modeling.

References

- J. L. Abkowitz, R. D. Holly, and W. P. Hammond. Cyclic hematopoiesis in dogs: Studies of erythroid burst forming cells confirm an early stem cell defect. *Exp. Hematol.*, 16: 941–945, 1988.
- M. Adimy and F. Crauste. Global stability of a partial differential equation with distributed delay due to cellular replication. *Nonlin. Analysis.*, 54:1469–1491, 2003.
- M. Adimy and F. Crauste. Modeling and asymptotic stability of a growth factor-dependent stem cell dynamics model with distributed delay. *Disc. Cont. Dyn. Syst. Series-B*, 8, 2007.
- M. Adimy and L. Pujo-Menjouet. A singular transport model describing cellular division. *C.R. Acad. Sci. Paris*, 332:1071–1076, 2001.
- M. Adimy and L. Pujo-Menjouet. A mathematical model describing cellular division with a proliferating phase duration depending on the maturity of cells. *Electron. J. Differential Equations*, 107:14 pp., 2003.
- M. Adimy, F. Crauste, and S. Ruan. A mathematical study of the hematopoiesis process with applications to chronic myelogenous leukemia. *SIAM J. Appl. Math.*, 65, 2005a.
- M. Adimy, F. Crauste, and S. Ruan. Stability and hopf bifurcation in a mathematical model of pluripotent stem cell dynamics. *Nonlin. Analysis.: Real World Appl.*, 6: 651–670, 2005b.
- M. Adimy, F. Crauste, and S. Ruan. Modelling hematopoiesis mediated by growth factors with applications to periodic hematological diseases. *Bull. Math. Biol.*, 68:2321–2351, 2006.

- D. Angeli, J. E. Jr. Ferrell, and E. D. Sontag. Detection of multistability, bifurcations, and hysteresis in a large class of biological positive-feedback systems. *Proc. Natl. Acad. Sci. USA*, 101:1822–1827, 2004.
- R. Apostu and M.C. Mackey. Understanding cyclical thrombocytopenia: A mathematical modeling approach. *J. Theor. Biol.*, 251:297–316, 2008.
- C. P. Bagowski and J. E. Jr. Ferrell. Bistability in the jnk cascade. *Curr. Biol.*, 11: 1176–1182, 2001.
- C. Balduini, C. Stella, V. Rosti, G. Bertolino, P. Noris, and E. Ascari. Acquired cyclic thrombocytopenia thrombocytosis with periodic defect of platelet function. *Brit. J. Haematol.*, 85:718–722, 1993.
- S. Basu, G. Hodgson, M. Katz, and A. R. Dunn. Evaluation of role of G-CSF in the production, survival, and release of neutrophils from bone marrow into circulation. *Blood*, 100(3):854–861, 2002.
- J. Bélair and M. Mackey. A model for the regulation of mammalian platelet production. *Ann. N.Y. Acad. Sci.*, 504:280–282, 1987.
- J. Bélair, M.C. Mackey, and J.M. Mahaffy. Age-structured and two-delay models for erythropoiesis. *Math. Biosci.*, 128:317–346, 1995.
- C.L. Bennett, J.A. Weeks, and M.R. Somerfield et al. Use of hematopoietic colony-stimulating factors: comparison of the 1994 and 1997 american society of clinical oncology surveys regarding asco clinical practice guidelines. health services research committee of the american society of clinical oncology. *J. Clin. Oncol.*, 17:3676–3681, 1999.
- J. Bernard and J. Caen. Purpura thrombopénique et megacaryocytopenie cycliques mensuels. *Nouv. Rev. franc. Hémat.*, 2:378–386, 1962.
- S. Bernard, J. Belair, and M. Mackey. Oscillations in cyclical neutropenia: New evidence based on mathematical modeling. *J. Theor. Biol.*, 223:283–298, 2003.

- N. Bessonov, A. Ducrot, and V. Volpert. Modeling of leukemia development in the bone marrow. *Proc. of the annual Symposium on "Mathematics applied in Biology and Biophysics (Tom XLVIII, v.2)*, pages 79–88, 2005.
- N. Bessonov, L. Pujot-Menjouet, and V. Volpert. Cell modeling of hematopoiesis. *J. Math. Model. Nat. Phenomena*, 1, 2006.
- A. Beuter, L. Glass, M.C. Mackey, and M.S. Titcombe. *Nonlinear Dynamics in Physiology and Medicine*. Springer-Verlag, 2003.
- E. Beutler, M. A. Lichtman, B. S. Collier, and T. Kipps. *Williams Hematology*. McGraw-Hill, New York, 1995.
- U. S. Bhalla, P. T. Ram, and R. Iyengar. Map kinase phosphatase as a locus of flexibility in a mitogen-activated protein kinase signaling network. *Science*, 297:1018–1023, 2002.
- S. P. Blythe, R. M. Nisbet, and W. S. C. Gurney. The dynamics of population models with distributed maturation periods. *Theor. Popul. Biol.*, 25:289–311, 1984.
- RD. Butler, TM Waites, RE Lamar, JD Hainsworth, FA Greco, and DH Johnson. Timing of g-csf administration during intensive chemotherapy for breast cancer (abstract). *Am Soc Clin Oncol*, 11:1411, 1992.
- G.S. Chatta, T.H. Price, R.C. Allen, and D. C. Dale. Effects of in vivo recombinant methionyl human granulocyte colony-stimulating factor on the neutrophil response and peripheral blood colonyforming cells in healthy young and elderly adult volunteers. *Blood*, 84:2923–2929, 1994.
- G. Chikkappa, and H. Burlington G. Borner, A. D. Chanana, E. P. Cronkite, S. Ohl, M. Pavelec, and J. S. Robertso. Periodic oscillation of blood leukocytes, platelets, and reticulocytes in a patient with chronic myelocytic leukemia. *Blood*, 47:1023–1030, 1976.
- O.A. Clark, G.H. Lyman, A.A. Castro, L.G. Clark, and B. Djulbegovic. Colony-stimulating factors for chemotherapy-induced febrile neutropenia: a meta-analysis of randomized controlled trials. *J. Clin. Oncol.*, 23:4198–4214, 2005.
- T. Cohen and D. P. Cooney. Cyclical thrombocytopenia: Case report and review of literature. *Scand. J. Haemat.*, 16:133–138, 1974.

- C. Colijn and M. Mackey. A mathematical model of hematopoiesis: II. Cyclical neutropenia. *J. Theor. Biol.*, 237:133–146, 2005a.
- C. Colijn and M. Mackey. A mathematical model of hematopoiesis: I. Periodic chronic myelogenous leukemia. *J. Theor. Biol.*, 237:117–132, 2005b.
- C. Colijn, D. C. Dale, C. Foley, and M.C. Mackey. Observations on the pathophysiology and mechanisms for cyclic neutropenia. *Math. Model. Natural Phenom.*, 1:45–69, 2006a.
- C. Colijn, A.C. Fowler, and M. C. Mackey. High frequency spikes in long period blood cell oscillations. *J. Math. Biol.*, 53:499–519, 2006b.
- C. Colijn, C. Foley, and M.C. Mackey. G-CSF treatment of canine cyclical neutropenia: A comprehensive mathematical model. *Exp. Hematol.*, 35:898–907, 2007.
- F. R. Cross, V. Archambault, M. Miller, and M. Klovstad. Testing a mathematical model of the yeast cell cycle. *Mol. Biol. Cell.*, 13:52–70, 2002.
- D. C. Dale and W. P. Hammond. Cyclic neutropenia: A clinical review. *Blood Rev.*, 2: 178–185, 1988.
- D. C. Dale, C. J. Cottle, T. E. Boxer, B. Cham, M. H. Freedman, G. Kannourakis, S. E. Kinsey, R. Davis, D. Scarlata, B. Schwinzer, C. Zeidler, and K. Welte. Severe chronic neutropenia: Treatment and follow-up of patients in the severe chronic neutropenia international registry. *Am. J. Hematol.*, 72:82–93, 2003.
- K. Dan, K. Inokuchi, E. An, and T. Nomura. Cell mediated cyclic thrombocytopenia treated with azathioprine. *Brit. J. Haematol.*, 77:365–379, 1991.
- J. T. Dancy, K. A. Deubelbeiss, L. A. Harker, and C. A. Finch. Neutrophil kinetics in man. *J. Clin. Invest.*, 58:705–715, 1976.
- L. Danielson and J. Harmenberg. Intermittent G-CSF in cyclic neutropenia. *Eur. J. Hematol.*, 48:123–124, 1992.
- K. A. Deubelbeiss, J. T. Dancy, L. A. Harker, and C. A. Finch. Neutrophil kinetics in the dog. *J. Clin. Invest.*, 55:833–839, 1975.

- M. Dicato, S. Meyer, and F. Ries. Reduced G-CSF dosage in cyclic neutropenia gives satisfactory clinical laboratory and economic results. *Blood*, 80:413, 1992.
- A. Ducrot and V. Volpert. On a model of leukemia development with a spatial cell distribution. *J. Math. Model. Nat. Phenomena*, page In press, 2008.
- C. D. R. Dunn. Cyclic hematopoiesis: The biomathematics. *Exp. Hematol.*, 11:779–791, 1983.
- J. Dyson, Villela-Bressan, and G.F. Webb. An age and maturity structured model of cell population dynamics , in *Mathematical Models in Medical and Health Science*, (M. Horn, G. Simonnett, and G.F. Webb, Eds.). pages 99–116, 1998.
- J. Eller, I. Györi, J. Zollei, and F. Krizsa. Modelling thrombopoiesis regulation I: Model description and simulation results. *Comput. Math. Applic.*, 14:841–848, 1987.
- C. Engel, M. Scholz, and M. A. Loeffler. Computational model of human granulopoiesis to simulate the hematotoxic effects of multicycle polychemotherapy. *Blood*, 104: 2323–2331, 2004.
- K. Engstrom, A. Lundquist, and N. Soderstrom. Periodic thrombocytopenia or tidal platelet dysgenesis in a man. *Scand. J. Haemat*, 3:290–292, 1966.
- D. Fargue. Reductibilité des systèmes héréditaires à des systèmes dynamiques. *Comptes Rendus de l'Académie des Sciences*, B277:471–473, 1973.
- D. Fargue. Reductibilité des systèmes héréditaires. *Inter. J. Nonlin. Mech.*, 9:331–338, 1974.
- J. E. Ferrell. Self-perpetuating states in signal transduction: positive feedback, double-negative feedback, and bistability. *Curr. Opin. Chem. Biol.*, 6:140–148, 2002.
- J. E. Jr. Ferrell and E.M. Machleder. The biochemical basis of an all-or-none cell fate switch in xenopus oocytes. *Science*, 280:895–898, 1998.
- G.V. Fisher. An introduction to chaos theory and some haematological applications. *Comp. Haematol. Int*, 3:43–51, 1993.

- C. Foley and M. Mackey. Dynamic hematological disease: A review. *J. Math. Biol.*, In press., 2008.
- C. Foley, S. Bernard, and M. Mackey. Cost-effective G-CSF therapy strategies for cyclical neutropenia: Mathematical modelling based hypotheses. *J. Theor. Biol.*, 238:754–763, 2006.
- P. Fortin and M.C. Mackey. Periodic chronic myelogenous leukemia: Spectral analysis of blood cell counts and etiological implications. *Brit. J. Haematol.*, 104:336–245, 1999.
- M Fukuda, M Nakato, and et al Kinoshita A. Optimal timing of g-csf administration in patients receiving chemotherapy for non-small cell lung cancer (nscL) (abstract). *Am Soc Clin Oncol*, 12:1549, 1993.
- L. Glass and M.C. Mackey. *From Clocks to Chaos: The Rhythms of Life*. Princeton University Press, Princeton, N.J., 1988.
- W.M. Gray and J. Kirk. Analysis by analogue and digital computers of the bone marrow stem cell and platelet control mechanisms. In *Proc. Conf. Computers for Analysis and Control in Medical and biological Research*, pages 120–124, UK, 1971. IEE.
- M. D. Green, H. Koelbl, J. Baselga, A. Galid, V. Guillem, P. Gascon, S. Siena, R. I. Lalisang, H. Samonigg, M. R. Clemens, V. Zani, B. C. Liang, J. Renwick, and M. J. Piccart. A randomized double-blind multicenter phase iii study of fixed-dose single-administration pegfilgrastim versus daily filgrastim in patients receiving myelosuppressive chemotherapy. *Ann. Oncol.*, 14:29–35, 2003.
- F. Grignani. Chronic myelogenous leukemia. *Crit. Rev. Oncology-Hematol.*, 4:31–66, 1985.
- D. Guerry, D. Dale, D. C. Omine, S. Perry, and S. M. Wolff. Periodic hematopoiesis in human cyclic neutropenia. *J. Clin. Inves.*, 52:3220–3230, 1973.
- I. Györi and J. Eller. Modelling thrombopoiesis regulation II: Mathematical investigation of the model. *Comput. Math. Applic.*, 14:849–859, 1987.
- W. P. Hammond, T. H. Price, L. M. Souza, and D. C. Dale. Treatment of cyclic neutropenia with granulocyte colony stimulating factor. *New Eng. J. Med.*, 320: 1306–1311, 1989.

- Y.A. Hannun. Apoptosis and the dilemma of cancer chemotherapy. *Blood*, 89:1845–1853, 1997.
- Matthew E. Hardee, Murat O. Arcasoy, Kimberly L. Blackwell, John P. Kirkpatrick, and Mark W. Dewhirst. Erythropoietin Biology in Cancer. *Clin Cancer Res*, 12(2):332–339, 2006. doi: 10.1158/1078-0432.CCR-05-1771.
- C. Haurie, M. C. Mackey, and D. C. Dale. Cyclical neutropenia and other periodic hematological diseases: A review of mechanisms and mathematical models. *Blood*, 92: 2629–2640, 1998.
- C. Haurie, M. C. Mackey, and D. C. Dale. Occurrence of periodic oscillations in the differential blood counts of congenital, idiopathic and cyclical neutropenic patients before and during treatment with G-CSF. *Exper. Hematol*, pages 401–409, 1999a.
- C. Haurie, R. Person, D. C. Dale, and M.C. Mackey. Haematopoietic dynamics in grey collies. *Exper. Hematol.*, 27:1139–1148, 1999b.
- C. Haurie, D. C. Dale, R. Rudnicki, and M. C. Mackey. Modeling complex neutrophil dynamics in the grey collie. *J. Theor. Biol.*, 204:505–519, 2000a.
- C. Haurie, D. C. Dale, R. Rudnicki, and M. C. Mackey. Modeling complex neutrophil dynamics in the grey collie. *J. Theor. Biol.*, 204:504–519, 2000b.
- N. Hayashi, H. Kinoshita, E. Yukawa, and S. Higuchi. Pharmacokinetic and pharmacodynamic analysis of subcutaneous recombinant human granulocyte colony stimulating factor (lenograstim) administration. *J. Clin. Pharmacol.*, 39:583–592, 1999.
- N. Hayashi, H. Aso, M. Higashida, H. Kinoshita, S. Ohdo, E. Yukawa, and S. Higuchi. Estimation of RHG-CSF absorption kinetics after subcutaneous administration using a modified Wagner-Nelson method with a nonlinear elimination model. *Eur. J. Pharm. Sci.*, 15:151–158, 2001.
- T. Hearn, C. Haurie, and M.C. Mackey. Cyclical neutropenia and the peripheral control of white blood cell production. *J. theor. Biol*, 192:167–181, 1998.
- E. S. Henderson, T. A. Lister, and M. F. Greaves, editors. *Leukemia*. Saunders, 1996.

- R. Hoffman, R.A. Bridell, K. van Besien, E.F. Srouf, T. Guscar, N.W. Hudson, and A. Ganser. Acquired cyclic amegakaryocytic thrombocytopenia associated with an immunoglobulin blocking the action of granulocyte-macrophage colony-stimulating factor. *New England Journal of Medicine*, 321:97–102, 1989.
- F.A. Holmes, J.A. OShaughnessy, S. Vukelja, S.E. Jones, J. Shogan, M. Savin, J. Glaspy, M. Moore, L. Meza, I. Wiznitzer, T.A. Neumann, L.R. Hill, and B.C. Liang. Blinded, randomized, multicenter study to evaluate single administration pegfilgrastim once per cycle versus daily filgrastim as an adjunct to chemotherapy in patients with high-risk stage ii or stage iii/iv breast cancer. *J. Clin. Oncol.*, 20:727–731, 2002.
- M. Horwitz, K. F. Benson, Z. Duan, F.-Q. Li, and R. E. Person. Hereditary neutropenia: dogs explain human neutrophil elastase mutations. *TRENDS Mol. Med.*, 10:163–170, 2004.
- L. G. Israels and E. D. Israels. *Mechanisms in Hematology*. Core Health Services Inc., 2002.
- S. Jayabose and C. Sandoval. Recombinant human granulocyte colony stimulating factor in cyclic neutropenia: Use of a new 3-day-a-week regimen. *Am. J. Ped. Hematol. Oncol.*, 16(4):338–340, 1994.
- K. Kaushansky, N. Lin, A. Grossmann, J. Humes, K.H. Sprugel, and V.C. Broudy. Thrombopoietin expands erythroid, granulocyte-macrophage, and megakaryocyte progenitor cells in normal and myelosuppressed mice. *Experimental Hematology*, 24: 256–269, 1996.
- N. D. Kazarinoff and P. van den Driessche. Control of oscillations in hematopoiesis. *Science*, 203:1348–1350, 1979.
- C. M. Kearns, W. C. Wang, N. Stute, J.N. Ihle, and W. E. Evans. Disposition of recombinant human granulocyte colony-stimulating factor in children with severe chronic neutropenia. *J. Pediatr.*, 123(3):471–479, 1993a.
- C. M. Kearns, W. C. Wang, N. Stute, Ihle J. N., and W. E. Evans. Disposition of recombinant human granulocyte colony stimulating factor in children with severe chronic neutropenia. *J. Pediatr.*, 123:471–479, 1993b.

- B. J. Kennedy. Cyclic leukocyte oscillations in chronic myelogenous leukemia during hydroxyurea therapy. *Blood*, 35:751–760, 1970.
- F. Kimura, Y. Nakamura, K. Sato, N. Wakimoto, T. Kato, T. Tahara, M. Yamada, N. Nagata, and K. Motoyoshi. Cyclic change of cytokines in a patient with cyclic thrombocytopenia. *British Journal of Haematology*, 94:171–174, 1996.
- E. A. King-Smith and A. Morley. Computer simulation of granulopoiesis: Normal and impaired granulopoiesis. *Blood*, 36:254–262, 1970.
- G. Koumakis, M. Vassilomanolakis, V. Barbounis, E. Hatzichristou, S. Demiri, G. Plataniotis, F. Pamouktsoglou, and A.P. Efremidis. Optimal timing (preemptive versus supportive) of granulocyte colony-stimulating factor administration following high-dose cyclophosphamide. *Oncology*, 56:28–35, 1999.
- M.J. Koury. Programmed cell death (apoptosis) in hematopoiesis. *Exp. Hematol.*, 20:391–394, 1992.
- M.J. Koury and M.C. Bondurant. The mechanisms of erythropoietin action. *Am. J. Kidney Dis.*, 18:20–23, 1991.
- T. Kuwabara, Y. Kato, S. Kobayashi, H. Suzuki, and Y. Sugiyama. Nonlinear pharmacokinetics of a recombinant human granulocyte colony-stimulating factor derivative (nartograstim): Species differences among rats, monkeys and humans. *J. Pharmacol. Exp. Ther.*, 271(3):1535–1543, 1994.
- A. Lasota and M.C. Mackey. Global asymptotic properties of proliferating cell populations. *J. Math. Biol.*, 19:437–62, 1984.
- J.E. Layton and N.E. Hall. The interaction of G-CSF with its receptor. *Frontiers in Biosci.*, 11:3181–3189, 2006.
- M. L. Lewis. Cyclic thrombocytopenia: A thrombopoietin deficiency. *J. Clin. Pathol.*, 27:242–246, 1974.
- M. Loeffler and K. Pantel. A mathematical model of erythropoiesis suggests an altered plasma volume control as cause for anemia in aged mice. *Exper. Gerontol*, 25:483–495, 1990.

- M. Loeffler, K. Pantel, H. Wulff, and H.E. Wichmann. A mathematical model of erythropoiesis in mice and rats. part i: Structure of the model. *Cell Tissue Kinet.*, 22: 13–20, 1989.
- B. I. Lord, M. H. Bronchud, S. Owens, J. Chang, A. Howell, L. Souza, and T. M Dexter. The kinetics of human granulopoiesis following treatment with granulocyte colony stimulating factor in vivo . *Proceedings of the National Academy of Sciences, USA*, 86: 9499–9503, 1989.
- J. Lotem and L. Sachs. Hematopoietic cytokines inhibit apoptosis induced by transforming growth factor bl and cancer chemotherapy compounds in myeloid leukemic cells. *Blood*, 80:1750–1757, 1992.
- N. MacDonald. Cyclical neutropenia: Models with two cell types and two time lags. In A.J. Valleron and P.D.M. Macdonald, editors, *Biomathematics and Cell Kinetics*, pages 287–295. Elsevier/North-Holland, Amsterdam, 1978a.
- N. MacDonald. *Time Lags in Biological Models*. Springer-Verlag, 1978b.
- M. C. Mackey. Periodic auto-immune hemolytic anemia: An induced dynamical disease. *Bull. Math. Biol.*, 41:829–834, 1979a.
- M. C. Mackey. A unified hypothesis for the origin of aplastic anemia and periodic haematopoiesis. *Blood*, 51:941–956, 1978a.
- M. C. Mackey. Cell kinetic status of haematopoietic stem cells. *Cell Prolif.*, 34:71–83, 2001.
- M. C. Mackey. A unified hypothesis for the origin of aplastic anemia and periodic haematopoiesis. *Blood*, 51:941–956, 1978b.
- M. C. Mackey. Dynamic haematological disorders of stem cell origin. In J. G. Vassileva-Popova and E. V. Jensen, editors, *Biophysical and Biochemical Information Transfer in Recognition*, pages 373–409. Plenum Publishing Corp., New York, 1979b.
- M. C. Mackey and L. Glass. Oscillations and chaos in physiological control systems. *Science*, 197:287–289, 1977.

- M. C. Mackey, A. A. G. Aprikyan, and D. C. Dale. The rate of apoptosis in post mitotic neutrophil precursors of normal and neutropenic humans. *Cell. Prolif.*, 36:27–34, 2003.
- M.C. Mackey and P. Dormer. Continuous maturation of proliferating erythroid precursors. *Cell and Tissues kinetics*, 15:381–392, 1982.
- M.C. Mackey and A. Rudnicki. Global stability in a delayed partial differential equation describing cellular replication. *J. Math. Biol.*, 33:89–109, 1994.
- J. Mahaffy, J. Belair, and M. Mackey. Hematopoietic model with moving boundary condition and state dependent delay: Applications in erythropoiesis. *J. Theor. Bio.*, 190:135–146, 1998a.
- J. M. Mahaffy, J. Bélair, and M.C. Mackey. Hematopoietic model with moving boundary condition and state dependent delay. *J. theor. Biol.*, 190:135–146, 1998b.
- B.R. Meisenberg, T.A. Davis, Melaragno, R. A.J., Stead, and R.L. Monroy. A comparison of therapeutic schedules for administering granulocyte colony-stimulating factor to nonhuman primates after high-dose chemotherapy. *Blood*, 79:2267–2272, 1992.
- J. Melo. The diversity of BCR-ABL fusion proteins and their relationship to leukemia phenotype. *Blood*, 88:2375–2384, 1996.
- K. Mempel, T. Pietsch, T. Menzel, C. Zeidler, and K. Welte. Increased serum levels of granulocyte colony stimulating factor in patients with severe congenital neutropenia. *Blood*, 77:1919–1922, 1991.
- N. Metropolis, A. Rosenbluth, M. Rosenbluth, A. Teller, and E. Teller. Equation of state calculations by fast computing machines. *Journal of Chemical Physics*, 21:1087–1092, 1953.
- A. R. Migliaccio, G. Migliaccio, D. C. Dale, and W. P. Hammond. Hematopoietic progenitors in cyclic neutropenia: Effect of granulocyte colony stimulating factor in vivo. *Blood*, 75:1951–1959, 1990.
- G. Molineux, O. Kinstler, B. Briddell, C. Hartley, P. McElroy, P. Kerzic, W. Sutherland, G. Stoney, B. Kern, F.A. Fletcher, A. Cohen, E. Korach, T. Ulich, I. McNiece,

- P. Lockbaum, M.A. Miller-Messana, S. Gardner, T. Hunt, and G. Schwab. A new form of filgrastim with sustained duration in vivo and enhanced ability to mobilize pbpc in both mice and humans. *Exp. Hematol.*, 27:1724–1734, 1999.
- A. Morley. Cyclic hemopoiesis and feedback control. *Blood Cells*, 5:283–296, 1979.
- A. Morley. A platelet cycle in normal individuals. *Aust. Ann. Med.*, 18:127–129, 1969.
- A. Morley and F. Stohlman. Cyclophosphamide induced cyclical neutropenia. *New England Journal of Medicine*, 282:643–646, 1970.
- A. Morley, E. A. King-Smith, and F. Stohlman. The oscillatory nature of hemopoiesis. In F. Stohlman, editor, *Hemopoietic Cellular Proliferation*, pages 3–14. Grune & Stratton, New York, 1969.
- G. Morstyn, L. Campbell, G. Lieschke, J.E. Layton, Maher D., M. O'Connor, M. Green, W. Sheridan, M. Vincent, K. Alton, L. Souza, K. McGrath, and R.M. Fox. Treatment of chemotherapy-induced neutropenia by subcutaneously administered granulocyte colony-stimulating factor with optimization of dose and duration of therapy. *J. Clin. Oncol.*, 7:1554–1562, 1989.
- J. P. Novak and E. Necas. Proliferation differentiation pathways of murine haematopoiesis: correlation of lineage fluxes. *Cell. Prolif.*, 27:597–633, 1994.
- M. O'Dwyer, B. J. Druker, M. Mauro, M. Talpaz, D. Resta, B. Peng, E. Buchdunger, J. Ford, S. Fernandes Reese, R. Capdeville, and C. L. Sawyers. STI571: A tyrosine kinase inhibitor for the treatment of CML. *Annals of Oncology*, 11:155, 2000.
- J. S. Orr, J. Kirk, K.G. Gray, and J.R. Anderson. A study of the interdependence of red cell and bone marrow stem cell populations. *British Journal of Haematology*, 15:23–24, 1968.
- I. Ostby, L. S. Rusten, G. Kvalheim, and P. Grottum. A mathematical model for reconstitution of granulopoiesis after high dose chemotherapy with autologous stem cell transplantation. *J. Math. Biol.*, 47:101–136, 2003.

- I. Ostby, G. Kvalheim, L. S. Rusten, and P. Grottum. Mathematical modeling of granulocyte reconstitution after high-dose chemotherapy with stem cell support: Effect of posttransplant G-CSF treatment. *J. Theor. Biol.*, 231:69–83, 2004.
- E. M. Ozbudak, M. Thattai, H. N. Lim, B. I. Shraiman, and A. van Oudenaarden. Multistability in the lactose utilization network of *Escherichia coli*. *Nature*, 427:737–740, 2004.
- H. Ozer, J.O. Armitage, C. L. Bennett, J. Crawford, G. D. Demetri, P. A. Pizzo, C. A. Schiffer, T. J. Smith, G. Somlo, J. C. Wade, J. L. Wade, R. J. Winn, A. J. Wozniak, and M. R. Somerfield. Update of recommendations for the use of hematopoietic colony-stimulating factors: Evidence-based, clinical practice guidelines. *Journal of Clinical Oncology*, 10:3288, 1997.
- S. E. Palmer, K. Stephens, and D. C. Dale. Genetics, phenotype, and natural history of autosomal dominant cyclichematopoiesis. *Am J Med Genet.*, 66:413–422, 1996.
- J. C. Panetta, M. N. Kirstein, A.J. Gajjar, G. Nair, M. Fouladi, and C. F. Stewart. A mechanistic mathematical model of temozolomide myelosuppression in children with high-grade gliomas. *Math. Biosc.*, 186:29–41, 2003.
- J. R. Park. Cytokine regulation of apoptosis in hematopoietic precursor cells. *Curr. Opin. Hematol.*, 3:191–196, 1996.
- J. R. Pomerening, E. D. Sontag, and J. E. Jr. Ferrell. Building a cell cycle oscillator: hysteresis and bistability in the activation of *cdc2*. *Nat. Cell Biol.*, 5:346–351, 2003.
- T. H. Price, G. S. Chatta, and D. C. Dale. Effect of recombinant granulocyte colony stimulating factor on neutrophil kinetics in normal young and elderly humans. *Blood*, 88:335–340, 1996.
- L. Pujo-Menjouet and M. Mackey. Contribution to the study of periodic chronic myelogenous leukemia. *C. R. Biologies*, 327:235–244, 2004.
- L. Pujo-Menjouet, S. Bernard, and M. Mackey. Long period oscillations in a G_0 model of hematopoietic stem cells. *SIAM J. Appl. Dyn. Syst.*, 4:312–332, 2005.

- Z. Rahman, L. Esparza-Guerra, H.Y. Yap, G. Fraxchini, G. Bodey, and G. Hortobagyi. Chemotherapy-induced neutropenia and fever in patients with metastatic breast carcinoma receiving salvage chemotherapy. *Cancer*, 79:1150–1157, 1997.
- P. Ranlov and A. Videbaek. Cyclic haemolytic anaemia synchronous with Pel-Ebstein fever in a case of Hodgkin’s disease. *Acta Medica Scandinavica*, 100, 1963.
- J. Reeve. An analogue model of granulopoiesis for the analysis of isotopic and other data obtained in the non-steady state. *Br. J. Haematol.*, 25:15–32, 1973.
- A. Ritchie, A. Gotoh, J. Gaddy, S.E. Braun, and H.E. Broxmeyer. Thrombopoietin upregulates the promoter conformation of p53 in a proliferation-independent manner coincident with a decreased expression of bax: potential mechanisms for survival enhancing effects. *Blood*, 90:4394–4402, 1997.
- I. Roeder. Quantitative stem cell biology: Computational studies in the hematopoietic system. *Curr Opin Hematol*, 13:222–228, 2006.
- L.K. Roskos, P. Lum, P. Lockbaum, G. Schwab, and B.-B. Yang. Pharmacokinetic/pharmacodynamic modeling of pegfilgrastim in healthy subjects. *J. Clin. Pharmacol.*, 46:747–757, 2006.
- S.I. Rubinow and J.L. Lebowitz. A mathematical model of neutrophil production and control in normal man. *J. Math. Biol.*, 1:187–225, 1975.
- P. Salamon, P. Sibani, and R. Frost. *Facts, Conjectures, and Improvements for Simulated Annealing*. Society for Industrial and Applied Mathematics, Philadelphia, 2002.
- M. Santillan and M. C. Mackey. Influence of catabolite repression and inducer exclusion on the bistable behavior of the lac operon. *Biophys.*, 86:1281–1292, 2004.
- M. Santillan, J. Mahaffy, J. Belair, and M. Mackey. Regulation of platelet production: The normal response to perturbation and cyclical platelet disease. *J. Theor. Bio.*, 206: 585–603, 2000.
- M. Santillan, M. C. Mackey, and E.S. Zeron. Origin of bistability in the lac operon. *Biophys. Journal*, 92:3830–3842, 2007.

- S. Schmitz. *Ein mathematisches Modell der zyklischen Haemopoese*. PhD thesis, Universitat Koln, 1988.
- S. Schmitz, M. Loeffler, J. B. Jones, R. D. Lange, and H. E. Wichmann. Synchrony of bone marrow proliferation and maturation as the origin of cyclic haemopoiesis. *Cell Tissue Kinet.*, 23:425–441, 1990.
- S. Schmitz, H. Franke, J. Brusis, and H. E. Wichmann. Quantification of the cell kinetic effects of G-CSF using a model of human granulopoiesis. *Exp. Hematol.*, 21:755–760, 1993.
- S. Schmitz, H. Franke, M. Loeffler, H. E. Wichmann, and V. Diehl. Reduced variance of bone-marrow transit time of granulopoiesis: A possible pathomechanism of human cyclic neutropenia. *Cell Prolif.*, 27:655–667, 1994.
- S. Schmitz, H. Franke, H. E. Wichmann, and V. Diehl. The effect of continuous G-CSF application in human cyclic neutropenia: A model analysis. *Br. J. Haematol.*, 90: 41–47, 1995.
- M. Scholz, C. Engel, and M. Loeffler. Modelling human granulopoiesis under polychemotherapy with G-CSF support. *J. Math. Biol.*, 50:397–439, 2005.
- W. Sha, J. Moore, K. Chen, A. D. Lassaletta, C.S. Yi, J. J. Tyson, and J. C. Sible. Hysteresis drives cell-cycle transitions in xenopus laevis egg extracts. *Proc. Natl. Acad. Sci. USA*, 100:975–980, 2003.
- L.F. Shampine. Solving odes and ddes with residual control. *Appl. Num. Math.*, 52: 113–127, 2005.
- E. Shochat, S. M. Stemmer, and L.A. Segel. Human haematopoiesis in steady state and following intense perturbations. *Bull. Math. Biol.*, 64:861–886, 2002.
- E. Shochat, V. Rom-Kedar, and L.A. Segel. G-csf control of neutrophils dynamics in the blood. *Bull. Math. Biol.*, 69:2299–2338, 2007.
- D. Shvitra, R. Laugaly, and Y. S. Kolesov. Mathematical modeling of the production of white blood cells. In G. Marchuk and L.N. Belykh, editors, *Mathematical Modeling in Immunology and Medicine*, pages 211–223, Amsterdam, 1983. North-Holland.

- K. Skomorovski and Z. Agur. A new method for predicting and optimizing thrombopoietin (tpo) therapeutic protocols in thrombocytopenic patients and in platelet donors [abstract]. *The Hematol. Journal*, Suppl. 1:185, 2001.
- K. Skomorovski, H. Harpak, A. Ianovski, M. Vardi, T.P. Visser, S.C.C. Hartong, H. H.D.M. van Vliet, G. Wagemaker, and Z. Agur. New tpo treatment schedules of increased safety and efficacy: pre-clinical validation of a thrombopoiesis simulation model. *Brit. J. Haematol*, 123:683–691, 2003.
- S.H. Strogatz. *Nonlinear dynamics and chaos : with applications to physics, biology, chemistry, and engineering*. Cambridge, MA, Westview Press, 2000.
- N. Stute, V.M. Santana, J.H. Rodman, M.J. Schell, J.N. Ihle, and W.E. Evans. Pharmacokinetics of subcutaneous recombinant human granulocyte colony-stimulating factor in children. *Blood*, 79(11):2849–2854, 1992.
- J. Swinburne and M.C. Mackey. Cyclical thrombocytopenia: Characterization by spectral analysis and a review. *J. Theor. Med.*, 2:81–91, 2000.
- H. Takatani, H. Soda, M. Fukuda, M. Watanabe, A. Kinoshita, T. Nakamura, and M. Oka. Levels of recombinant human granulocyte colony stimulating factor in serum are inversely correlated with circulating neutrophil counts. *Antimicrob. Agents Chemother.*, 40:988–991, 1996.
- V. Vainstein, Y. Ginosara, M. Shohamb, D.O. Ranmara, A. Ianovskib, and Z. Agur. The complex effect of granulocyte colony-stimulating factor on human granulopoiesis analyzed by a new physiologically-based mathematical model. *J. Theor. Biol.*, 234(3): 311–327, 2005.
- S. Viswanathan and P. W. Zandstra. Towards predictive models of stem cell fate. *Cytotechnology.*, 41:75–92, 2003.
- G. K. von Schulthess and N. A. Mazer. Cyclic neutropenia (CN): A clue to the control of granulopoiesis. *Blood*, 59:27–37, 1982.
- G.K. von Schulthess and U. Gessner. Oscillating platelet counts in healthy individuals: Experimental investigation and quantitative evaluation of thrombocytopoietic feedback control. *Scand. J. Haematol.*, 36:473–479, 1986.

- K. Watari, S. Asano, N. Shirafuji, H. Kodo, K. Ozawa, F. Takaku, and S. Kamachi. Serum granulocyte colony stimulating factor levels in healthy volunteers and patients with various disorders as estimated by enzyme immunoassay. *Blood*, 73:117–122, 1989.
- G.F. Webb. *Theory of nonlinear age-dependent population dynamics*. Monographs and Textbooks in Pure and Applied Mathematics no. 89, 1985.
- H. E. Wichmann, M. Loeffler, and S. Schmitz. A concept of hemopoietic regulation and its biomathematical realization. *Blood Cells*, 14:411–429, 1988.
- H.E. Wichmann, M.D. Gerhardt, H. Spechtmeier, and R. Gross. A mathematical model of thrombopoiesis in the rat. *Cell Tissue Kinet*, 12:551–567, 1979.
- G.T. Williams and C.A. Smith. Molecular regulation of apoptosis: Genetic controls on cell death. *Cell*, 74:777–779, 1993.
- M. Yanabu, S. Nomura, T. Fukuroi, T. Kawakatsu, H. Kido, K. Yamaguchi, M. Suzuki, T. Kokawa, and K. Yasunaga. Periodic production of antiplatelet autoantibody directed against GP IIIa in cyclic thrombocytopenia. *Acta Haematol.*, 89:155–159, 1993.
- N. Yildirim and M. C. Mackey. Feedback regulation in the lactose operon: a mathematical modeling study and comparison with experimental data. *Biophys.*, 84:2841–2851, 2003.
- N. Yildirim, M. Santillan, D. Horike, and M. C. Mackey. Dynamics and bistability in a reduced model of the lac operon. *Chaos*, 14:279–292, 2004.
- W.C. Zamboni. Pharmacokinetics of pegfilgrastim. *Pharmacotherapy*, 23:9S–14S, 2003.